UNIVERSITY OF
KWAZULU-NATAL

INYUVESI
YAKWAZULU-NATALI

AFLATOXIN B_1 MODULATES OXIDATIVE STRESS AND APOPTOSIS IN HUMAN EMBRYONIC KIDNEY CELLS

Nomali Zanele Dlamini
214518974
BSc, BMedSc (Hons) (UKZN)

Submitted in fulfilment of the requirements for the degree of Master of Medical Science in the Discipline of Medical Biochemistry and Chemical Pathology

School of Laboratory Medicine and Medical Sciences

College of Health Sciences

University of KwaZulu-Natal

Durban, South Africa

2019

DECLARATION

I, **Miss Nomali Zanele Dlamini**, declare as follows:

1. The research reported in this thesis, except where otherwise indicated, and is my original research.
2. This thesis has not been submitted for any degree or examination at any other university.
3. This thesis does not contain other person's data, pictures, graphs or other information, unless specifically acknowledged as being sourced from other persons.
4. This thesis does not contain other persons' writing, unless specifically acknowledged as being sourced from other researchers. Where other written sources have been quoted, then:
    a. Their words have been re-written, but the general information attributed to them has been referenced
    b. Where their exact words have been used, then their writing has been placed in italics, inside quotation marks and referenced.
5. This thesis does not contain text, graphics or tables copied and pasted from the Internet, unless specifically acknowledged, and the source being detailed in the thesis and in the References sections.
6. The research described in this study was carried out in the Discipline of Medical Biochemistry and Chemical Pathology, School of Laboratory Medicine and Medical Sciences, College of Health Sciences, University of KwaZulu-Natal, Howard College Campus, Durban, under the supervision of Dr RB Khan.

Signed: _____ Date: _____

DEDICATION

Myself

My family

In loving memory of my eldest sister

Sthembiso Mbuyisa

3-01-1983 to **23-11-2013**

ACKNOWLEDGEMENTS

I would like to express my heartfelt appreciation to GOD almighty and to the following people:

Dr RB Khan

Words are not enough to describe my appreciation for giving this opportunity. I will always be grateful for the patient guidance, advice and encouragement you have provided for me in the course of this study not only as a supervisor but also as an inspiring female mentor. Thank you for believing in me and for the time you invested in me. I would also like to thank you for teaching me the laboratory techniques, allowing me to be hands on and responding to my queries promptly. I have been extremely lucky to have a supervisor like you.

My family

Thank you for your unconditional love and support and allowing me to follow my dreams. My dearest father for being my rock in everything and the support you have shown me is remarkable. My mother and dearest sisters for always believing in me, always offering to help and motivating me to chase my dreams.

My friends

The close companionships I found through my Honours and master's years, Priscilla Mhlanga, Thobeka Madide, Ntombi Benede while going through their own life and Masters' life they kept supporting me with personal and academic issues, I wouldn't have made it throughout the year without their support. Nomalungelo Mahlalela, thank you for showing me that being kind, polite and smart are good qualities to have when working with people.

Academic staff and post graduate staff

I would like to give thanks to the staff and students especially Angela, Yandisa, Lloyd and Lebo from the Department of Medical Biochemistry for their help in the laboratory, advice and moral support.

UKZN - College of Health Sciences

Thank you for financial support as a post graduate student and for running expenses throughout the course of my Masters.

ABBREVIATIONS

Ab	Antibody
ADP	Adenosine diphosphate
AFs	Aflatoxins
AFAR	Aflatoxin aldehyde reductase
AFB_1-lys	Aflatoxin B_1 lysine adduct
AFB_1	Aflatoxin B_1
AFB_2	Aflatoxin B_2
AFG_1	Aflatoxin G_1
AFG_2	Aflatoxin G_2
AFM_1	Aflatoxin M_1
AFM_2	Aflatoxin M_2
AFBO	Aflatoxin B_1-8,9-epoxide
AIF	Apoptosis inducing factor
Amp	Amperes
APAF-1	Apoptotic protease activating factor-1
APS	Ammonium persulphate
AREs	Antioxidant response elements
ATM	Ataxia telangiectasia mutated
ATP	Adenosine triphosphate
Bax	Bcl-2-associated X
BCA	Bicinchoninic acid
Bcl-2	B-cell lymphoma/leukemia-2
BHT	Butylated hydroxytoluene
BSA	Bovine serum albumin
Ca^{2+}	Calcium
CAT	Catalase
CARD	Caspase-recruitment domains
CCM	Complete culture medium
cDNA	Complementary DNA
CHK	Check point kinase
c-IAP	Cellular inhibitor of apoptosis

CO_2	Carbon dioxide
COX	Cyclooxygenase
$CuSO_4$	Copper (II) sulfate solution
Cyt-c	Cytochrome-c
CYP	Cytochrome P_{450}
D	Days
DED	Death effector domain
dH_2O	Distilled water
DISC	Death-inducing signaling complex
DMEM	Dulbecco's Modified Eagles Medium
DMSO	Dimethyl sulfoxide
DNA	Deoxyribonucleic acid
dNTP	Deoxynucleotide
ds-	Double-stranded
e^-	Electron
EDTA	Ethylenediaminetetraacetic acid
FADD	Fas-associated death domain
$FADH_2$	Flavin adenine dinucleotide
FasL	Fatty acid synthetase-ligand
FasR	Fatty acid synthetase-receptor
Fe	Iron
Fe^{2+}	Ferrous ion
FCS	Foetal calf serum
G	Gram
G6PD	Glucose-6-phosphate dehydrogenase
GAPDH	Glyceraldehyde-3-phosphate dehydrogenase
GGT	γ-glutamyl transpeptidase
GR	Glutathione reductase
GSH	Glutathione
GSSG	Glutathione disulphide
GPx	Glutathione peroxidase
GST	Glutathione -S- transferase

hr/hrs	Hours
H^+	Hydrogen ion/proton
H_2O	Water
H_2O_2	Hydrogen peroxide
H_3PO_4	Phosphoric acid
HBMECs	Human brain microvascular endothelial cells
HCC	Hepatocellular carcinoma
HCl	Hydrochloric acid
Hek293	Human embryonic kidney cells
HRP	Horseradish peroxidase
Hsp70	Heat shock protein 70
Huh7	Epithelial cells of human hepatocellular carcinoma
HUVECs	Human umbilical vein endothelial cells
IAP	Inhibitory apoptosis protein
IC	Inhibitory concentration
IC_{50}	Half maximal inhibitory concentration
IgG	Immunoglobulin G
KCl	Potassium chloride
kDa	Kilodaltons
LDH	Lactate dehydrogenase
L-glu	L-glutamine
LMPA	Low Melting Point Agarose
LOOH	Lipid hydroperoxides
LOX	Lipoxygenases
M	Minute
M	Molar
MDA	Malondialdehyde
Mg	Milligram
MgCl	Magnesium chloride
Ml	Millilitre
mM	Millimolar
Mn	Manganese

MOMP	Mitochondrial outer membrane permeability
mRNA	Messenger ribonucleic acid
MTT	3-(4,5-dimethylthiazol-2-yl)-2,5-diphenyltetrazolium bromide
NaCl	Sodium chloride
Na_2EDTA	Disodium ethylenediaminetetraacetic acid
NADH	Nicotinamide adenine dinucleotide hydrogen
NADPH	Nicotinamide adenine dinucleotide phosphate
$NaNO_3$	Sodium nitrate
NaOH	Sodium hydroxide
NEDD	*N*-(1-naphthyl)ethylenediamine
Ng	Nanogram
NFH_2O	Nuclease free water
NF-κB	Nuclear factor kappa-light-chain-enhancer of activated B-cells
Nm	Nanometer
No	Number
NO	Nitric oxide
NO_2^-	Nitrite
NO_3^-	Nitrate
Nrf-2	Nuclear factor-erythroid 2-related factor 2
NAT	N-transferase
O_2	Molecular oxygen/ Singlet oxygen
O_2^-	Superoxide anion
OD	Optical density
OH^-	Hydroxyl radicals
$ONOO^-$	Peroxynitrite
p53	Protein 53
PARP	Poly (ADP-ribose) polymerase
PBS	Phosphate buffer saline
PCR	Polymerase Chain Reaction
pH	Potential hydrogen
PHS	Phosphatidyl serine
PS	Prostaglandin H synthase

PSF	Penicillin-streptomycin-fungizone
PUFAs	Polyunsaturated fatty acids
qPCR	Quantitative polymerase chain reaction
RBI	Relative band intensity
RFU	Relative fluorescence units
RIP	Receptor-interacting protein
RLU	Relative light units
ROS	Reactive Oxygen Species
RNA	Ribonucleic acid
RNS	Reactive nitrogen species
Rpm	Revolutions per minute
RT	Room temperature
S	Seconds
ss-	Single-stranded
SA	South Africa
SCGE	Single Cell Gel Electrophoresis
SD	Standard deviation
SDS	Sodium dodecyl sulphate
SDS-PAGE	Sodium dodecyl sulphate polyacrylamide gel electrophoresis
SEM	Standard error of the mean
SOD	Superoxide dismutase
SULF	Sulfanilamide
TBA	Thiobarbituric acid
TBARS	Thiobarbituric acid reactive substances
TCA	Tricarboxylic acid
TEMED	Tetremethylethylenediamine
Tris	Trisaminomethane
Tris-HCl	Trisaminomethane hydrochloride
TRAIL	TNF-Related Apoptosis-Inducing Ligand
TRADD	TNF receptor-associated death domain
TNF	Tumor necrosis factor
TNFL	TNF-ligand

TNFR	TNF- receptors
TTBS	Tris-buffer Saline Tween-20
UKZN	University of KwaZulu-Natal
V	Voltage
VCl_3	Vanadium (III) chloride
Zn	Zinc

TABLE OF CONTENTS

LIST OF FIGURES

CHAPTER 2

ABSTRACT

Introduction: Aflatoxin B_1 (AFB_1) is produced by filamentous fungal strains of *Aspergillus flavus* and *Aspergillus parasiticus* that infect field crops, therefore AFB_1 is a frequent contaminant of dietary staples such as rice, maize and peanuts. Humans and animals are exposed to AFB_1 through consumption of contaminated foods, predisposing them to various diseases. AFB_1 is a potent hepatotoxin that has been classified by the International Agency of Research on cancer (IARC) as a group1 carcinogen. The carcinogenic effects of AFB_1 have been attributed to the metabolism of this toxin to an epoxide that promotes the production of free radicals, mitochondrial toxicity and induction of cell death. With the increasing prevalence of kidney associated diseases in humans, and the AFB_1-associated kidney toxicity observed in animals, this study investigated the cytotoxic effects/mechanism of AFB_1 in human embryonic kidney (Hek293) cells.

Methods: Hek293 cells were exposed to AFB_1 (0-100µM) for 24hrs. The effect on cell viability was assessed using the methylthiazol tetrazolium (MTT) assay, which also produced the half maximal inhibitory concentration (IC_{50}) used in subsequent assays. Free radical production was evaluated by quantifying malondialdehyde (MDA) and nitrate concentration, while DNA fragmentation was determined using the single cell gel electrophoresis (SCGE) assay and DNA gel electrophoresis. Damage to cell membranes was ascertained using the lactate dehydrogenase (LDH) assay. The concentration of ATP, reduced glutathione (GSH), necrosis, annexin V and caspase activity was measured by luminometry. Western blotting and quantitative PCR was used to assess the expression of proteins and genes associated with apoptosis and oxidative stress.

Results and discussion: The MTT assay revealed a reduction in cell viability of Hek293 cells as the AFB_1 concentration was increased, with a half maximum inhibitory concentration (IC_{50}) of 32.60 µM. The decreased viability corresponded to decreased ATP concentration. The upregulation of Hsp70 indicated that oxidative stress was induced in the AFB_1-treated cells. While this implies an increased production of free radicals, the accompanying upregulation of the antioxidant system indicates the activation of defense mechanisms to prevent cellular damage. Thus, membrane damage associated with increased radical formation was prevented as indicated by the reduced LDH release and necrosis. In addition, cytotoxic effects were evident as AFB_1 activated the intrinsic pathway of apoptosis with corresponding increased DNA fragmentation, p53 and Bax upregulation and increased caspase activity, but externalisation of phosphatidylserine (PS), a major hallmark of apoptosis, did not occur in AFB_1 treated Hek293 cells.

Conclusion: The results suggest that AFB_1 induced oxidative stress leading to cell death by the intrinsic pathway of apoptosis in Hek293 cells.
Keywords : Aflatoxin B_1 (AFB_1), oxidative stress, apoptosis, Hek293 cells

CHAPTER 1 : INTRODUCTION

1.1 BACKGROUND

Fungi belonging to *Aspergillus, Penicillium* and *Fusarium* genera are frequent contaminants of a variety of agricultural commodities that form part of the South African staple diet (da Rocha *et al.*, 2014, Alshannaq and Yu, 2017, Misihairabgwi *et al.*, 2019). These contaminating fungi produce toxic low molecular weight secondary metabolites (mycotoxins) due to compromised environmental conditions such as high temperatures and increased humidity (Liu and Wang, 2016). Mycotoxins persist in food despite cooking and processing, and consumption of contaminated food commodities can cause diseases and death in humans and animals (da Rocha *et al.*, 2014).

Aflatoxins are mycotoxins that are produced by the filamentous fungi *Aspergillus flavus* and *Aspergillus parasiticus* that are found on peanuts, wheat, corn, beans and rice products (de Oliveira and Corassin, 2014, Alshannaq and Yu, 2017). It is postulated that aflatoxin B_1 (AFB_1) is the most potent member of the aflatoxin family, and has been classified as a group 1 carcinogen by the International Agency for Research on cancer (IARC) (Chen *et al.*, 2016). The carcinogenic effects of AFB_1 are based on its metabolism; AFB_1 is bioactivated to a potent AFB_1-8,9-epoxide by cytochrome P_{450} (CYP), but this can be detoxified by the phase 2 glutathione (GSH) pathway (Kumar *et al.*, 2017, Deng *et al.*, 2018). The AFB_1-8,9-epoxide targets guanine residues of DNA forming adducts that result in well-known mutations associated with adduct formation, most notably the Ras oncogene and p53. The epoxide also forms adducts at lysine residues of proteins, as observed with albumin, the albumin-lysine adduct is used as a biomarker for AFB_1 exposure (Rushing and Selim, 2018).

Aflatoxin B_1 exposure is implicated in hepatocellular carcinoma and increased lung cancer risk. Cytotoxic effects related to these organs have been demonstrated in human hepatocellular carcinoma (HepG2) cells (Liu *et al.*, 2014, Li *et al.*, 2017) and human bronchial epithelial (BEAS-2B) cells (Zhang *et al.*, 2014) . Oxidative stress is one mechanism that may pre-dispose to AFB_1-induced cell injury, because free radical damage to DNA and protein are associated with carcinogenesis. AFB_1 exposure is also linked to aberrant cell death mechanisms especially apoptosis. In addition to its carcinogenic capability, previous studies have reported that AFB_1 is

also mutagenic, genotoxic and immunotoxic to mammals (Kumar *et al.*, 2017). Studies also demonstrate AFB_1 to be nephrotoxic and induce renal damage in rats, and suggests that prolonged exposure has the potential to induce kidney disease (Abdel-Hamid and Firgany, 2015, Kumar *et al.*, 2017, Asa *et al.*, 2018, Yilmaz *et al.*, 2018). However, the biochemical mechanism underlying the mechanism of AFB_1 effects in human kidney has not been elucidated.

Kidney damage in rats is not surprising since the kidney is the principal route for excretion of biotransformed water-soluble metabolites (Pizzorno, 2015). Drugs and metabolites are selectively taken up and concentrated by the renal tubular cells before excretion in the urine, therefore high intracellular concentrations of toxic substances may be retained mainly in the renal medulla (Pizzorno, 2015, Câmara *et al.*, 2017). As a result, direct toxic damage to renal tubules and renal papillae may predispose to kidney disease (Câmara *et al.*, 2017).

Apart from a variety of physiological functions performed by the kidneys, they also possess biotransformation capabilities. The kidneys have been reported to express metabolizing enzymes cytochrome P_{450} (CYP) including CYP2B6 which is involved the metabolism of diverse environmental chemicals (Zanger and Schwab, 2013). In addition, CYP3A4 and CYP3A5 are also expressed in the kidney; it has been reported that CYP3A4 and CYP3A5 are involved in AFB_1 metabolism (Knights *et al.*, 2013, Zanger and Schwab, 2013).

Toxic phase 1 intermediates require conjugation with GSH. The kidneys are reliant on an adequate GSH supply to function normally. This is based on the exposure to high concentrations of oxidants and reactive electrophiles (Pizzorno, 2015). GSH protects against oxidative stress which is essential for mitochondrial and cellular homeostasis and aids in the detoxification of xenobiotics. Detoxification of chemicals involves conjugation with GSH to form GSH adducts that are considered less toxic and can be excreted from cells via the mercapturic acid pathway (Pizzorno, 2015).

1.2 PROBLEM STATEMENT

Wheat and maize are a major part of the diet, and are considered the most staple foods in South Africa (Misihairabgwi *et al.*, 2019). Maize and its products are highly prone to mycotoxin contamination both in the field and in storage. One of the potent mycotoxins elaborated, AFB_1, is

considered the most toxic amongst mycotoxins and has been reported to possess carcinogenic, mutagenic and hepatoxic effects, which confer major health risks to humans and animals. Moreover, it has been linked to the development of hepatocellular carcinoma (Deng *et al.*, 2018) and nephrotoxic effects in rat kidney (Abdel-Hamid and Firgany, 2015, Asa *et al.*, 2018, Yilmaz *et al.*, 2018). Several studies using human cell lines have indicated aberrant apoptosis and oxidative stress as mechanisms for AFB_1-mediated cytotoxicity. Cytotoxicity to human lymphocytes by the induction of apoptosis and necrosis in human lymphocytes has been reported by Al-Hammadi (2014)(Al-Hammadi *et al.*, 2014). Pro-apoptotic activity of AFB_1 was also demonstrated in HepG2 and BEAS-2B cells (Liu *et al.*, 2014, Zhang *et al.*, 2014, Li *et al.*, 2017). AFB_1 has also demonstrated cytotoxicity to human peripheral blood mononuclear cells (PBMCS) by impairment of oxidative status (Bernabucci *et al.*, 2011). The biochemical mechanisms underlying the effects of AFB_1 in kidney cells has not been investigated in humans. Considering the essential role of the kidney as an excretory organ in the body, the effects of AFB_1 in kidney cells requires investigation.

1.3 AIM OF THE STUDY

This study aimed to determine the cytotoxic effects of AFB_1 on human embryonic kidney (Hek293) cells.

1.4 HYPOTHESIS

Null hypothesis: Acute exposure (single dose in 24 hours) to AFB_1 has no effect in Hek293 cells.
Alternate hypothesis: Acute exposure (single dose in 24 hours) to AFB_1 induces oxidative stress and apoptosis in Hek293 cells.

1.5 OBJECTIVES OF THE STUDY

This study was conducted to determine the

- changes in cell viability after administration of various AFB_1 concentrations in Hek293 cells to derive the IC_{50}
- effect of AFB_1 on production of free radicals in Hek293 cells
- antioxidant responses induced by AFB_1 in Hek293 cells
- cell death pathways triggered by AFB_1 in Hek293 cells

CHAPTER 2 : LITERATURE REVIEW

This study investigated the effects of aflatoxin B_1 (AFB_1) on Hek293 cells. The literature review established what is known about the mycotoxin AFB_1 which colonizes various food commodities and is a health concern worldwide. Given the challenges posed by AFB_1 in food toxicology, food security and public health, this chapter covers what has been reported on the effects of AFB_1 on human and animal health. It also establishes the gap in literature, since AFB_1 effects in the human kidney have not been investigated.

2.1 MYCOTOXINS

Mycotoxins are toxic low molecular weight (below 700kDa) secondary metabolites produced by a variety of fungi or mould. There are over 400 different mycotoxins, with new ones still being classified (da Rocha *et al.*, 2014, Yao *et al.*, 2015). The genera *Aspergillus, Fusarium, Penicillium* and *Alternaria* are deemed as the most mycotoxin producing fungi (da Rocha *et al.*, 2014, Carvajal-Moreno, 2015). The synthesis of mycotoxins by these toxigenic species depends extensively on the internal parameters of fungal strains (biochemical, physical and genetic), but also on external factors such as humidity and temperature (Misihairabgwi *et al.*, 2019, Zinedine and El Akhdari, 2019). Therefore, mycotoxins are produced when fungi reach maturity; and their production can occur in the field, before harvest, post-harvest, during processing, packaging, distribution and storage in different grains and agricultural commodities (Liu and Wang, 2016).

The occurrence of mycotoxins in human and animal food is a significant problem adversely affecting food quality in developing countries as well as developed countries (da Rocha *et al.*, 2014, Alshannaq and Yu, 2017). The detrimental effects include a decrease in nutritional value of food and reduced yields in crop and livestock. It has been reported that approximately 25-50% of products produced worldwide, particularly basic foodstuffs are contaminated with mycotoxins (da Rocha *et al.*, 2014, Misihairabgwi *et al.*, 2019). Most mycotoxins are not affected by food processing; for example cooking and they can be converted to toxic intermediates by metabolism in humans and animals (Alshannaq and Yu, 2017). In addition, the metabolism of mycotoxins to their toxic form can potentially pose risks to human health, resulting in disease and death in mammals.

Exposure to mycotoxins occurs when fungal infected crops are directly consumed by livestock, for example wheat, corn, oats and sorghum (Alshannaq and Yu, 2017). However, indirect contamination may occur when the toxigenic fungus has been eradicated during processing, but the mycotoxins remain in the final product. The main route of exposure to mycotoxins in humans is through the ingestion of contaminated plant and animal products, including food derived from these products such as cheese, milk and meat (Figure 2.1) (da Rocha *et al.*, 2014, Alshannaq and Yu, 2017). However, inhalation and dermal contact may also be important routes of exposure. Direct effects of mycotoxins range from acute disease where exposure to the toxin may result in severe health conditions prior to death, these conditions are expected after exposure to high levels of mycotoxin (da Rocha *et al.*, 2014, Alshannaq and Yu, 2017, Zinedine and El Akhdari, 2019). Chronic disease manifestations may result from prolonged exposure to small quantities of the toxin. The diseases resulting from mycotoxin exposure are known as mycotoxicosis. Mycotoxicosis usually remain unrecognized except when large numbers of people are affected with no apparent connection to a known aetiological agent (Alshannaq and Yu, 2017, Zinedine and El Akhdari, 2019).

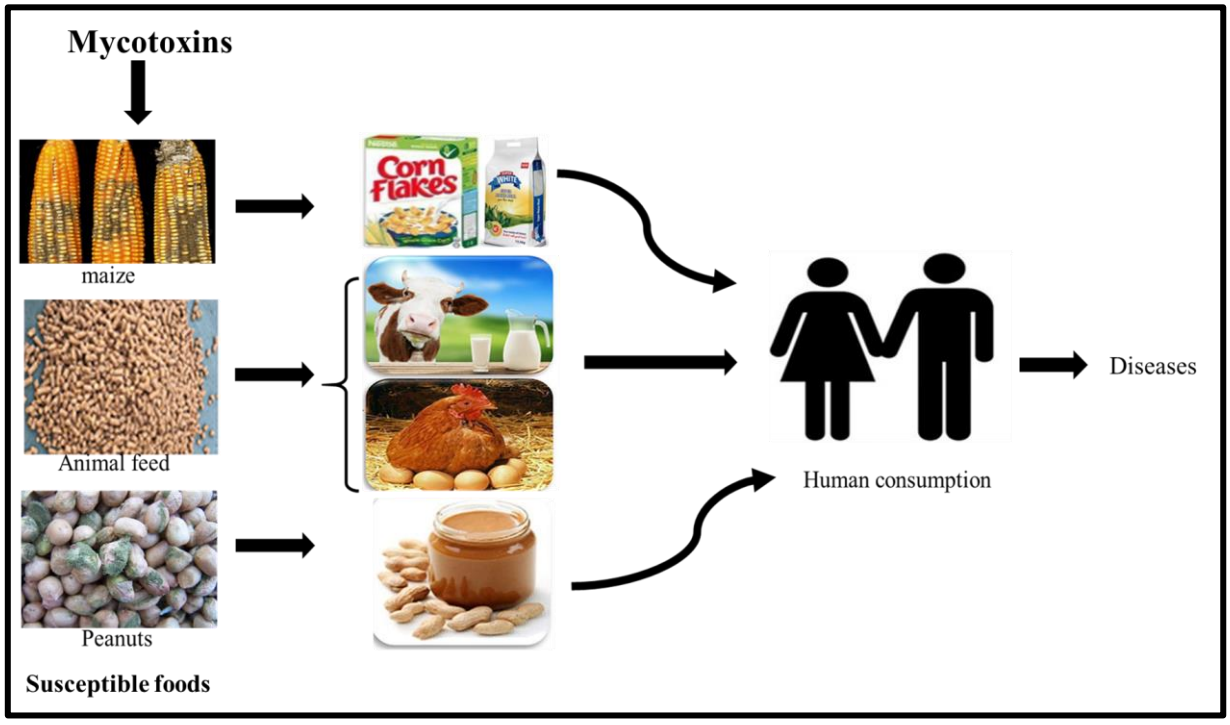

Figure 2.1 : The main route of exposure to mycotoxins humans and animals (Prepared by author).

‘Turkey-X disease’ marked a breakthrough in the association of mycotoxin-contamination with disease in animals. The plague occurred in the early 1960’s, and was marked by the death of turkey poults in England after consumption of a peanut meal that originated from Brazil and Africa (Alshannaq and Yu, 2017). The secondary metabolite responsible for the death of the birds was produced by *Aspergillus flavus* and studies of these toxins ensued. The genus *Aspergillus*, first described in 1729 by Pier Antino Micheli, is more common in warmer tropical and subtropical areas than in moderate areas of the world. *Aspergillus* species are filamentous saprophytic fungi that can produce active compounds like aflatoxins, penicillic acid, ochratoxins, citrinin, sterigmatocystin and other important metabolites (Yao *et al.*, 2015, Misihairabgwi *et al.*, 2019).

2.2 AFLATOXINS

Aflatoxins (AFs) are a class of structurally related toxic metabolites produced by the fungal strains *Aspergillus flavus* and *Aspergillus parasiticus* that are normally found in soil and organic materials (Kumar *et al.*, 2017). There are approximately 20 known aflatoxins that are frequently found as contaminants in maize grains, cereals, peanuts, rice and oil seeds (de Oliveira and Corassin, 2014). There are favourable conditions for aflatoxin production, these include high moisture during harvest, dry weather near crop maturity and insufficient drying and storage of crops (Figure 2.2). Post harvesting conditions such as storage (long periods of storage, excess heat and moisture, pest related damage) and food processing also influences the production of aflatoxins (Figure 2.2). The identification of aflatoxins was linked to the discovery that a ground nut contaminated with *Aspergillus flavus* lead to a turkey disease that killed approximately 100 000 turkey poultry birds in England (da Rocha *et al.*, 2014, Yao *et al.*, 2015). Aflatoxins therefore pose a threat to human and animal health, their toxicity can result in kidney and liver damage, cause carcinogenic, mutagenic and immunosuppressive effects (Carvajal-Moreno, 2015).

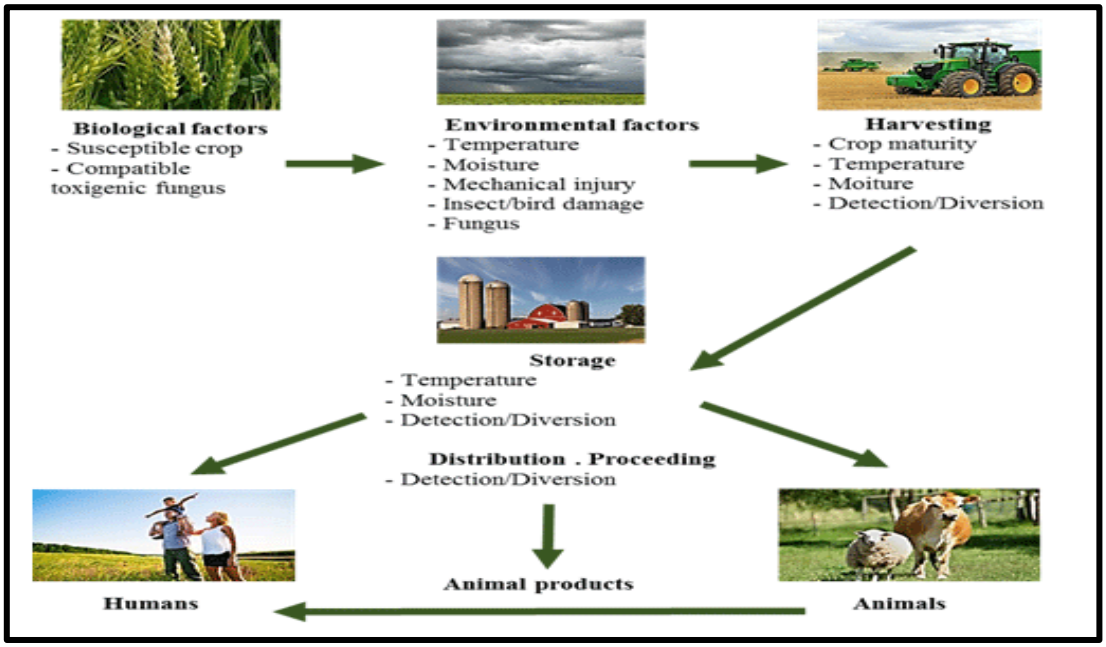

Figure 2.2 : The factors influencing aflatoxin production and occurrence in the food chain. Adapted from (Fernandes *et al.*, 2017).

2.2.1 Physical and chemical properties of aflatoxins

Aflatoxins are colourless to pale yellow crystalline solids with low molecular weight and display fluorescence under UV light. Aflatoxins are unstable under UV light in the presence of oxygen and extreme pH levels (<3 or >10). Under alkaline conditions the lactone ring opens and aflatoxins are destroyed, but this is a reversible reaction upon acidification (Kumar, 2018). Ammoniation causes irreversible opening of the lactone ring at high temperatures and pressure resulting in decarboxylation of aflatoxins (Kumar, 2018). Aflatoxins have high decomposition temperatures ranging from 237˚C to 320˚C; this makes them stable at temperatures present when cooking or boiling food, milk and alcoholic fermentation (Bbosa *et al.*, 2013c) and their destruction is not easily achieved. They are slightly soluble in water and easily soluble in moderately polar solvents such as methanol, chloroform and dimethyl sulfoxide (de Oliveira and Corassin, 2014, Kumar, 2018). Due to the lipid solubility, aflatoxins are readily absorbed from the site of exposure, across the cell membranes into the blood stream. They are then distributed to various tissues or organs especially the liver where they are biotransformed (Kumar, 2018).

2.2.2 Types of aflatoxins

Of the approximately 20 known aflatoxins, only aflatoxin B_1 (AFB_1), AFB_2, AFG_1, AFG_2, AFM_1 and AFM_2 (Figure 2.3) are usually found in foods. The B and G denotes the blue and green fluorescent colours produced under ultraviolet light, while the subscript numbers 1 and 2 indicate the major and minor compounds respectively (Deng *et al.*, 2018, Kumar, 2018). Less toxic oxidative metabolites of aflatoxin produced by farm animals after ingestion of contaminated feed include AFM_1, AFM_2, AFG_1 and AFG_2 (Figure 2.3). Even though the metabolites are less toxic than the parent compound, AFM_1 in dairy milk can cause liver illness in humans especially among infants and children (Kumar, 2018). The toxicity of aflatoxins decreases in the order $B_1>G_1>B_2>G_2$.

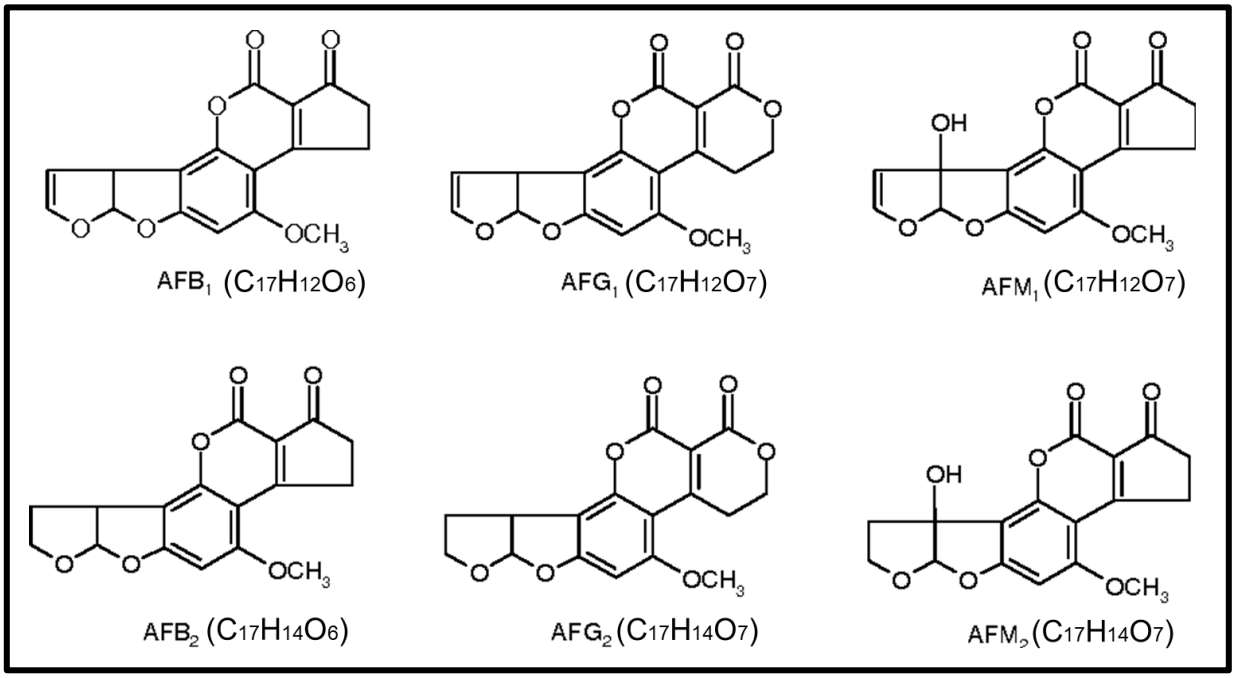

Figure 2.3 : Different types of aflatoxins, AFB_1 (Mw=312.27g/mol), AFB_2 (Mw=314.29g/mol), AFG_1 (Mw=328.276g/mol), AFM_1 (Mw=328.276g/mol) AFG_2 (Mw=330.29g/mol), AFM_2 (Mw=330.29 g/mol) (Musleh *et al.*, 2017).

2.3 AFLATOXIN B_1

Aflatoxin B_1 (AFB_1) is found as a contaminant in peanuts and grains such as maize, sorghum and rice. It is the most potent of the aflatoxin family and has been reported to have mutagenic, hepatocarcinogenic, teratogenic and genotoxic abilities, it causes immunosuppression in animals and can influence how cells are produced in the body (Liu and Wang, 2016). It has been classified

as a group 1 carcinogen in humans by the WHO-international agency for research on cancer (Al-Ouqaili, 2018). Although AFB_1 mainly targets the liver, it also affects other organs and tissue, including lungs and kidney.

2.3.1 Structure

Aflatoxin B_1 ($C_{17}H_{12}O_6$) has a difuro-coumaro-cyclopentenone structure fused with a lactone ring of the coumarin structure with oxygen (O_2) at positions 1, 4 and 11 (Marchese *et al.*, 2018). The difuro terminus of this compound has a 2,3 double bond which is essential for the carcinogenicity of this toxin (Figure 2.4). On condition that the bond is single, the carcinogenic properties of AFB_1 are lost but toxicity is still retained (Kumar, 2018, Marchese *et al.*, 2018).

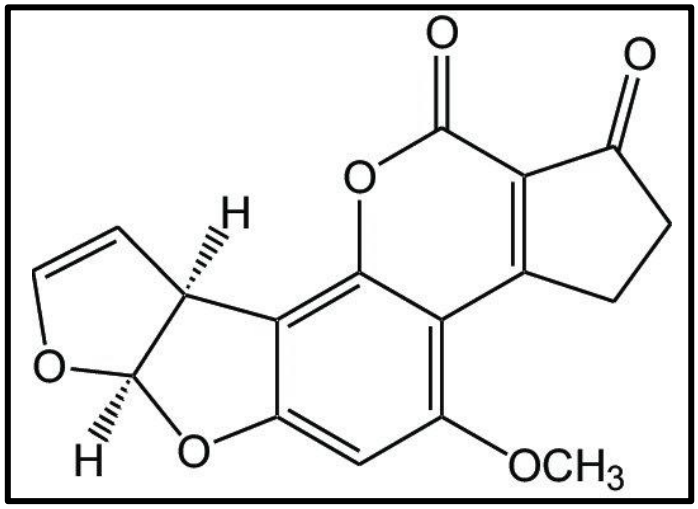

Figure 2.4 : The chemical structure of aflatoxin B_1 ($C_{17}H_{12}O_6$) (Hedström and Mattiasson, 2015).

2.3.2 Metabolism

2.3.2.1 The cytochrome P450 (CYP) enzyme system

Cytochrome P_{450} (CYP) enzymes are so named because they are bound to membranes within a cell (cyto) and comprise of a haem pigment (chrome and P) that absorbs light at a wavelength of 450nm when exposed to carbon monoxide (Guengerich, 2015). Each CYP gene is assigned a number that relates it to a specific group, a letter that represents the gene's subgroup and a number given to the specific gene within the group (Guengerich, 2015). For example, the cytochrome P_{450} gene found in group 3, subgroup A and gene 1 will be written as CYP3A1. There are about 60 CYP genes in

humans (Raunio *et al.*, 2015). The CYP family play a role in the synthesis and metabolism of numerous endogenous molecules and chemicals including cholesterol, steroid hormones and bile acids. They also break down xenobiotics like ingested medication and toxins found within cells (Knights *et al.*, 2013, Raunio *et al.*, 2015).

2.3.2.2 Metabolism of AFB_1

The bioactivation and detoxification of AFB_1 in the body requires the activity of metabolizing enzymes (Figure 2.3). The CYP family is responsible for AFB_1 bioactivation in the liver and lipoxygenases (LOX) and prostaglandin H synthase (PHS) are necessary for its biotransformation in the lung (Bbosa *et al.*, 2013c, Deng *et al.*, 2018). In poultry species the CYP2A6, CYP3A37, CYP1A1 and CYP1A5 are responsible for AFB_1 bioactivation. Human CYP1A2 and CYP3A4 in the liver and CYP3A5 and CYP2B6 in the kidney play a role in the activation of AFB_1 to a reactive toxic metabolite, aflatoxin B_1-8,9-epoxide (AFBO) which facilitates its carcinogenic and cytotoxic effects (Knights *et al.*, 2013, Liu and Wang, 2016).

The conjugation of AFBO with GSH is a major route of detoxification leading to the excretion of the epoxide (Figure 2.5). Conjugation with GSH disrupts AFBO ability to bind to DNA and proteins forming an inert metabolite that is then converted to a mercapturic acid adduct through a series of enzymatic reactions including γ-glutamyl transpeptidase (GGT), dipeptidase (PEP) and N-acetyltransferase (NAT) and then can be excreted in urine (Rushing and Selim, 2018). This is an important pathway of for detoxification of AFB_1 as a carcinogen even though depletion of GSH results in high levels of reactive oxygen species (ROS) causing oxidative damage (Marchese *et al.*, 2018, Rushing and Selim, 2018).

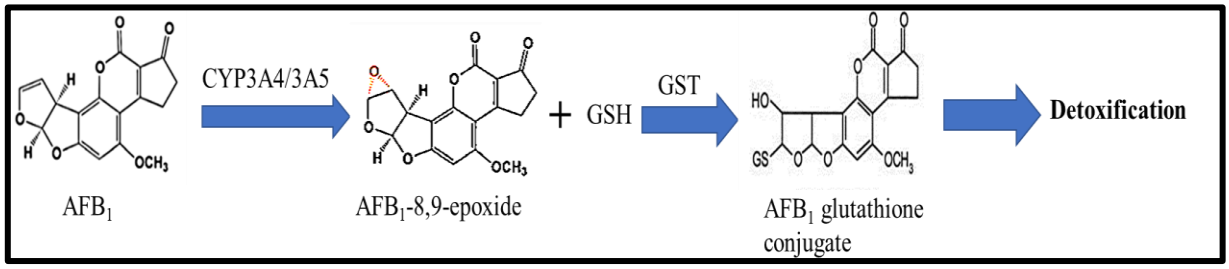

Figure 2.5 : The biotransformation of AFB_1 by enzymes CYP3A4/3A5 to form a reactive AFB_1-8,9-epoxide with a functional group denoted in red. The epoxide can conjugate with GSH in a reaction catalysed by the enzyme glutathione-S-transferase (GST) for protective effects forming an AFB_1 glutathione conjugate that can be detoxified thus minimizing the toxicity of AFB_1 (Stewart *et al.*, 1999).

2.3.3 Biochemical effects of AFBO

2.3.3.1 DNA

The detrimental effects of AFB_1 have been attributed to the metabolism of this toxin. The reactive metabolite AFBO reacts with the N7 atom of guanine and forms a pro-mutagenic DNA adduct aflatoxin-N7-guanine which can cause gene mutations resulting in damage to DNA (Figure 2.6) (Bbosa *et al.*, 2013c).The most common mutation found in human hepatocytes exposed to AFB_1 is a G-T transversion on codon 249 of the p53 gene. The tumour suppressor protein p53 regulates various cellular functions including DNA repair, cell cycle progression and apoptosis (Marchese *et al.*, 2018, Rushing and Selim, 2018). Many cancers including hepatocellular carcinoma (HCC) possess mutations in p53 which is thought to alter the tumour suppressive functions of p53 leading to formation of cancerous cells (Marchese *et al.*, 2018). Epidemiological studies in humans in aflatoxin risk regions have revealed a positive correlation between p53 mutations and aflatoxin presence in HCC patients, giving strong evidence that AFB_1 exposure results in HCC development in humans by mutating p53 (Szymańska *et al.*, 2004, Kirk *et al.*, 2005, Rushing and Selim, 2018). In addition, it has been reported that AFBO exerts an inhibitory effect on the biological processes including DNA synthesis, DNA repair, DNA-dependent RNA synthesis and protein synthesis (Deng *et al.*, 2018, Marchese *et al.*, 2018).

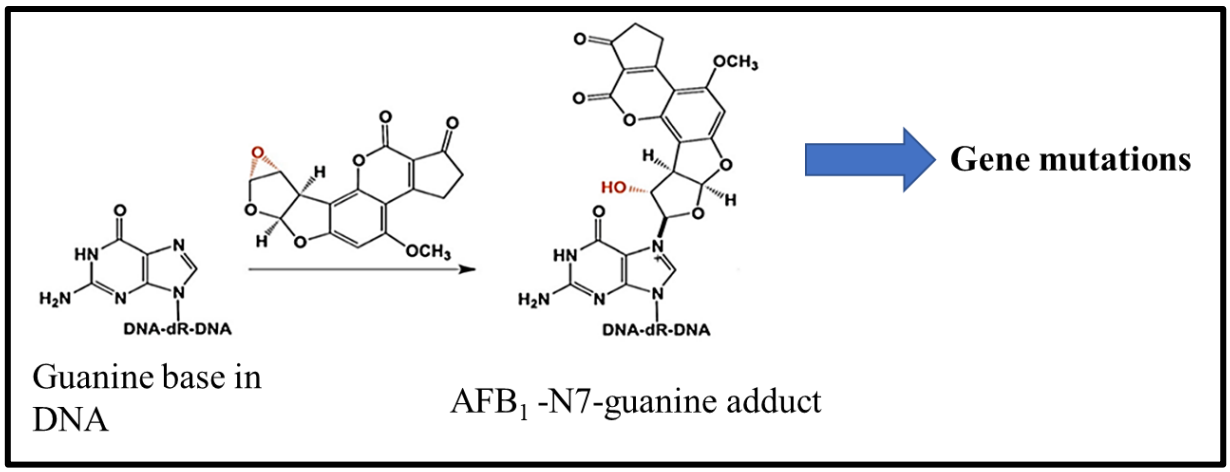

Figure 2.6 : The reactive metabolite AFBO can react with guanine bases at the N7 atom in DNA to form the AFB_1-N7-dG adduct that can potentially cause gene mutations resulting in DNA damage and can be the onset of many diseases (Stewart *et al.*, 1999).

2.3.3.2 Proteins

The reactive metabolite AFBO has a highly unstable nature, which can cause the metabolite to spontaneously hydrolyse before binding to any macromolecules resulting in the formation of AFB_1-dihydrodiol which is in equilibrium with an open ring aldehyde called AFB_1 aldehyde (Figure 2.7) (Roebuck *et al.*, 2009, Bbosa *et al.*, 2013c, Rushing and Selim, 2018). The AFB_1 aldehyde can form Schiff base derived adducts in cellular proteins by covalently binding to the N-termini and lysine side chains forming AFB_1 lysine adducts (AFB_1-lys) and these proteins adducts have been implicated in AFB_1 acute toxicity (Figure 2.7) (Roebuck *et al.*, 2009, Rushing and Selim, 2018). The AFB_1 aldehyde can undergo further metabolism by aflatoxin aldehyde reductase (AFAR) into AFB_1 dialcohol eliminating its protein binding potential (Figure 2.7). Protein binding of AFBO and AFB_1 aldehyde usually occurs on serum albumin, which has a half of approximately 20 days making it a reliable biomarker of AFB_1 exposure (Rushing and Selim, 2018).

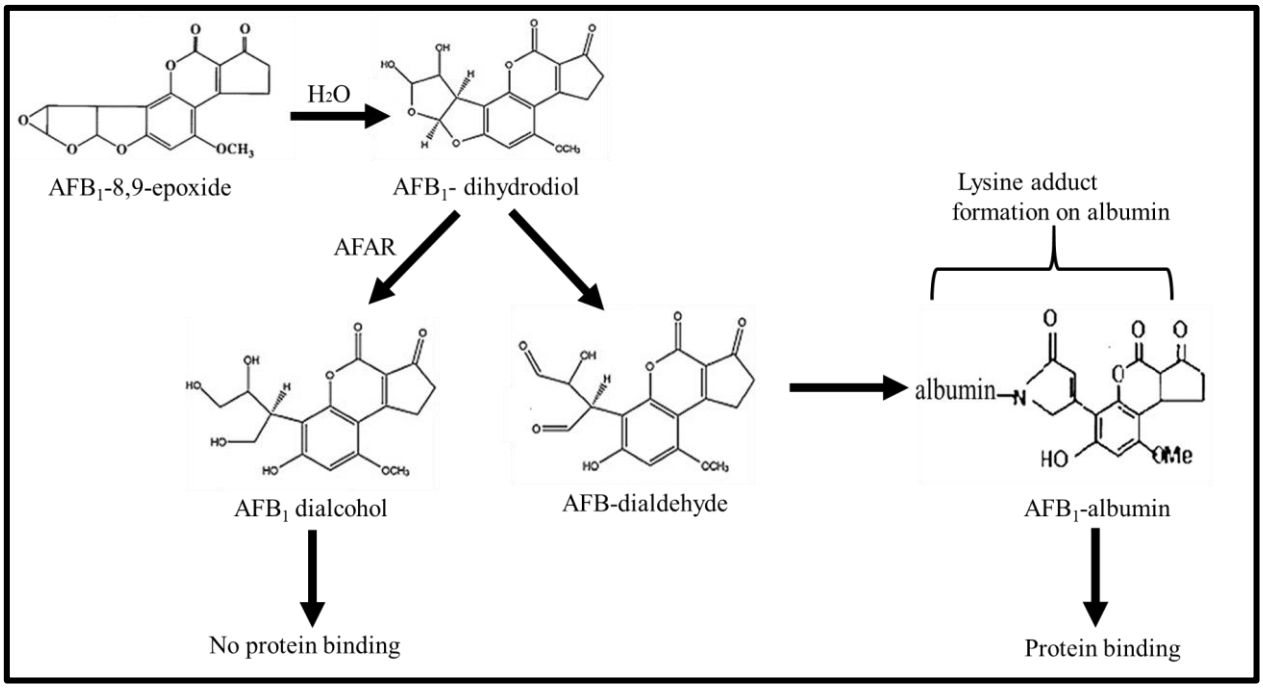

Figure 2.7 : The mechanism by which the AFB_1 epoxide enhances its biochemical effects on proteins by binding to lysine residues resulting in adduct formation, hence protein binding. The reduction enzymatic activity of aflatoxin-aldehyde reductase (AFAR) reducing AFB_1- diahydrodiol to AFB_1-dialcohol limits binding of the epoxide to proteins reducing it effects (Prepared by author).

2.3.3.3 Lipids

The accumulation of aflatoxins and its metabolites have been reported to induce lipid peroxidation in cells resulting in cell membrane damage (Bbosa *et al.*, 2013c). Lipid peroxidation is described

as a process in which oxidants such as free radicals attack lipids comprising of carbon-carbon double bond(s) especially polyunsaturated fatty acids (PUFAs) (Ayala *et al.*, 2014). This process involves the abstraction of hydrogen from a carbon with an insertion of oxygen resulting in lipid peroxyl radicals and hydroperoxides (Figure 2.8). In response to lipid peroxidation cells may promote survival or induce cell death. Under minimal lipid peroxidation rates cells, stimulate an antioxidant response for their maintenance and survival whereas at high lipid peroxidation rates the extent of oxidative damage overwhelms the cells repair capacity and cells may activate cell death signalling pathways (Ayala *et al.*, 2014). Lipid peroxidation can result in the formation of many oxidation products including malondialdehyde (MDA), lipid hydroperoxides (LOOH), propanal and 4-hydroxynonenal (4-HNE) (Ayala *et al.*, 2014).

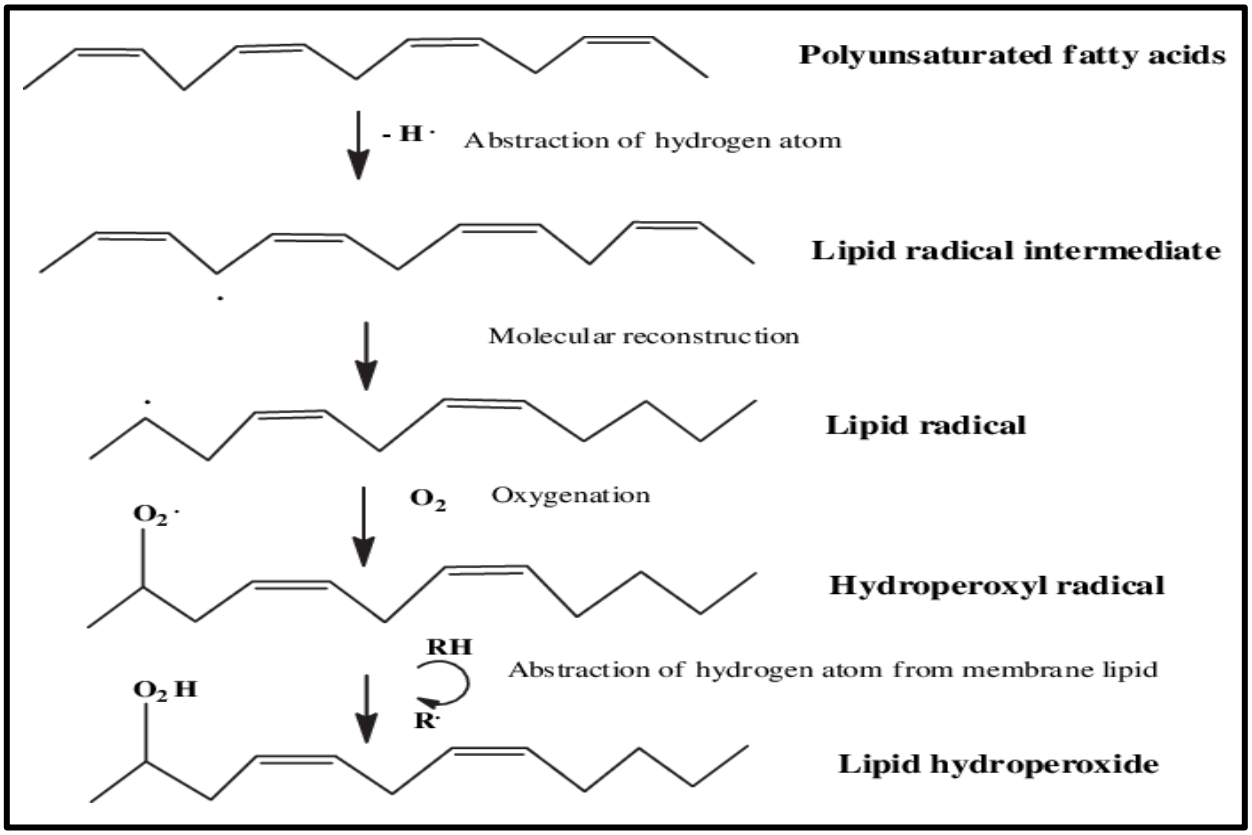

Figure 2.8 : The peroxidation of lipids in cells adapted from (Basu, 2007).

The accumulation of the AFBO metabolite depletes glutathione, an antioxidant which is used as part of the detoxification process. The depletion of GSH leads to the accumulation of abnormally high concentration of free radicals in cells, thus affecting cell membrane integrity (Bbosa *et al.*,

2013b, Rushing and Selim, 2018). Deficiency in GSH also enhances damage to essential cellular macromolecules including DNA and proteins (Bbosa *et al.*, 2013b, Rushing and Selim, 2018).

2.4 OXIDATIVE STRESS

Humans and animals require energy to survive. The production of this energy is dependent on mitochondria which utilise the oxygen (O_2) breathed in to produce energy in the form of ATP. To facilitate this activity, mitochondria have an electron transport chain (ETC) that passes electrons through a series of complexes, generating a hydrogen gradient that culminates in the reduction of O_2 to ATP and water (Yong *et al.*, 2019). This activity can result in the production of highly reactive metabolites known as free radicals within cells. Free radical production can induce oxidative stress when there is an imbalance between the production of reactive oxygen species (ROS) and the biological ability of antioxidants to clear the toxicity of the reactive metabolites (Di Meo *et al.*, 2016). This imbalance has been considered as an important molecular mechanism underlying cell injury that can result in irreparable oxidative injury and even cell death when it gets beyond control.

2.4.1 Production of free radicals

Studies have reported that there are two sources of ROS production; the endogenous such as oxygen leakage from the mitochondria during oxidative phosphorylation and exogenous including xenobiotics, chlorinated compounds, pathogens and inflammatory cytokines. The major endogenous ROS in living cells is the superoxide anion radical (O_2^-). Other ROS derived from the metabolism of molecular oxygen include singlet oxygen (O_2), hydrogen peroxide (H_2O_2), peroxynitrite ($ONOO^-$) and the highly reactive hydroxyl radical ($^{\cdot}OH$) (Figure 2.9) (Ling and Kuo, 2018). Deleterious effects of oxygen result from its metabolic reduction to these highly reactive and toxic species.

Reactive oxygen species are not always harmful metabolic by-products; they normally exist in all aerobic cells as mediators in many biological processes (Liu and Wang, 2016). When tightly regulated they can act as intracellular signalling molecules, but a critical imbalance resulting from excess ROS production, antioxidant depletion or both can result in oxidative stress (Liu and Wang, 2016).

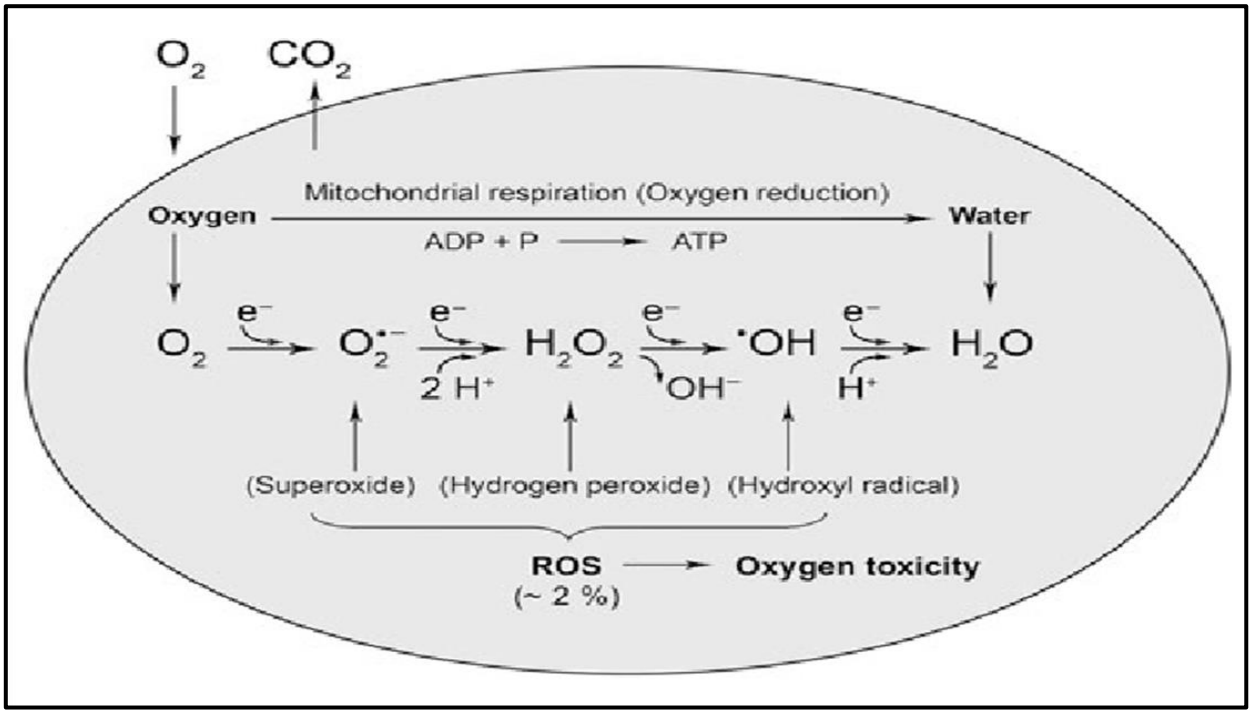

Figure 2.9 : The production of ROS as a consequence of mitochondrial respiration (Kutschera and Niklas, 2013).

2.4.2 Antioxidant response

Redox balance is required in cells, therefore an antioxidant defence system consisting of antioxidant enzymes is provided. The expression of antioxidant enzymes such as superoxide dismutase (SOD), catalase, and glutathione peroxidase (GPx) is tightly controlled by antioxidant response elements (AREs) and activated nuclear related factor-2 (Nrf-2), which is a redox sensitive transcription factor (Liu and Wang, 2016). The Nrf-2 promotes the induction of target genes such as glutathione-S-transferases (GST), glutathione reductases (GR) and GPx that are responsible for cell survival. When cells are subjected to ROS, Nrf-2 is activated as an adaptive response to protect cells from impending oxidative stress; it translocates to the nucleus where it transactivates genes that encode different antioxidant enzymes, which act to maintain cell homeostasis (Liu and Wang, 2016).

Superoxides are scavenged by SOD in a dismutation reaction that converts O_2^- to H_2O_2 and O_2 (Figure 2.9, 2.10). Superoxide anions can also react with nitric oxide (NO) to produce $ONOO^-$, the instigator of nitrosative stress (Figure 2.10). Hydrogen peroxide may be converted into water by the enzymes catalase or GPx and inductive changes or variability in the expression of these

enzymes can influence cellular redox potential (Figure 2.10) (Ling and Kuo, 2018). However, Nrf-2 activation by ROS limits the capacity of cells to escape from injury because they also stimulate cell death signals leading to the execution of apoptosis (Liu and Wang, 2016).

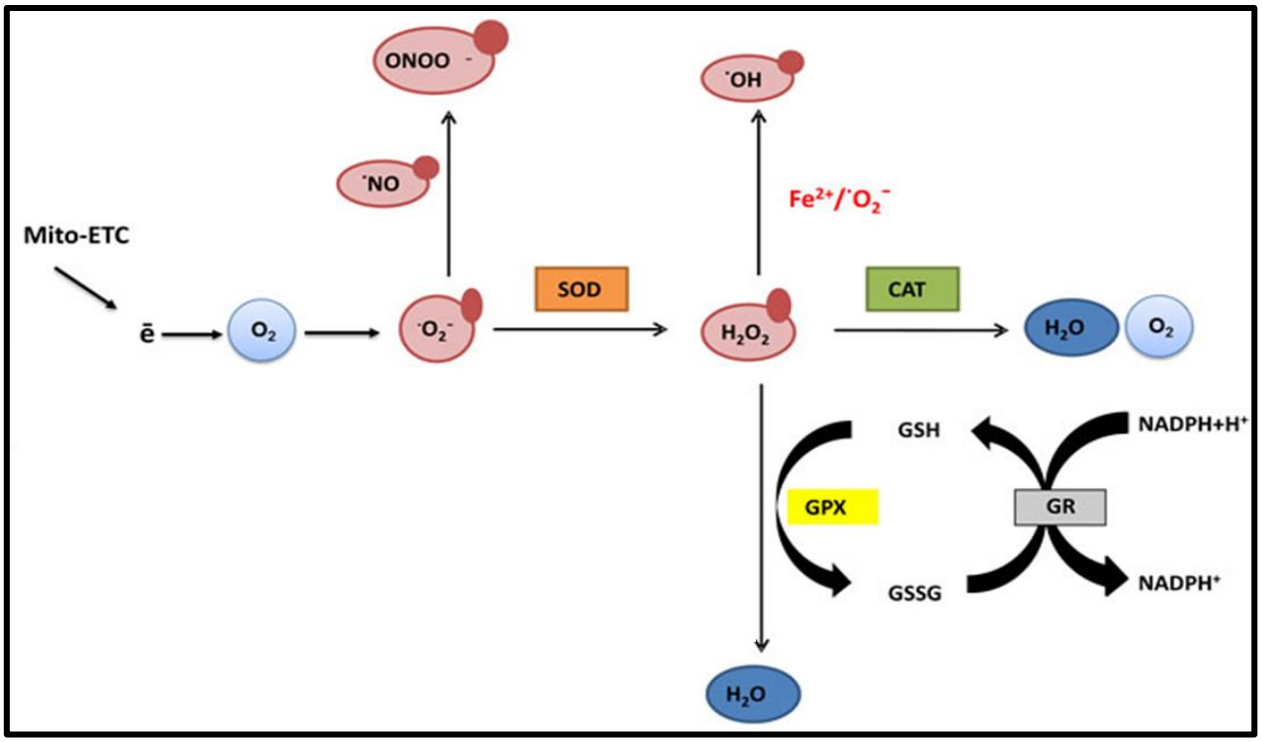

Figure 2.10 : The scavenging and protective effects of antioxidants against ROS (Sznarkowska *et al.*, 2017)

It has been reported that CYP is a key enzymatic complex in the mitochondria associated with electron leakage, which is one of the important sources of intracellular ROS generation, thus implicating CYP enzymes in the production of ROS. Therefore, bioactivation of AFB_1 by the CYP enzymes results in an increase in ROS production and the generated reactive species can result in lipid peroxidation of membranes and oxidative modification of proteins and DNA (Liu and Wang, 2016). In addition, the accumulation of AFB_1 and its metabolites in the body especially the AFBO depletes the GSH which is an important antioxidant that prevents cellular damage caused by ROS (Carvajal-Moreno, 2015). The depletion of GSH is therefore due to the formation of high amounts of epoxides and ROS in the body resulting in oxidative stress. The expression of GSH could increase protection against AFB_1-induced hepatocarcinogenesis (Liu and Wang, 2016).

Excessive ROS can attack lipids, protein and DNA, and induce oxidative injury that inactivates biological activity of these important cellular macromolecules (Di Meo *et al.*, 2016, Elwahab, 2017). The increase in ROS also reduces the cleaning ability of antioxidants such as SOD, GPx, glutathione reductase (GR) and non-enzymatic antioxidants like GSH resulting in oxidative stress (Elwahab, 2017).

2.5 MECHANISMS OF CELL DEATH

2.5.1 Apoptosis

Apoptosis is a form of programmed cell death that occurs in multicellular organisms in balance with cell division. It is a highly regulated process that serves to eliminate unwanted /unnecessary cells. Apoptosis is carried out by a family of protease enzymes called caspases (cysteine aspartyl-specific proteases) which cleave target proteins; their activity is essential for successful apoptosis (Pfeffer and Singh, 2018). Apoptosis occurs in two main pathways, viz. the intrinsic or mitochondrial pathway, and the extrinsic or death receptor pathway (Figure 2.6). These pathways are linked and the molecules used in one pathway can influence the other (Li *et al.*, 2018).

The extrinsic pathway of apoptosis occurs when a death signal binds to a death receptor; the known death receptors are TNF receptor (TNFR1) and a related protein called Fas (CD95), and their ligands are TNF ligand (TNFL) and Fas ligand (FasL) respectively (Figure 2.11). The death receptors contain intracellular death domains that recruit adaptor proteins, a TNF associated death domain (TRADD) and a Fas-associated death domain (FADD), as well as a cysteine aspartate protease like caspase 8. Binding of the ligand to the death receptor results in the activation of death domains and recruitment of adaptor proteins forming a death inducing signalling index (DISC) complex (Liu and Wang, 2016). The DISC complex initiates the activation of pro-caspase 8 to caspase 8, an initiator caspase that initiates apoptosis by cleaving other downstream executioner caspases (Figure 2.11) (Pfeffer and Singh, 2018).

The intrinsic pathway results when a signal received from signalling molecules such as ataxia telangiectasia mutated (ATM) and check point kinase (CHK) activate the p53 gene. p53 recruits proteins such as Bax/Bak to increase mitochondrial permeability by forming pores that allow the release of pro-apoptotic molecules including cytochrome c into the cytosol (Pfeffer and Singh, 2018). The intrinsic pathway can also be initiated by caspase 8 when it cleaves Bid to t-Bid, thus

facilitating Bax activation (Figure 2.11). Cytochrome c binds to Apaf-1 in the cytosol and forms a wheel-like heptamer that contains caspase activation and recruitment domains (CARDs); pro-caspase 9 binds its respective CARD domain and becomes activated into caspase 9 (Figure 2.11).

Caspase 8 and caspase 9 are both able to cleave and activate pro-caspase 3 to caspase 3, an effector caspase (Figure 2.11). Caspase 3 directs the changes cell morphology that are hallmarks of apoptosis, including cell shrinkage, membrane blebbing, DNA fragmentation and condensation, and formation of apoptotic bodies that are removed by phagocytes (Pfeffer and Singh, 2018).

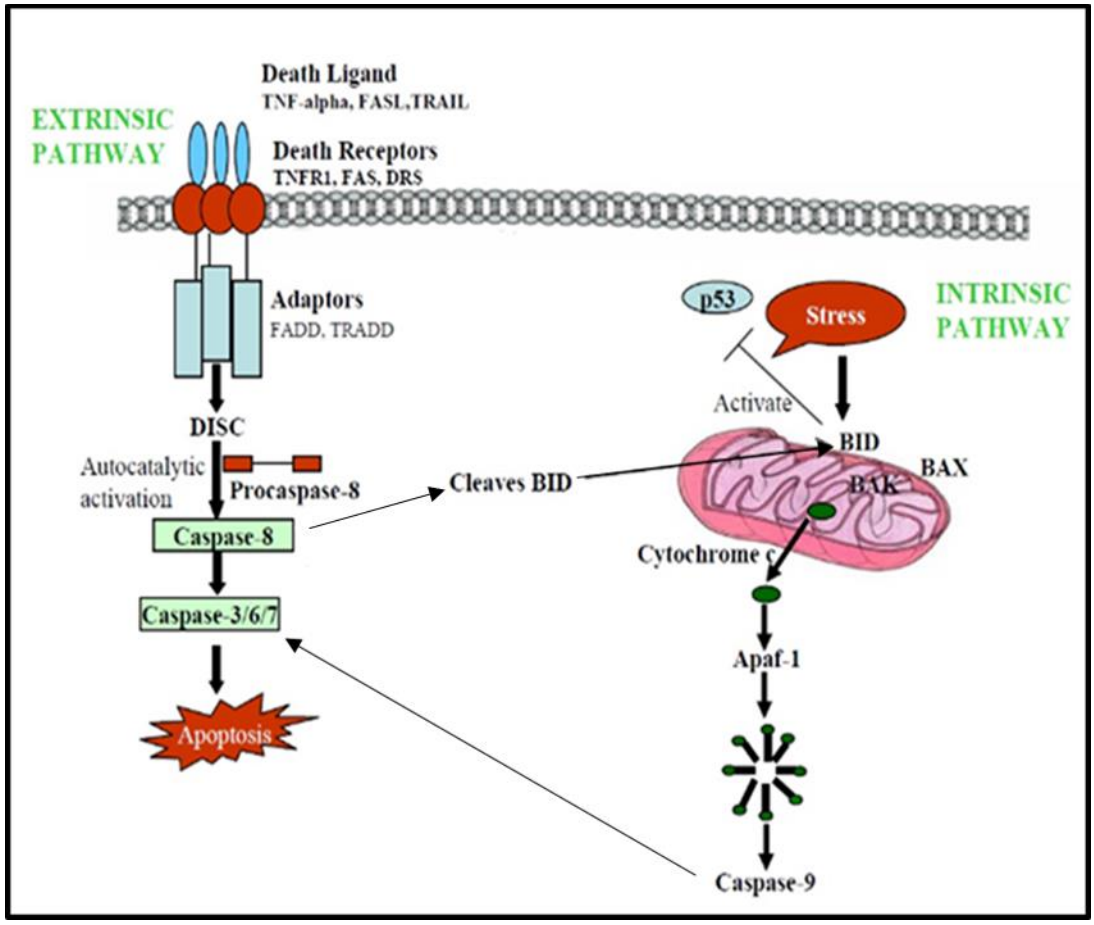

Figure 2.11 : The intrinsic and extrinsic pathways of apoptosis (Rampal *et al.*, 2012)

Apoptosis is a self-managed operation that kills damaged cells and maintains minimal damage to surrounding tissues. Defective apoptotic processes have been reported in various diseases and it

has been reported that AFB_1 was able to induce apoptosis in hepatocytes, bone marrow, lung cells or human bronchial epithelial cells (Chen *et al.*, 2016).

2.5.2 Necrosis

Necrosis is a form of cell death that is considered accidental, unprogrammed or due to cell injury and occurs when ATP is depleted (Jog and Caricchio, 2014). This form of cell death results from different stimuli such as cellular stress, heat, osmotic shock, high concentrations of H_2O_2 and toxin exposure that initiate changes at the cellular level. Under pathological conditions an increase in ROS produced by the mitochondria can induce damage in biomolecules which can lead cells towards necrosis.

The morphological characteristics of necrosis include swelling of the cell membrane, chromatin condensation and irregular DNA degradation (Figure 2.12) (Escobar *et al.*, 2015). The increased cellular swelling results in the breakdown of plasma membranes which releases cytoplasmic contents into the extracellular space (Figure 2.12). The necrotic process occurs in the absence of phagocytosis and its final stage is mainly characterized by the loss of cell membrane integrity (Escobar *et al.*, 2015).

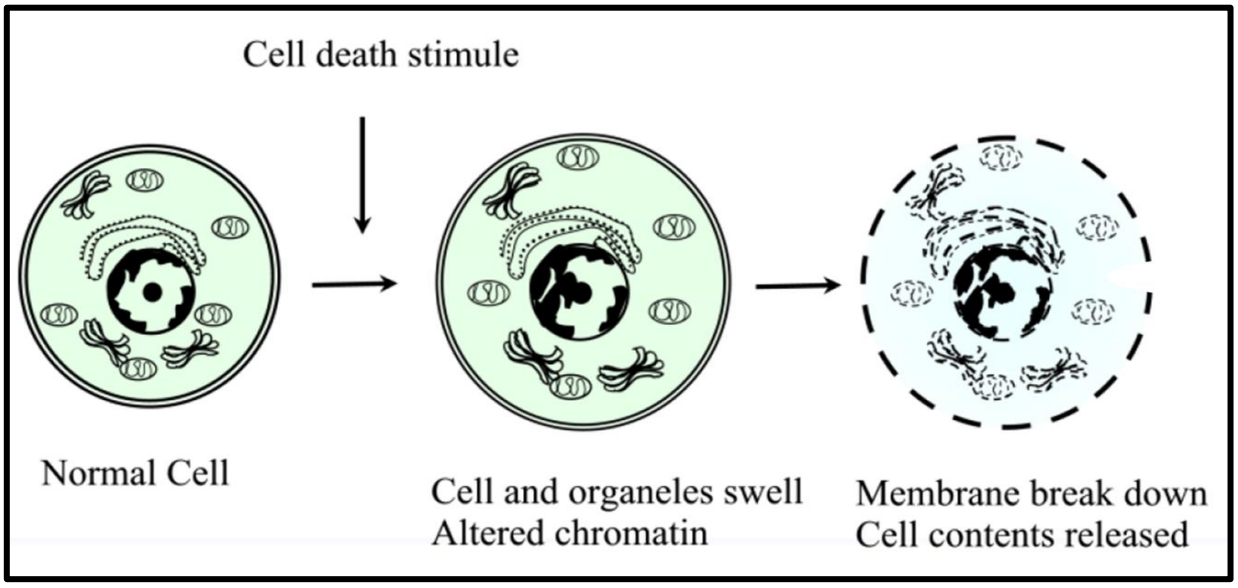

Figure 2.12 : The morphological characteristics of necrotic cell death (Escobar *et al.*, 2015).

2.6 EFFECTS OF AFB_1

2.6.1 Multiple organs and cell lines

Aflatoxin B_1 (AFB_1) has reported to affect several body organs including the liver, brain, heart skeletal muscle and different body systems. AFB_1 exposure is associated with enlargement of the liver, congestion of the liver parenchyma, necrosis of hepatocytes and liver cancer (Hussain *et al.*, 2008). It has also been reported that AFB_1 induced a decrease in protein content in the liver, heart, and skeletal muscle in animals due to its ability to inhibit metabolic systems such as protein synthesis thus leading to liver and heart damage (Wangikar *et al.*, 2005). People working in food industries get exposed to AFB_1 when they inhale contaminated dust during processing; this may lead to lung cancer (Van Vleet *et al.*, 2002, Zhang *et al.*, 2014). Studies with experimental animals have demonstrated that AFB_1 induces pulmonary adenomas and tumours in both the peripheral and central nervous system (Coulombe Jr, 1994). AFB_1 is also known to alter neurotransmitters and their precursors in mouse brains (Coulombe Jr, 1994).

It has been reported that the consumption of AFB_1 diets induced an increase in MDA levels and a reduction in GSH levels resulting in oxidative stress in the spleen of broilers, and that excessive apoptosis in splenic lymphocytes correlated with an increase in oxidative stress (Chen *et al.*, 2016), Furthermore, (Yilmaz *et al.*, 2018) also showed that AFB_1 significantly decreased antioxidant activity such as glutathione peroxidase (GPx), GSH, catalases, superoxide dismutase (SOD) and glucose-6-phosphate dehydrogenase (G6PD) in the heart and kidney tissues of AFB_1-treated rats which can lead to cardiac and renal damage (Yilmaz *et al.*, 2018). In a comparative study, (Qureshi *et al.*, 2015) revealed that AFB_1 affected cell viability of human umbilical vein endothelial cells (HUVEC), human brain microvascular endothelial cells (HBMEC) as well as immortalized epithelial cells of human hepatocellular carcinoma (Huh7). It was also observed that at high AFB_1 concentrations, an 85% cell death rate was induced in HBMEC and only 22% in HUVEC, while no cell death was observed in Huh7. It was further revealed that low concentrations of AFB_1 induced DNA adduct formation in HBMECs, while no adduct formation was observed at low and high AFB_1 concentrations in HUVECs (Qureshi *et al.*, 2015). However, high concentrations of AFB_1 induced DNA adduct formation in Huh7. This showed that AFB_1 was converted to its reactive metabolite AFBO in HBMECs and Huh7, which had varying activities of biotransformation enzymes. In addition to the cytotoxic effects of AFB_1 in cell cultures, Al Ouqaili

(2018) also showed that high AFB_1 concentrations inhibited growth of hematopoietic stem cells (HSCs) hence decreasing viability of treated cells (Al-Ouqaili, 2018).

While AFB_1 mainly targets the liver, it was recently reported to induce myocardial toxicity in rats. Ge *et al.* (2017) revealed that the consumption of AFB_1 by rats lead to disruption of the mitochondrial membrane and disorganisation of the cristae, an indication of mitochondrial damage (Ge *et al.*, 2017). It was found that myocardial apoptosis was significantly higher after treatment with AFB_1 relative to the control as the activities of caspase 3, Bax and BCl_2 were upregulated in the cardiac tissue. Due to AFB_1 lipophilicity, its distribution in blood and the excretion by kidney, the kidney may also be susceptible to its toxic effects. Various studies have also reported that AFB_1 is nephrotoxic and induces renal damage in rats (Abdel-Hamid and Firgany, 2015, Asa *et al.*, 2018, Yilmaz *et al.*, 2018).

2.7 TOXIC EFFECTS ON THE KIDNEY

2.7.1 Kidney structure and function

The kidneys are a pair of bean-shaped organs located on either side of the spine, below the ribs and behind the belly that play a vital role in the body because they remove wastes and excess fluid from the body. The kidneys also remove acid produced by cells of the body and maintain a healthy balance of water, salts and minerals such as calcium, sodium, and potassium in the blood (Lawrence *et al.*, 2018). Without this balance, heart, muscles, nerves and other tissues in the body won't be able to function properly, as all blood in the body passes through the kidney properly. Blood enters the kidney, waste gets removed and salt, water and minerals are adjusted if necessary. The filtered blood is transferred to different parts of the body and waste is turned into urine, which collects in the pelvis, a structure that drains down a tube called the ureter to the bladder.

The most important part of each kidney are the nephrons (Figure 2.13) (Lawrence *et al.*, 2018). Each kidney is made up of approximately 1 million nephrons. Nephrons are tiny filtering units and each nephron includes a filter called a glomerulus and a tubule (Figure 2.13). Nephrons work in a two-step process; the glomerulus filters blood and the tubule restore the needed substances to the blood and removes waste (Figure 2.13). If blood stops flowing into a kidney that could result in kidney failure (Lawrence *et al.*, 2018).

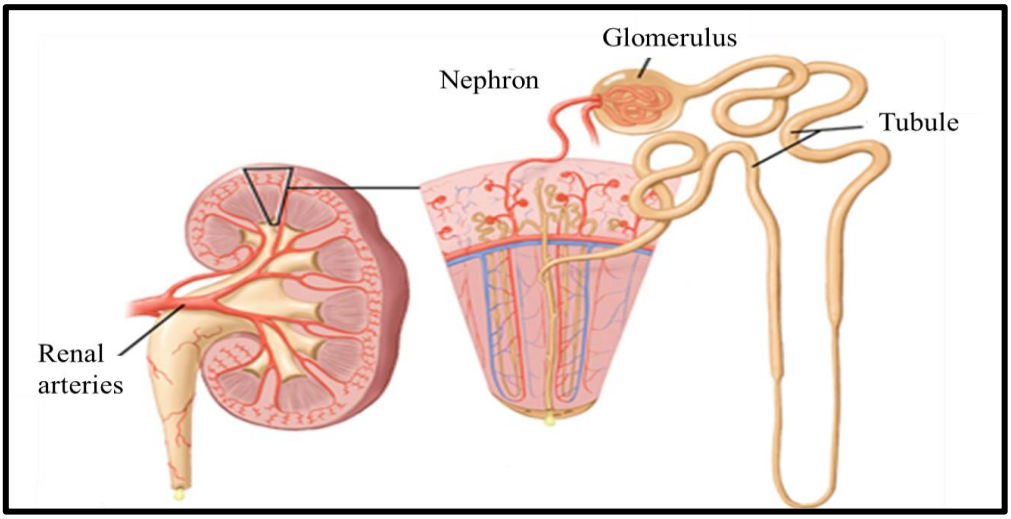

Figure 2.13 : The structure of a human kidney adapted from (Glassock and Rule, 2016).

Due to their critical role as an excretory organ, the kidney receives a disproportionate percentage of blood flow, thus exposing the kidneys to high concentrations of circulating toxins. In addition, the workload imposed increases their nutrient, oxygen and energy requirements (Moosa *et al.*, 2015). The kidneys not only facilitate many vital functions in the body, but it has been reported that they possess a significant metabolizing capacity. The kidney expresses a variety of enzymes involved in metabolism including CYP2B6, CYP3A4, CYP3A5, CYP4A11, CYP4F2, CYP4F8, CYP4F11 and CYP4F12 (Knights *et al.*, 2013).

2.7.2 The Human embryonic kidney (Hek293) cell line

The Hek 293 cell line was derived from primary human embryonic kidney cells that were obtained from a health aborted foetus and is an adherent cell line. The Hek 293 cell line is understood to be of epithelial origin and has been transformed with sheared adenovirus 5 DNA (Stepanenko and Dmitrenko, 2015). Due to its high metabolic nature, easy reproduction and maintenance makes its one of the most used cell lines in biotechnology and cell biology studies. These cells are used as models of human renal cells in invitro studies (Stepanenko and Dmitrenko, 2015).

2.7.3 Effects of AFB_1 on the kidney

Different parts of the nephron are exposed to aflatoxins before they are excreted, thus AFB_1 and its metabolites may lead to nephrotoxicity (Coulombe Jr, 1994, Sharma *et al.*, 2011, Bbosa *et al.*, 2013a). The reduction in protein induced by aflatoxin has been attributed to increased necrosis of

the kidney (Sharma *et al.*, 2011, Bbosa *et al.*, 2013a). AFB_1 has been implicated in kidney tumour formation in experimental animals and a mixture of aflatoxin B and aflatoxin G was reported to cause approximately 80% of renal and hepatic tumours in hamsters (Coulombe Jr, 1994, Bbosa *et al.*, 2013a). There were also renal lesions with features of megalocytosis in the proximal renal tubes.

In Africa, AFB_1 exposure lead to the development of fatty and hemorrhagic kidney syndrome abnormal development of glomerular epithelial cells, thickening of the glomerular basement membrane and degenerative changes in renal tubular cells in birds (Hussain *et al.*, 2008, Bbosa *et al.*, 2013a). In other animals, a reduction in the glomerular filtration rate, glucose reabsorption and tubular transport of electrolytes and organic anions, reduced glutamate-oxaloacetate and pyruvate transaminases was observed in rats. These changes were attributed to aflatoxins and other metabolites as well as the produced ROS. In cultured kidney cell lines, AFB_1 was implicated in the induction of aggregated and condensed chromatin, mitochondrial degeneration and loss of microvilli (Bbosa *et al.*, 2013a).

The reported information clarifies that AFB_1 poses a great challenge to human health and even though the main target organ for this toxin is the liver, it can also be toxic to other parts of the body including the kidney which is one of the important body organs. Studies have reported the effects of AFB_1 on other organ systems like the liver, and studies have been done on mouse/rat kidneys but a gap in literature came to light as studies on the effects of AFB_1 in the human kidney have not been have been reported. The methodology employed to evaluate the effects of AFB_1 on human embryonic kidney (Hek293) cells will be discussed in the following chapter.

CHAPTER 3 : MATERIALS AND METHODS

This chapter describes the protocol principles and procedures followed to evaluate the effects of aflatoxin B_1 (AFB_1) on Hek293 cells. It provides information on the materials used for this particular study, how the cells were maintained prior to treatment and how cell treatments were prepared. The instruments used to collect data and statistical tests used to analyse the data collected are also described.

3.1 MATERIALS

The mycotoxin AFB_1 was purchased from Sigma Aldrich (Johannesburg South Africa (S.A)), the human embryonic kidney (Hek293) cell line was purchased from Highveld Biological in Johannesburg, South Africa (SA). Tissue culture reagents were purchased from Whitehead Scientific (Johannesburg, SA). The methylthiazol tetrazolium (MTT) salt, phosphate buffered saline (PBS) tablets were purchased from Capital Laboratory Supplies, SA. Reagents for the thiobarbituric acid (TBA) reactive substances assay (TBARS) and nitric oxide synthase (NOS) assay were procured from Capital Laboratory Supplies, SA. The lactate dehydrogenase (LDH) cytotoxicity detection kit was purchased from Roche (Manheim, Germany). DNA fragmentation kit was purchased from Thermo fisher Scientific (Johannesburg, S.A) All western blotting reagents were purchased from Bio-Rad (Hercules, CA). The Cell Signalling Technology (CST) antibodies and Promega luminometry kits were purchased from Anatech (SA).Other reagents such as salts and solvents used for preparation of buffers were purchased from Merck (Darmstadt, Germany).

3.2 CELL CULTURE

3.2.1 Background

Cell culture is a technique in which cells are grown outside of the body in an artificial environment that mimics physiological conditions (Jedrzejczak-Silicka, 2017). Under appropriate conditions of temperature, pH, a solid support, fluid medium and aseptic conditions the cells can live and grow abundantly. This technique was developed by an American embryologist Ross Granville Harrison (1870-1959) in the first decade of the 20^{th} century and was first practised in 1907 at the Yale university (Jedrzejczak-Silicka, 2017). The development of cell culture techniques shed light to many possibilities in cell and tissue culture and as has been used as a tool in many applications.

3.2.2 Protocol

A vial of cryopreserved Hek293 cells was thawed at 37˚C and reconstituted in a 25 cm^3 flask, in 10 ml of complete culture medium (CCM) comprising of Dulbecco's Modified Eagle's Medium (DMEM) supplemented with 10% foetal calf serum (FCS), 1% L-glutamine, 1% penicillin streptomycin fungizone and 1.25 mM HEPES. The flask was placed in an incubator containing 5% CO_2 at 37˚C for 4 hours (4hrs). After 4hrs the CCM was discarded, the flask was replenished with 5 ml of CCM and incubated overnight (5% CO_2, 37ºC). The cells were maintained and monitored, the CCM was changed frequently until cells reached confluency. Confluent cells were counted using the trypan blue method for use in consecutive assays.

3.3 PREPARATION OF THE TREATMENTS

The aflatoxin B_1 stock solution (640 µM) was prepared by dissolving 1 mg AFB_1 5 ml of CCM. The AFB_1 stock was stored at 4˚C and diluted in CCM to obtain different AFB_1 concentrations required for the different treatments in subsequent assays. Untreated cells served as the control in all experiments.

3.4 MTT ASSAY

3.4.1 Background

The MTT (3- (4,5-dimethylthiazol-2-yl)-2-5-diphenyltetrazolium bromide) assay is a colorimetric assay used to evaluate cell viability or cytotoxicity (Adan *et al.*, 2016, Riss *et al.*, 2016). The determination of cell viability is principally guided by ascertaining mitochondrial function of cells by measuring the activity of mitochondrial enzymes such as succinate dehydrogenase (Adan *et al.*, 2016, Riss *et al.*, 2016). The MTT salt is a water-soluble tetrazolium dye that is reduced to a water insoluble purple formazan product in metabolically active cells using succinate dehydrogenase and NADH (Figure 3.1) (Adan *et al.*, 2016, Riss *et al.*, 2016). The intensity of the formazan product is directly proportional to the number of viable cells which can be measured at a specific wavelength using a spectrophotometer.

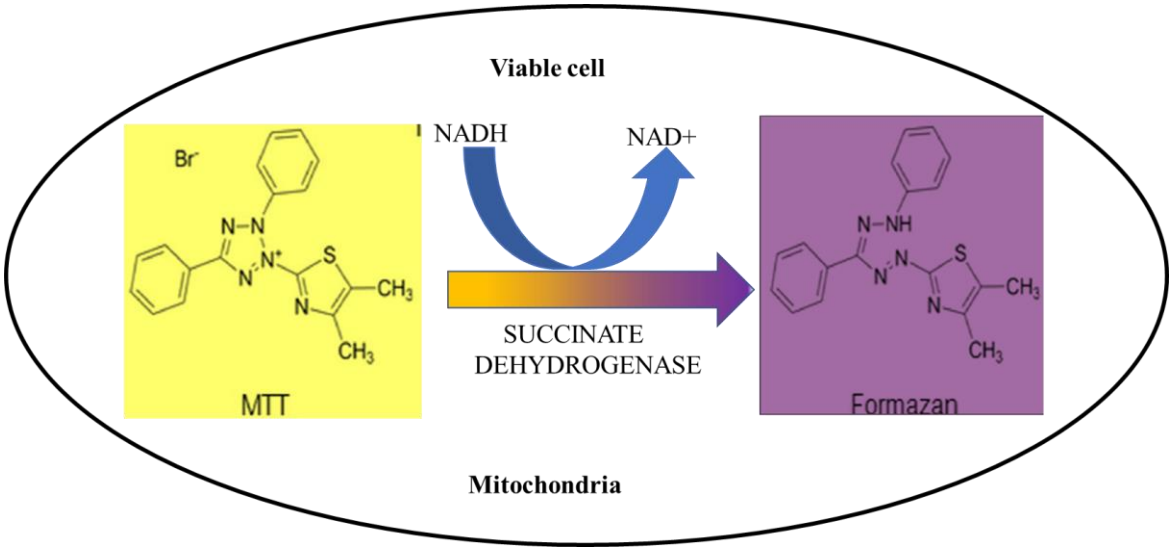

Figure 3.1 : The reduction of the yellow tetrazolium salt to purple formazan by metabolic active cells (Prepared by author).

3.4.2 Protocol

The toxicity and half inhibitory concentration of AFB_1 was evaluated using the MTT assay. The Hek293 cells were seeded at a density of 20000 cell/well (200 µl) in a 96 well microtiter plate in triplicates and incubated overnight (5% CO_2, 37ºC) for attachment. Treatments with different AFB_1 concentrations (0-100 µM) were prepared and the cells were treated with 300 µl of each treatment in triplicates and incubated (5% CO_2, 37˚C) for 24hrs.

Following incubation, the treatments were discarded, and the cells were incubated (37˚C, 5% CO_2) with 120 µl/ well of the MTT salt solution (4mg in 800 µl of 0.1M PBS and 4 ml of CCM) for 4hrs. The MTT salt solution was replaced with 100µl of the solubilising agent dimethyl sulfoxide (DMSO) for 1 hr at 37ºC to dissolve the formazan crystals. The absorbance of the samples was ascertained using the Bio-Tek µQuant plate reader (USA) at a wavelength of 570 nm and reference wavelength of 690 nm. The absorbance values were used to calculate % cell viability as follows: $\frac{av\ abs\ of control}{av\ abs\ of\ treatment}\ x\ 100$. The half maximum inhibitory concentration (IC_{50}) was obtained using GraphPad Prism v5.0 (GraphPad Software Inc., La Jolla, USA) by plotting a concentration response curve (log concentration vs cell viability of samples). The calculated IC_{50} was used to extrapolate a concentration lower (IC_{25}) and one concentration higher (IC_{75}) for use in subsequent assays.

3.5 ATP ASSAY

3.5.1 Background

The main energy source for all cellular activities is ATP, a nucleotide triphosphate produced mainly by mitochondria in all living cells that functions to store and supply cells with energy when necessary (Yong *et al.*, 2019). Mitochondrial toxicity and loss of membrane integrity impacts on the ability to synthesize ATP, the ATP levels of cells drastically decrease, and cells may die (Yong *et al.*, 2019).

The ATP assay is based on the luciferin and oxyluciferin reaction. During the reaction the enzyme luciferase catalyses the interaction between luciferin and oxygen to form oxyluciferin in the presence of Mg^{2+} and ATP, yielding a luminescent signal released in the form of light (Figure 3.2) which can be measured using a luminometer (Riss *et al.*, 2016). Since ATP is necessary for the reaction, there is a linear relationship between the intensity of luminescent signal produced and ATP concentration (Adan *et al.*, 2016, Riss *et al.*, 2016).

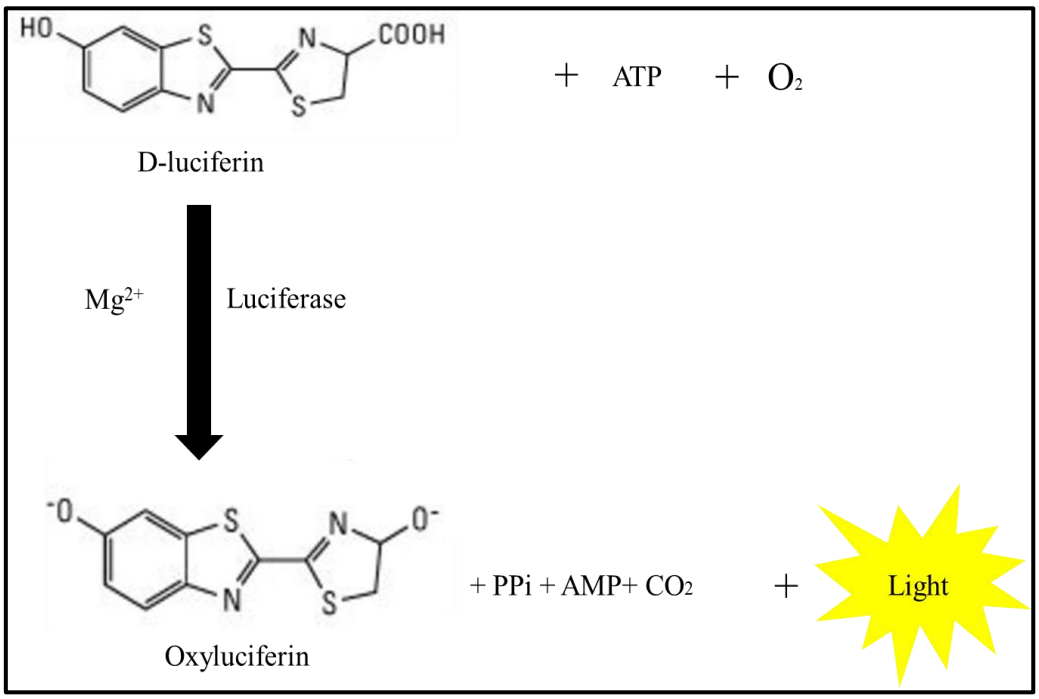

Figure 3.2 : Luciferase catalysed bioluminescence reaction in the presence magnesium ion (Mg^{2+}) and ATP (Prepared by author).

3.5.2 Protocol

The intracellular activity of ATP was quantified using the Promega Cell Titre-Glo® (#G7570) luminescent assay. The reagents were prepared according to the manufacturer's instructions. Hek293 cells were plated in a 96 well white luminometer plate at volume of 20000 cells/well (200 µl) and incubated overnight for adherence (5% CO_2, 37˚C). The cells were then treated with 300µl of AFB_1 concentrations (IC_{25}, IC_{50}, IC_{75}) in duplicates for 24hrs, the untreated cells served as the control. Following treatment, the treatment media was discarded, and the cells were gently washed 1x with 300 µl of 0.1 M PBS. The wells were replenished with 50 µl of 0.1 M PBS and 25 µl of Cell Titre-Glo® ATP reagent was added to each well. The plate was incubated at room temperature in the dark for 30 minutes. Luminescence was measured using a Modulus™ microplate luminometer (Turner Bio-Systems, Sunnyvale, California, USA) and data was expressed as relative light units (RLU).

3.6 TBARS ASSAY

3.6.1 Background

Lipid peroxidation occurs when hydrogen atoms in PUFAs containing a single electron are removed by free radicals leaving behind an unpaired electron on the carbon atom. The molecule undergoes molecular rearrangement, followed by a reaction with O_2 to generate a peroxyl radical. The peroxyl radicals may then attack membrane proteins, but are also capable of abstracting hydrogen atom from an adjacent fatty acid side chain thus propagating the chain of lipid peroxidation (Ayala *et al.*, 2014).

Lipid peroxidation results in the formation of highly reactive and unstable lipid peroxides. The decomposition of these peroxides results in malondialdehyde (MDA) formation. This intermediate can be quantified following its reaction with thiobarbituric acid (TBA) (Zeb and Ullah, 2016). The reaction between MDA and thiobarbituric acid (TBA) results in the formation of a pink chromogen which can be detected using a spectrophotometer at 532nm (Figure 3.3).

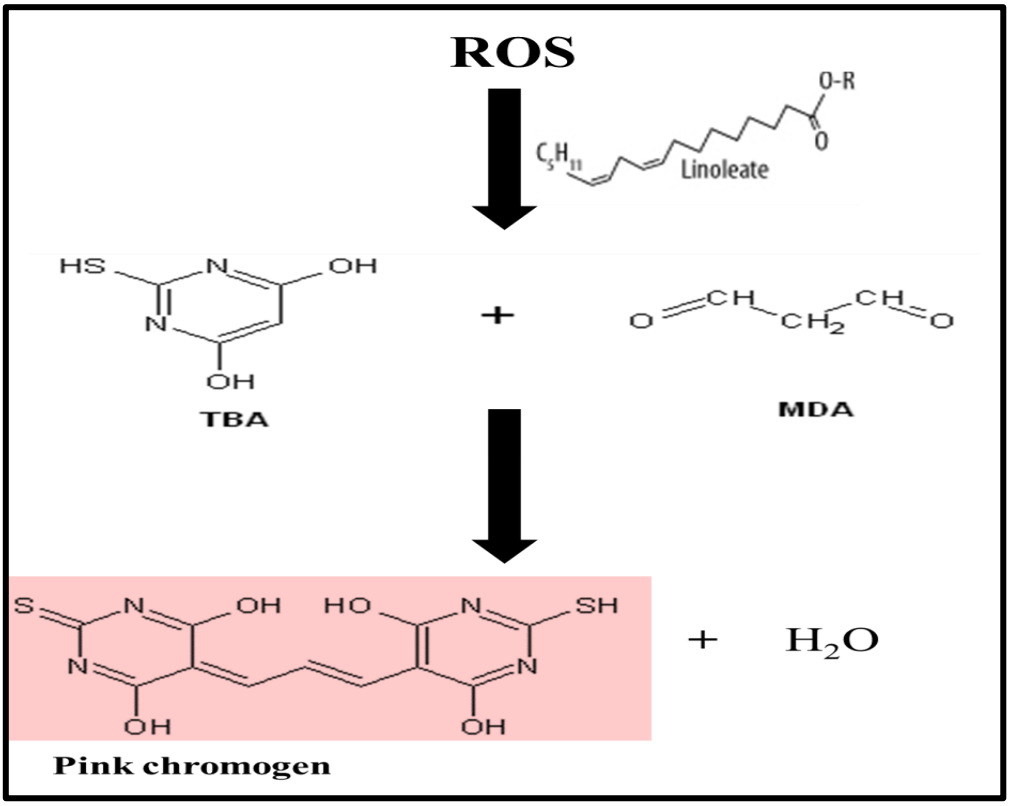

Figure 3.3 : The principle of the TBARS assay showing that thiobarbituric acid (TBA) reacts with MDA in the presence of heat or acid to produce a coloured product that is proportional to lipid peroxidation levels in samples (Prepared by author).

3.6.2 Protocol

Treatment media (200 µl) from the control and treatments were added to four clean labelled glass test tubes. Two additional tubes were prepared; viz. the negative (200 µl CCM) and positive (199 µl CCM + 1 µl MDA) controls. Each tube then received 200 µl of 2% and 7% phosphoric acid (H_3PO_4) each, followed by the addition of 400 µl of TBA/butylated hydroxytoluene (BHT) solution to every sample except the blank, which received 400 µl of 3 mM HCL. The tubes were briefly vortexed and the mixture in each tube was acidified by adding 200 µl of 1 M HCl. The tubes were boiled in a water bath for 15 minutes to allow for the hydrolysis of MDA adducts. The samples were left to cool to room temperature and 1500 µl of butanol was added to each tube. After vortexing each tube for 30 seconds, the tubes were allowed to stand so that samples can settle, and the two distinct phases were visualised. Thereafter, 200 µl of the upper phase of each sample was pipetted in triplicate in a 96-well plate and the plate was read using Bio-Tek µQuant spectrophotometer at 532 nm, with a reference wavelength of 600 nm. The average of 3 replicates

was calculated and divided by the absorption coefficient, 156 mM^{-1} and multiplied by 1000 to determine the average concentration of MDA (µM).

3.7 NITRIC OXIDE SYNTHASE (NOS) ASSAY

3.7.1 Background

Reactive nitrogen species are produced in all eukaryotic cells and are involved in the regulation of different physiological processes including differentiation, proliferation and metabolism. Nitric oxide (NO) is an unstable diatomic molecule which contains 1 unpaired electron which makes it a free radical. In mammalian cells, NO is formed from the enzymatic oxidation of L-arginine by nitric oxide synthases (Csonka *et al.*, 2015). NO is a highly reactive molecule with a short half-life in biological environments. NO undergoes oxidative degradation to form stable metabolites products, nitrates (NO_3^-) and nitrites (NO_2^-) (Csonka *et al.*, 2015). The NOS assay is based on the conversion of nitrate to nitrite by nitrate reductase, which is accomplished by vanadium chloride (VCl_3) in this assay. This is followed by the acidic Griess reaction (Figure 3.4). Under acidic conditions, nitrates react with sulfanilimide (SULF) to form a diazo compound which couples with N-(1-naphthyl) ethylenediamine (NEDD) to form a purple chromophoric azo-derivative that can be measured at 540/690nm (Csonka *et al.*, 2015).

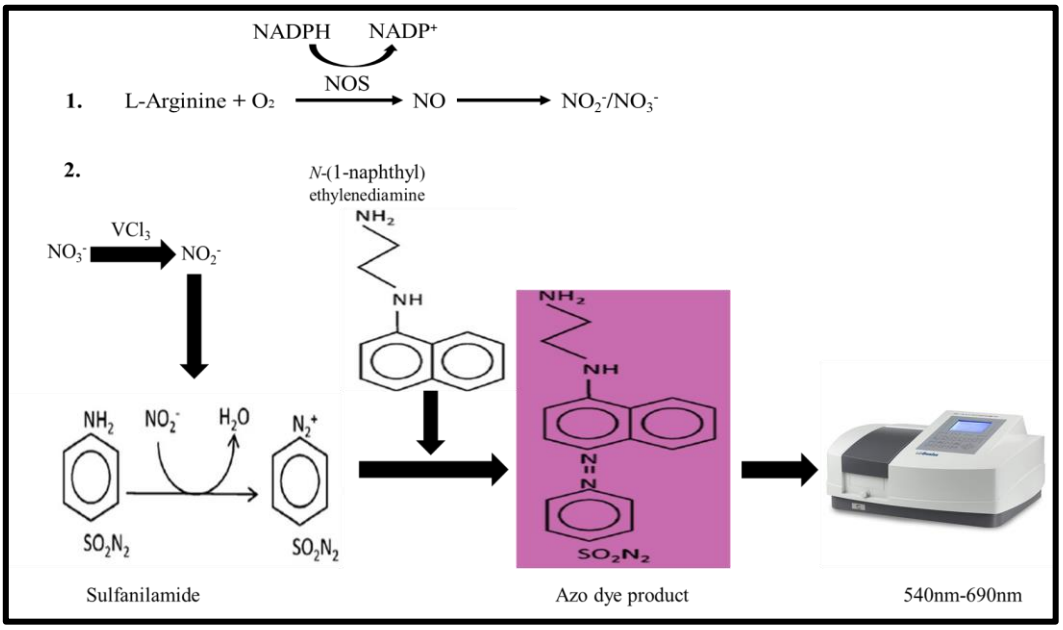

Figure 3.4 : 1. Nitrates (NO_3^-) and nitrites (NO_2^-) are formed nitric oxide (NO) in a reaction catalysed by the nitric oxide synthase (NOS) 2. The quantification of nitrites uses the GRIESS reaction to form a purple azo dye product that can be read spectrophotometrically at 540/690 nm (Prepared by author).

3.7.2 Protocol

Sodium nitrate standards (0 - 200 µM) were prepared and the retained supernatants from treatments with different AFB_1 concentrations, including the control samples were used. In a 96 well microtiter plate, 50 µl of samples/standard solution were pipetted into each well in duplicate. Sequentially, 50 µl of VCl_3, 25 µl of SULF, 50 µl of NEDD were added in quick succession to each well, and the plate was incubated at 37˚C for 30 minutes. The absorbances were read using Bio-Tek µQuant plate reader at a wavelength of 540 nm and a reference wavelength of 690 nm. A standard curve was constructed to extrapolate sample nitrate concentrations.

3.8 GSH ASSAY

3.8.1 Background

Reduced glutathione (GSH) is a tripeptide (L-γ-glutamyl-L-cysteinyl glycine) that serves as a key antioxidant to tissues and cells by providing a free thiol group (Salbitani *et al.*, 2017). The reduced form (GSH) provides reducing equivalents for the glutathione peroxidase (GPx) catalysed reduction reaction of lipid peroxides to their corresponding alcohols and hydrogen peroxide to water. (Salbitani *et al.*, 2017). During the GPx catalysed reaction the formation of a disulphide bond between two GSH molecules gives rise to oxidised glutathione (GSSG). The enzyme glutathione reductase (GR) recycles GSSG to GSH with simultaneous oxidation of $NADPH_2$ resulting in a decrease in GSH:GSSG ratio (Salbitani *et al.*, 2017) .

The quantification of GSH is based on a reaction catalysed by glutathione-S-transferase whereby a luciferin derivative is converted to luciferin in the presence of GSH. The light emitted is proportional to the amount of luciferin formed, which depends on the amount of GSH present (Elwahab, 2017). This makes the luminescent signal produced directly proportional to the amount of GSH present in a sample (Figure 3.5).

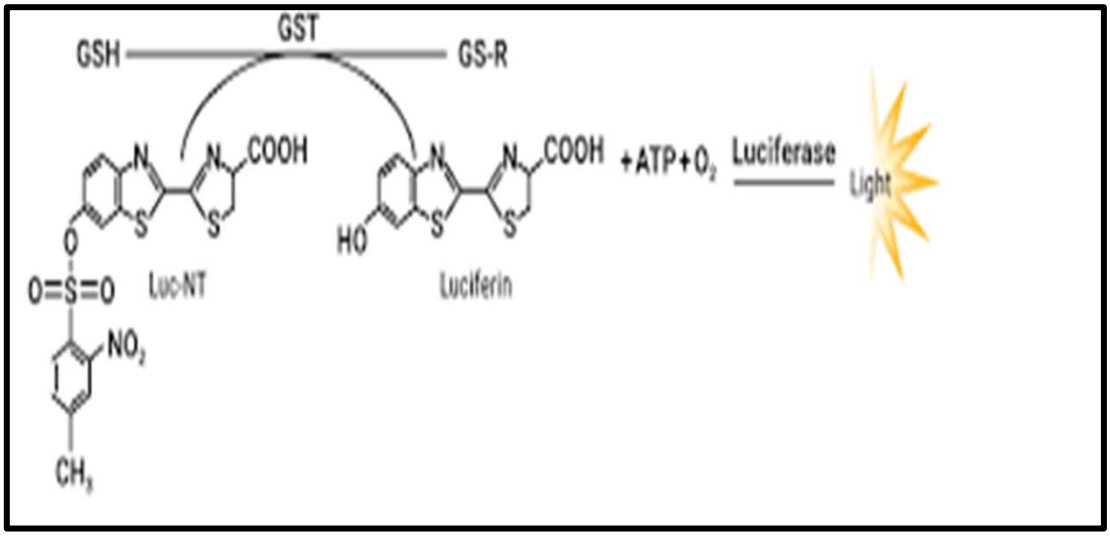

Figure 3.5 : Representation of luminometric measure of reduced glutathione (GSH) in samples (adapted from Promega protocols).

3.8.2 Protocol

The levels of intracellular GSH were quantified using the GSH-Glo^{TM} assay (#V6911, Promega, Madison, USA). Reagents were prepared according to the manufacturer's guidelines. A volume of 200 µl (20000 cells/well) were seeded into a white 96 well luminometer plate and left to attach overnight (5% CO_2, 37˚C). Following attachment, 24hr treatments with different concentrations of AFB_1 were done in duplicates and the plate was incubated at 37˚C in a humidified incubator containing 5% CO_2. The treatment media was then removed and the in the wells were replenished with 50 µl of 0.1 M PBS. Thereafter, 25 µl of 1x GSH-Glo reagent was added to each well and the plate was incubated at room temperature, away from light. After 30 minutes, 50 µl of reconstituted luciferin detection reagent was added to each well and the plate was incubated in the dark for 15 minutes. Luminescence was measured using the Modulus™ microplate luminometer (Turner Bio-Systems, Sunnyvale, California, USA) and the data was presented as RLU.

3.9 THE SINGLE CELL GEL ELECTROPHORESIS (SCGE) ASSAY

3.9.1 Background

The comet assay is commonly known as the single cell gel electrophoresis (SCGE) assay. It is a simple technique used to detect DNA fragmentation resulting from DNA damage in individual cells. The comet assay is based on the quantification of DNA fragments migrating from the nucleus

of the cell during electrophoresis (Nandhakumar *et al.*, 2011). The comet assay was initially used to detect double stranded DNA breaks, however in 1988 Singh and his colleagues optimised the protocol in alkalinic conditions thus allowing for the detection of DNA single strand breaks. The alkaline comet assay involved embedding cells in agarose gel on a microscopic slide and immersing the slides in lysis solution. The undamaged DNA in the nucleus remains intact within the comet head and does not migrate. However, when DNA is damaged the damaged the DNA strands unwind and electrophoretically migrates out of the nucleus into the agarose suspension due to attraction of negatively charged DNA towards the positively charged anode and yield a comet tail (Nandhakumar *et al.*, 2011). Jointly, the DNA tail and undamaged DNA resemble a comet (Figure 3.6). The longer and brighter the comets tails become, the more extensive is the damage to DNA (Nandhakumar *et al.*, 2011).

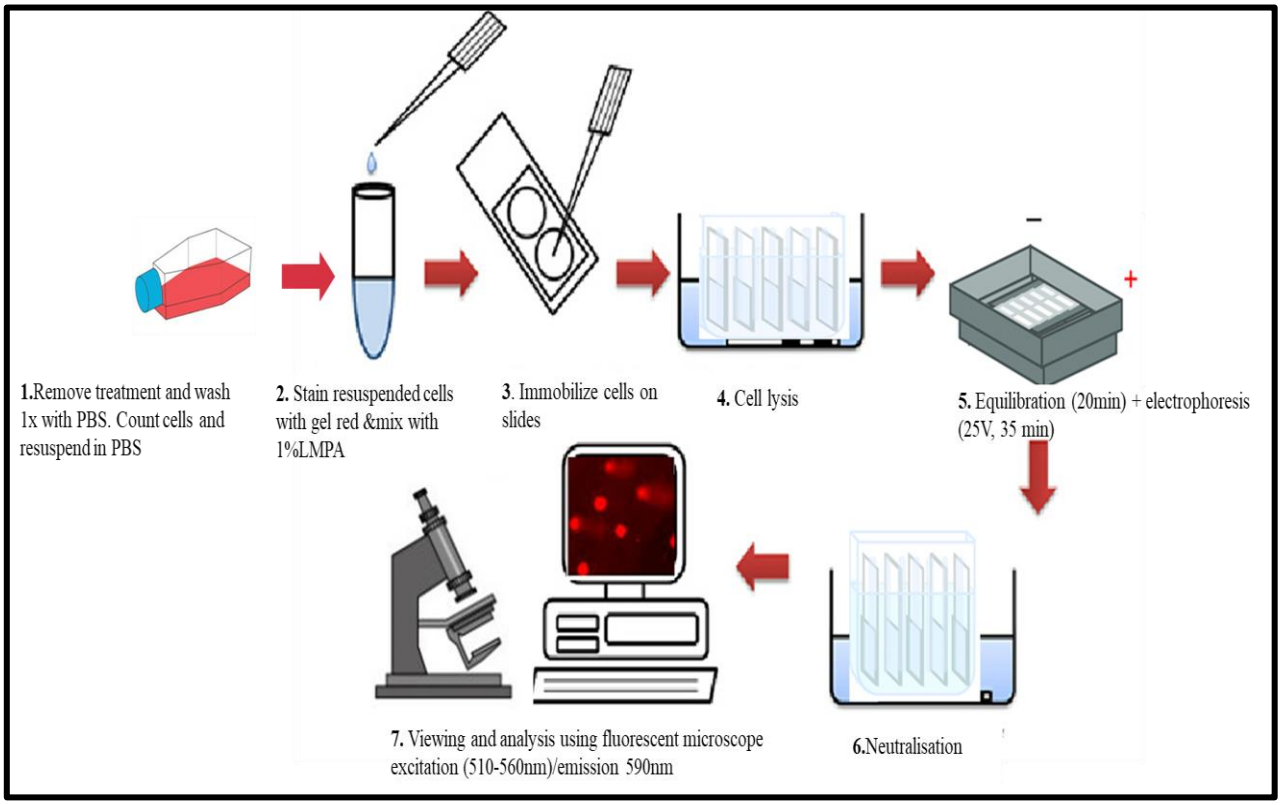

Figure 3.6 : Schematic representation of the SCGE assay procedure (Prepared by author).

3.9.2 Protocol

The comet/SCGE assay was used to detect DNA fragmentation in AFB_1-treated Hek293 cells. Slides with frosted ends were used and labelled in duplicates for each treatment (C, IC_{25}, IC_{50}, IC_{75}). Resuspended control and treated Hek293 cells were encompassed in 1% low melting point agarose (LMPA) sandwiched between a base layer comprising 2% LMPA and a top layer comprising 1% LMPA as each slide consisted of 3 gel layers. For the first gel layer, 800 µl of 2% LMPA was pipetted onto each slide, covered with a coverslip and left to set at 4°C for 10 minutes. The coverslip was removed and the second layer consisting of cell suspension (20000 cells in 400 µl of 1% LMPA and 1 µl gel red) was pipetted onto the slide, overlayed with a coverslip and left to set at 4°C for 10 minutes. Following removal of the coverslip, the third layer consisting of 400 µl of 1% LMPA was added, covered with a coverslip and left to set at 4°C for 10 minutes.

After all the layers were set the slides were immersed in cell lysis solution that was prepared fresh beforehand (100 mM EDTA, 2.5 M NaCl, 1% Triton X-100, 10% DMSO, and 10 mM Tris (pH 10) for an hour at 4°C. The slides were then allowed to equilibrate by immersing them in electrophoresis buffer (1mM Na_2EDTA and 300 mM NaOH, pH 13) for 20 minutes preceding electrophoresis (25V, 35 minutes at 37°C). The electrophoresed gels were rinsed 3 times with neutralising buffer (0.4 M Tris, pH 7.4) at 5-minute time intervals. The slides were then viewed under a under a fluorescent microscope [Olympus IXSI inverted microscope] with 510-560nm excitation and 590nm emission filters. Images were captured using Soft imaging system (Life Science - ©Olympus Soft Imaging Solutions v5) and 50 measurements of comet-tail length in µm were done for each treatment.

3.10 CASPASE ACTIVITY

3.10.1 Background

Cysteine aspartate proteases (caspases) are a family of protease enzymes that play an essential role in the initiation and execution of programmed cell death. Caspases are expressed in all cell types and are initially expressed as inactive zymogens and are only activated once an apoptotic signal is received (McIlwain *et al.*, 2013). This assay is based on the cleavage of conjugated aminoluciferin by caspases (Figure 3.7). Upon release of aminoluciferin, it reacts with luciferase in the presence

of ATP and molecular oxygen generating a luminescent signal that is proportional to the levels of caspase activity present in cells (Figure 3.7) (McIlwain *et al.*, 2013).

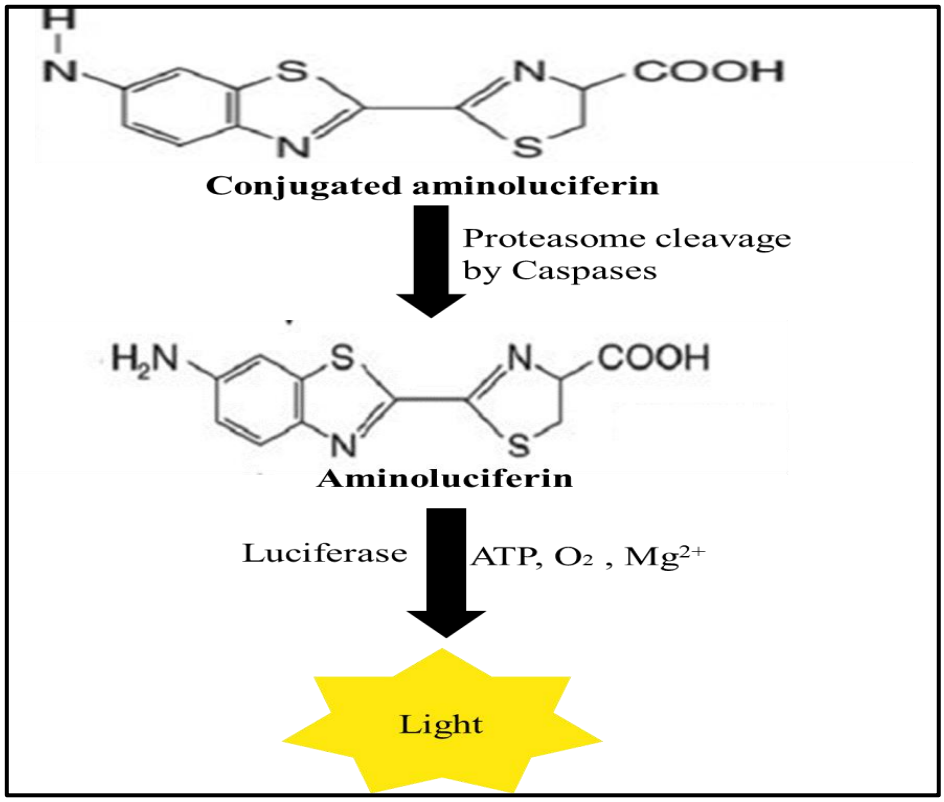

Figure 3.7 : Representation of proteasomal cleavage of conjugated aminoluciferin to aminoluciferin thereby producing light as a product which is directly proportional to caspase activity (Prepared by author).

3.10.2 Protocol

The activity of caspases 3/7, 8 and 9 were assessed using the Promega Caspase-Glo® assay [#G8090, #G8200, #G8210 (Madison, USA)] respectively. The reagents were prepared according to the manufacturer's directions. The cells were plated at a density of 20000/well in a 96-well white luminometer plate and incubated overnight (5% CO_2, 37˚C) and were then treated in duplicates with 300 µl of various concentrations of AFB_1 (IC_{25}, IC_{50}, IC_{75}) for 24hrs with untreated cells serving as the control. Following treatment, the cells were rinsed gently with 300 µl of 0.1 M PBS. Thereafter, 50 µl of 0.1 M PBS and 25 µl of Caspase-Glo®-3/7reagent was added into each well. The plate was incubated away from light for 30 minutes at room temperature. This procedure was repeated for caspase-8 and caspase-9 respectively. Luminescence was detected using the Modulus™ microplate luminometer (Turner Bio-Systems, Sunnyvale, California, USA) and the data was expressed as RLU.

3.11 ANNEXIN V ASSAY

3.11.1 Background

The annexin V assay was used to quantify the percentage of cells that are actively undergoing apoptosis and necrotic cell death within the cell population. This assay is guided by the principle that normal cells express the membrane phospholipid phosphatidylserine (PS) on the inner membrane (Figure 3.8) (Lakshmanan and Batra, 2013). When cells are damaged or undergo apoptosis, PS is exposed by flipping from the inner membrane to the outer membrane. The exposed PS is recognised by annexin V (Lakshmanan and Batra, 2013). Damaged membranes allow for a fluorescent DNA binding dye to enter the cells; the fluorescence is indicative of cells undergoing necrosis (Figure 3.8).

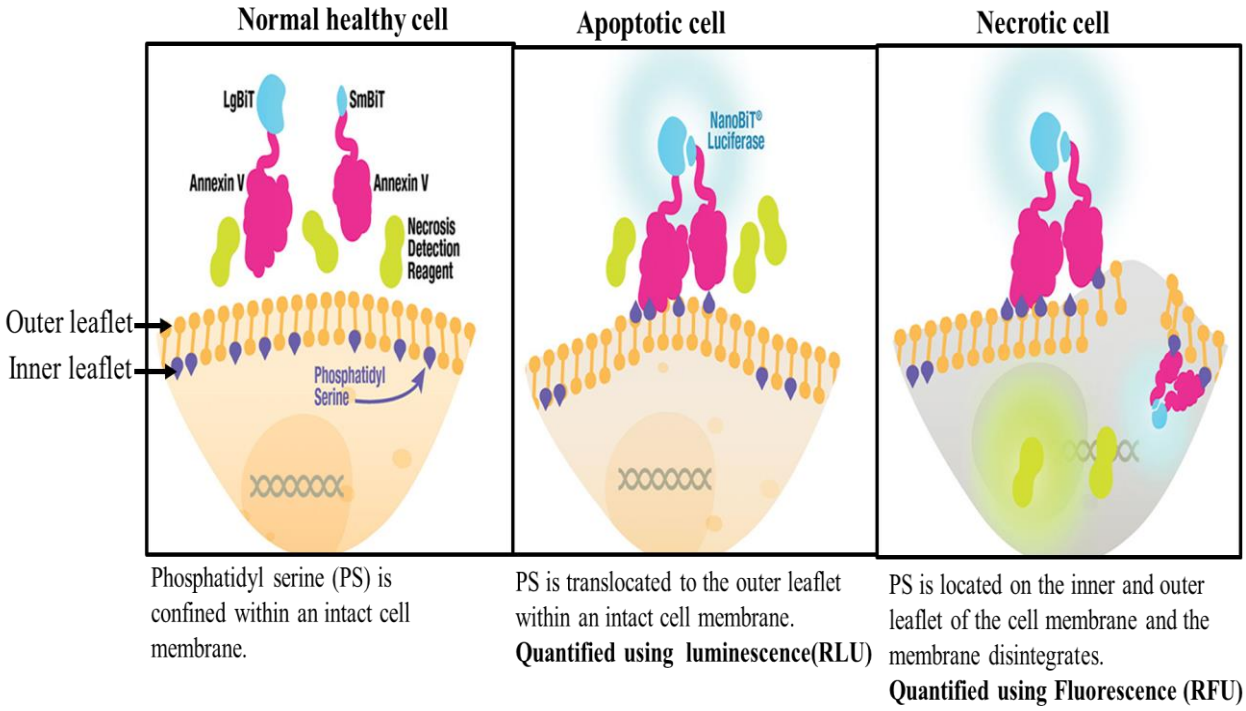

Figure 3.8 : The annexin V assay principle in the detection of apoptotic and necrotic cells (Prepared by author).

3.11.2 Protocol

Human embryonic kidney cells (Hek 293 cells) were seeded at a volume of 20000 cells/ml (200 µl) in a 96-well white luminometer plate, and incubated overnight to adhere (5% CO_2, 37˚C). The

2x detection reagent was prepared according to the manufacturer's instructions; 1µl of 1000x annexin NanoBit,1 µl 1000x $CaCl_2$, 1 µl 1000x Annexin V-SmBiT and 1µl 1000x Annexin V-LgBiT. After incubation the cells were treated with different concentrations of AFB_1 (C, IC_{25}, IC_{50}, IC_{75}) for 24 hrs, then treatment media was removed, and the cells were washed gently with 300 µl of 0.1M PBS and replenished with 50 µl of 0.1M PBS, then 25 µl of the detection reagent was loaded into each well and the plate was incubated at room temperature protected from light for 30 minutes. The luminescence and fluorescence were detected using Modulus™ microplate luminometer (Turner Biosystems) for apoptosis and necrosis and expressed in RLU and relative fluorescence units (RFU) respectively.

3.12 LDH ASSAY

3.12.1 Background

Lactate dehydrogenase (LDH) is a stable, cytosolic enzyme found in cells that can be released from damaged cells (Fiume *et al.*, 2014). When cell viability decreases, an increase in plasma membrane leakage occurs resulting in the release of LDH into the cell culture medium. The activity of LDH can be quantified using NADH produced during the conversion of lactate to pyruvate for the reduction of a yellow tetrazolium salt to form a red water-soluble formazan product (Figure 3.9) with quantifiable properties (Kumar *et al.,* 2018). The amount of formazan produced is directly proportional to the amount of LDH in the culture which in turn is proportional to the number of damaged cells (Kumar *et al.*, 2018). LDH release is considered as an early event in necrosis, but a late event in apoptosis.

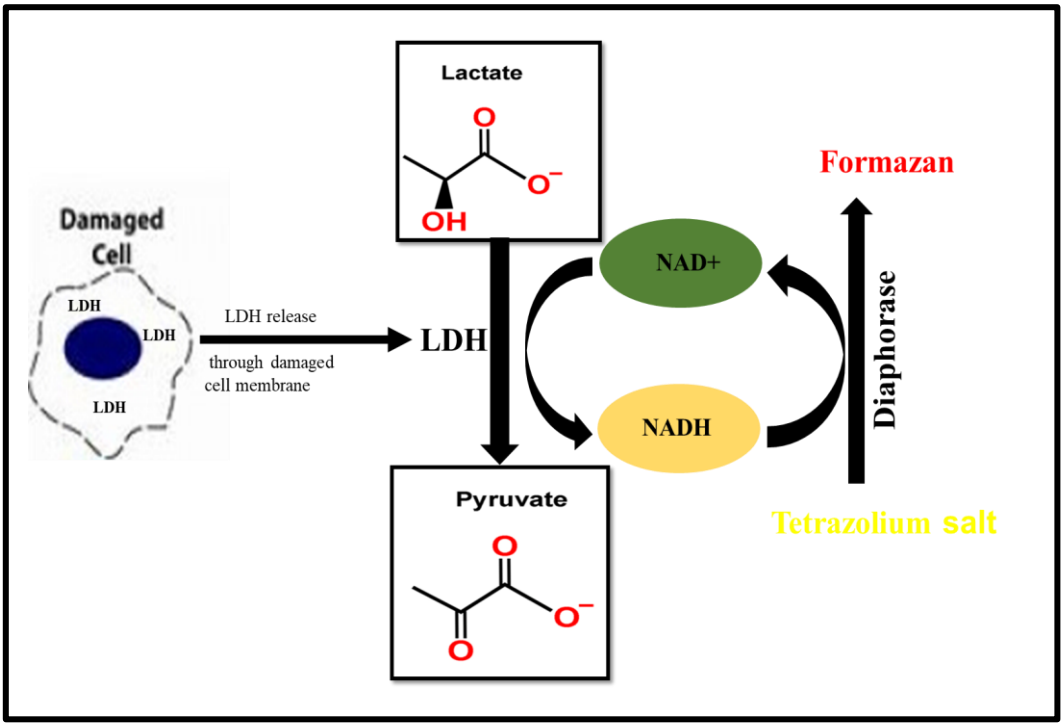

Figure 3.9 : Representation of LDH release from a damaged cell and its conversation to measurable red formazan by enzyme diaphorase (Prepared by author).

3.12.2 Protocol

Hek293 cells were treated with various concentrations of AFB_1 and the treatment supernatants were retained in eppendorf tubes labelled according to the different AFB_1 treatments. In a 96 well plate, 100 µl of the positive control (CCM only) and treatment supernatants (C, IC_{25}, IC_{50}, IC_{75}) were pipetted into each well, followed by the addition of 50 µl of the reaction mix (25 µl blue cap catalyst, 0.563 ml LDH reagent- 2). The plate was incubated in the dark at 37˚C for 30 minutes. Following incubation, 25 µl of stop solution was added and the absorbances were read at 490/690 using a Bio-Tek µQuant plate reader.

3.13 WESTERN BLOTTING

3.13.1 Background

Western blotting is a technique used for the isolation and quantification of proteins in biological samples. This is achieved by separating proteins through a gel and allowing them to migrate under the influence of and electric field (Figure 3.10) (Taylor and Posch, 2014). The rate of migration is

based on their shape and molecular mass. The proteins are transferred to a nitrocellulose membrane which is incubated with specific antibodies that bind to the protein of interest (Figure 3.10, 3.11, 3.12). The unbound antibody is washed off leaving only the bound antibody to the protein of interest (Taylor and Posch, 2014). Chemiluminescence is then used to detect the bound antibodies. Antibodies only bind to the protein of interest and only one band is visible. The thickness of the band corresponds to the amount of protein present.

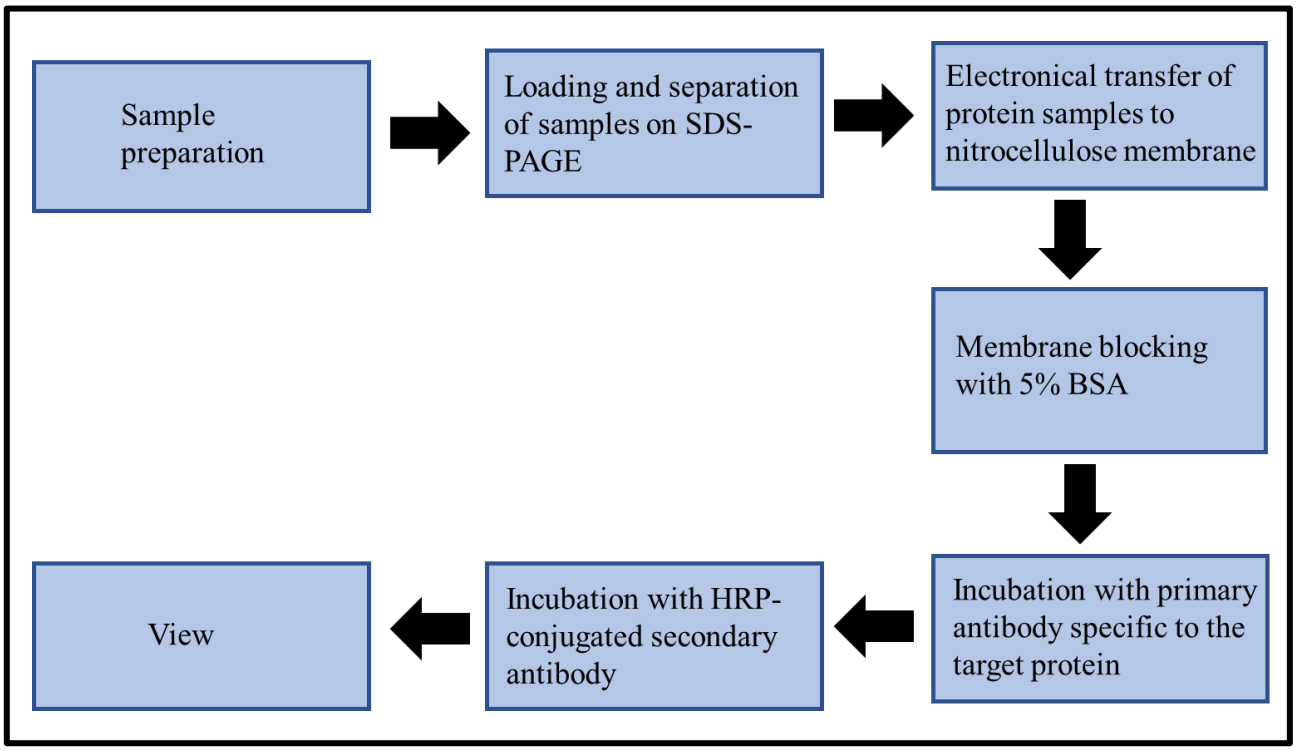

Figure 3.10 : Short overview presentation of the western blotting procedure (Prepared by author).

3.13.2 Protein isolation

Flasks of Hek293 cells were treated with IC_{25}, IC_{50}, IC_{75} concentrations of AFB_1 and the untreated flask served as the control. Cytobuster™ (Roche, Johannesburg, SA) reagent supplemented with protease and phosphatase inhibitors as per manufacture's guidelines was used for the isolation of proteins from cells. The treated cells were washed once with 5 ml of 0.1 M PBS and 300 µl of the cytobuster reagent was added to each flask, then the flasks were left on ice for 15 minutes. The cells were scraped and transferred to 1.5 ml eppendorf tubes and centrifuged (2000 rpm, 4°C, 5 minutes) for the separation of pellet and crude protein. After centrifugation the supernatant was

transferred into an eppendorf tube and was used for protein quantification using the bicinchoninic acid assay (BCA) assay.

3.13.3 Protein quantification and sample preparation

Bovine serum albumin (BSA) standards were prepared (0-1 mg/ml) and 25 µl per standard solution/sample was pipetted into a 96 well plate in duplicate. The BCA working solution was prepared (198 µl BCA:4 µl $CuSO_4$)) and 200 µl of this solution was added to each well and the plate was incubated at 37˚C, away from light for 30 minutes. Following incubation, the absorbances were read on a Bio-Tek spectrophotometer (USA) at 562 nm and a standard curve was constructed. Sample protein concentrations were calculated, and standardised to 1 mg/ml.

Standardized proteins were diluted in Laemli buffer (dH_2O, 10% SDS, β-mercaptoethanol, glycerol, 0.5 M Tris, 1% bromophenol blue) and the samples were boiled for 5 minutes at 100˚C for denaturation of protein.

3.13.4 SDS-PAGE and Transfer

The denatured protein samples were separated on SDS-PAGE. A 10% resolving gel and 4% stacking gel [10% SDS, Tris, Bis-acrylamide, dH_2O, 10% ammonium persulfate (APS), TEMED] was prepared and allowed to polymerise for an hour consecutively. Thereafter, the protein samples were subjected to an electric field (150 V) for 1 hr using a Bio-Rad compact power supplier. The electrophoresed gels were placed in transfer buffer (25 mM Tris, 192 mM glycine, 20% v/v methanol, pH 8.3) to allow equilibration between the gel and proteins. The proteins were then electro-transferred from the gel to a nitrocellulose membrane using a Transblot^{TM} turbo programme, the gel was sandwiched between two fibre pads soaked in transfer buffer in a transblot cassette and subjected to a current of (25 V,1.0 Amp, 45 minutes).

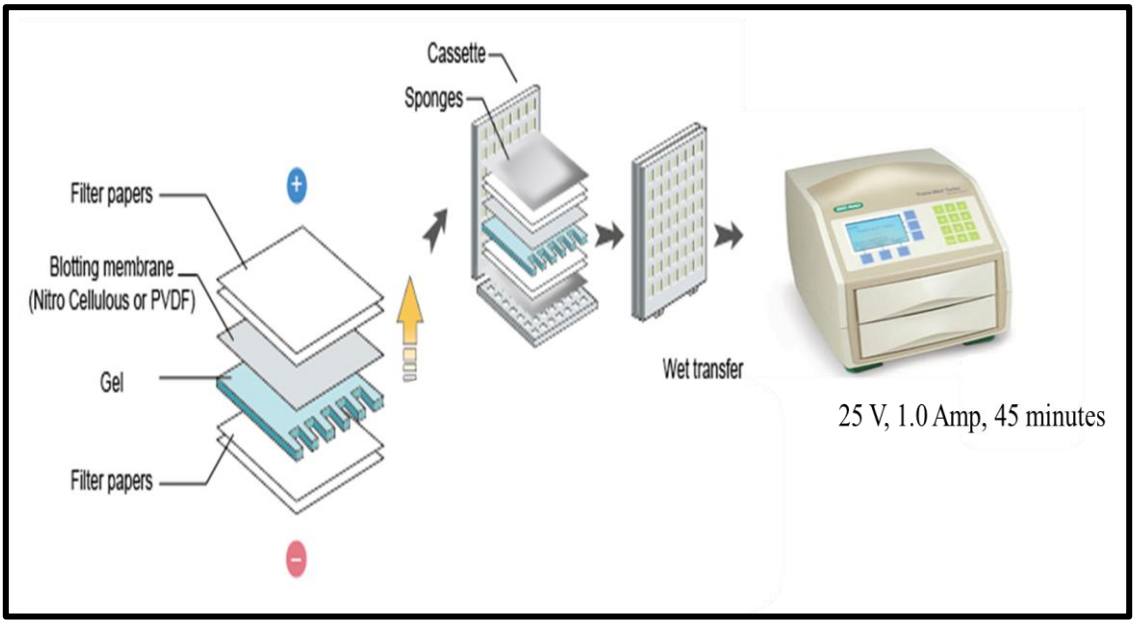

Figure 3.11 : The transfer procedure of migrated proteins from SDS gel to a nitrocellulose membrane adapted from creative diagnostics® western blot protocols.

3.13.5 Immunoprobing

Following transfer, the membranes were blocked with 5ml of 5% BSA in Tris buffered saline [dH_20, NaCl, KCl, Tris-HCl (pH7.5)] with tween 20 (TTBS) and incubated on the shaker for 2hrs. It was necessary to block the membrane in order to prevent non-specific binding of antibodies. Thereafter the membranes were incubated with specific primary antibodies [SOD2 (#13141S), GPx1 (#3286S), Nrf-2 (#12721S), c-Parp (#9542S), catalase (#12980S), Hsp70 (#46477S), p53 (#48818S), c-IAP (#7065S), Bax (#5023S), NF-κb (#8245S)] diluted in 5 % BSA,1:1000, for 1hour on shaker at room temperature, then overnight at 4˚C to allow for the binding of the antibody to its specific protein. Following overnight incubation, the membranes in primary antibodies were equilibrated to room temperature (1 hr on shaker), then the primary antibodies were removed, and membranes were subsequently washed 5 times (10 minutes) with TTBS to remove excess antibodies. This was followed by probing with horse radish peroxidase (HRP) conjugated secondary antibody [anti-mouse IgG (#7076S) for Hsp70and p53, anti-rabbit IgG (7074S) for SOD2, GPx1, Nrf-2, c-Parp, catalase, c-IAP, Bax and NF-κb)] diluted in 5ml of 5%BSA,1:2500, then incubation on shaker for 2 hrs. After incubation the membranes were washed 5 times with TTBS. For viewing, 150 µl of Clarity Western ECL Substrate (Bio-Rad) was added to the

membranes and images were captured using Molecular Imager® Chemidoc™ XRS and Bio-Rad imaging system.

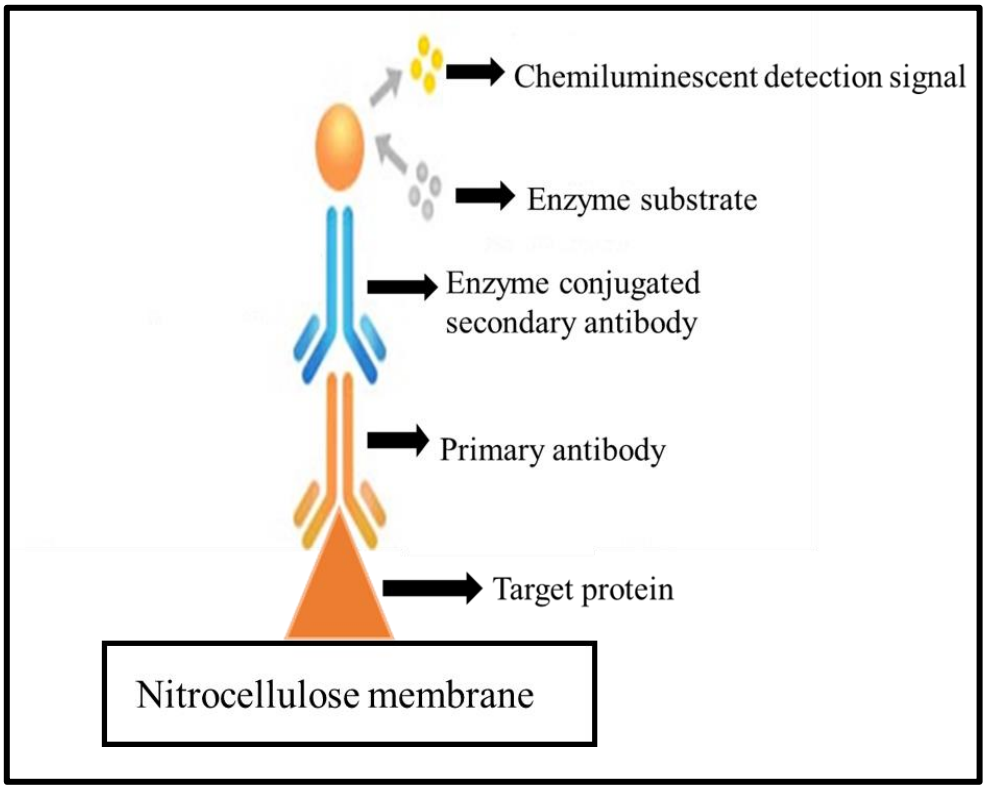

Figure 3.12 : The binding of primary antibody to the target protein followed by the secondary antibody conjugated enzyme which allows for emission of a chemiluminescent detection signal adapted from (Elab science ® western blot protocols).

To ensure the accuracy of results a housekeeping gene, β-actin was used to normalise the expression of proteins. The membranes were quenched after 1 wash with 5ml of H_20_2 (30 minutes). Membranes were washed again (1 wash with dH_20 and 1 wash with TTBS; 5 minutes each) before blocking with 5 % BSA for 1hr.Thereafter, the membranes were reprobed with HRP-labelled anti-human β-actin (1:5000 in 5 % BSA) for 1hr. The membranes were then washed 5x with TTBS and viewed as described above. The relative band density was calculated using band intensities of both the proteins of interest and the house keeping proteins and data was expressed as relative band density (RBI).

3.14 QUANTITATIVE PCR (qPCR)

3.14.1 Background

3.14.1.1 Polymerase chain reaction (PCR)

Polymerase chain reaction (PCR, Figure 3.13) is a technique used to amplify specific fragments of DNA in an enzyme reaction (Kralik and Ricchi, 2017). PCR occurs in cycles and in every cycle the number of specific DNA sections is doubled resulting in an exponential amplification of target DNA (Kralik and Ricchi, 2017). Each PCR cycle comprises of steps including denaturation, primer annealing and primer extension. The initial step denatures or separates the double-stranded DNA template by heat (94˚C for 15 seconds to 2 minutes) into single strands for replication by the thermostable DNA polymerase (Jalali *et al.*, 2017). In the next cycle the temperature is reduced to roughly 40-60˚C, allowing the oligonucleotide primers to anneal with the denatured DNA target and serve as primers for the enzyme DNA polymerase this step takes approximately 15-60 seconds. Lastly new DNA is synthesised as the reaction temperature is increased to the ideal temperature suited for the DNA polymerase. Most thermostable DNA polymerases temperatures range from 70-74˚C (Jalali *et al.*, 2017). The extension step allows for the synthesis of new DNA strands by the DNA polymerase that extend the annealed primers. The modification of basic PCR lead to the expansion of its application. The development of quantitative PCR enabled the quantification of target sequences in real time (Jalali *et al.*, 2017).

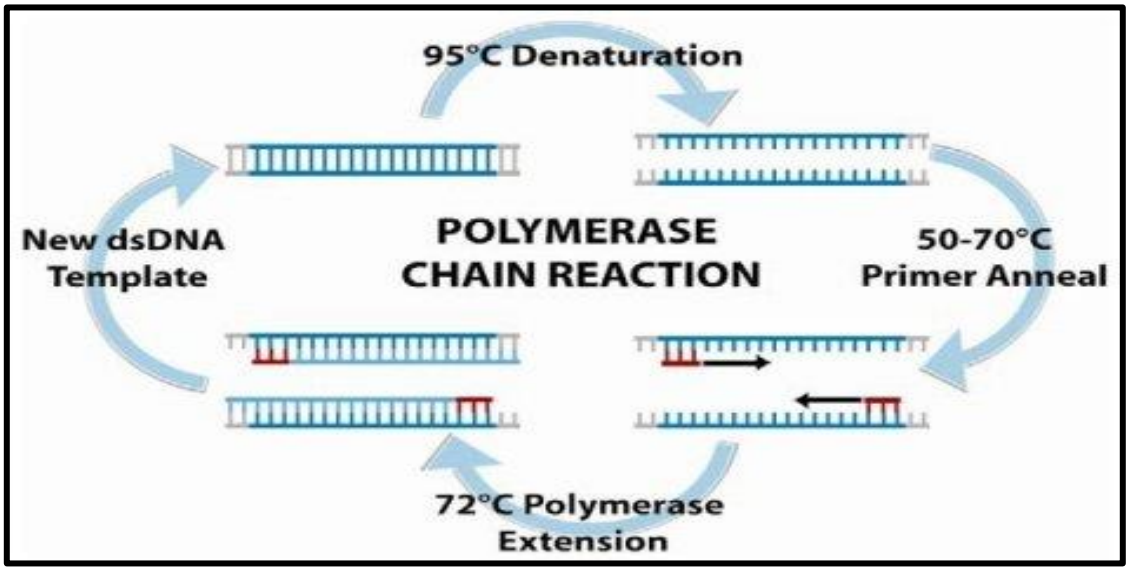

Figure 3.13 : Cycles of conventional PCR within the thermocycler instrument adapted from (Lui *et al.*, 2009)

3.14.1.2 qPCR

Quantitative polymerase reaction (qPCR) also referred to as real time PCR, is a technique that measures and detects PCR products. The process of qPCR occurs in two steps, firstly mRNA is isolated and then reverse transcribed to single stranded complementary DNA (cDNA) (Navarro *et al.*, 2015). Additional characterization of qPCR is based on the addition of a fluorescent dye, SYBR green that can bind to the minor groove of double stranded DNA (dsDNA) amplicons present, resulting in increased fluorescence upon DNA-binding that's proportional to the amount of PCR product produced at the end of each cycle (Jalali *et al.*, 2017, Kralik and Ricchi, 2017, Navarro *et al.*, 2015).

3.14.2 Protocol

3.14.2.1 RNA isolation

Hek293 cells were treated with different AFB_1 concentrations (IC_{25}, IC_{50}, IC_{75}) for 24hr, untreated cells served as the control. The cells were washed 1x with 0.1 M PBS and 500 µl of Trizol and 500 µl of 0.1 M PBS was added to each flask and the flasks were incubated at room temperature (RT) for 5 minutes. Following incubation, the flasks were scrapped, and the contents were transferred to 1.5 ml eppendorf tubes and stored at -80ºC.

Thereafter, to thawed samples 100 µl of chloroform was added, mixed vigorously for 15 seconds and samples were incubated at RT for 2-3 minutes. The samples were then centrifuged (12000 x g, 4˚C, 15 minutes). While working on ice, the upper aqueous phase was transferred to new 1.5 ml eppendorf tube and 250 µl of isopropanol was added to each tube, then the samples were stored overnight (-80˚C) overnight. Thawed samples were centrifuged (12000 x g, 4˚C, 20 minutes) and the supernatant was removed leaving only the pellet containing total RNA. The pellet was then washed with 500 µl of 75% cold ethanol and flicked to loosen the pellet. The tubes were then centrifuged again (7400 xg, 4˚C,15 minutes) and thereafter all ethanol was discarded, and the samples were air dried for 1-1.5hrs.

Thereafter the pellets were resuspended in 15 µl of nuclease free water (NFH_2O) and samples were incubated at RT for 2-3 minutes on ice and isolated RNA was quantified using a nanodrop 2000 (Thermo Fisher Scientific, Johannesburg, S.A.).The purity of RNA was determined using an

absorbance ratio of 260/280 nm, samples between 1.8-2 were considered as pure. RNA samples were standardized to 5000 ng/µl with nuclease free water (NFH_2O) and stored at -80˚C.

3.14.2.2 cDNA synthesis

Following the manufacturer's guidelines, RNA was reverse transcribed to cDNA using the iScript™ CDNA synthesis kit. A 20 µl reaction mixture (4 µl of 5x iScript reaction mix, 1 µl iScript reverse transcriptase, 11 µl NFH_2O and 4 µl RNA sample) was prepared for each sample. The prepared samples were placed in a thermocycler and reverse transcribed as follows: 25 °C for 5 minutes, 42 °C for 30 minutes, 85°C for 5 minutes and final hold at 4°C. The cDNA was diluted with 80 µl of NFH_20 to obtain a final volume of 100 µl and stored at -80 °C for further use.

3.14.2.3 qPCR

Working stock solutions of forward and reverse primers were prepared separately according to manufacture guidelines (6.25 µl SYBR green, 0.5 µl forward primer, 0.5 µl reverse primer, 3.75 µl of NFH_20 and 1.5 µl of cDNA) for both the gene of interest and housekeeping gene, this made up to a reaction volume of 12.5 µl. The gene of interest was 8-oxoguanine DNA glycosylase (OGG1) (Forward primer : 5'-GCATCGTACTCTAGCCTCCAC-3', Reverse primer : 5'-AGGACTTTGCTCCCTCCAC-3', 60°C). The house keeping gene was glyceraldehyde 3-phosphate dehydrogenase (GAPDH) (Forward primer : 5'-TCCCTGAGCTGAACGGGAAG-3', Reverse primer : 5'-GGAGGAGTGGGTGTCGCTGT-3'). Each treatment was done in triplicates in a plate that was covered with plastic and centrifuged (200 rpm, 37°C, 3 minutes) then placed in the CFX Touch™ Real Time PCR Detection System (Bio-Rad; Hercules, California, United States).The reaction was subjected to initial denaturation (95°C, 4 minutes), followed by an annealing phase (60°C, 40 seconds) which can be altered to accommodate different genes, and finally the extension phase (72°C for 30 seconds). To determine the initial amount of DNA present in samples a curve was plotted with fluorescent emission over time. The expression of the house keeping gene (GAPDH) was also quantified for normalization of the target gene expression. The data acquired was analysed using the Livak & Schmittgen (2001) method and presented as relative fold change in mRNA expression.

3.15 DNA fragmentation

3.15.1 Background

Deoxyribonucleic acid (DNA) is a negatively charged nucleic acid that when subjected to an electric field migrates from negative (anode) to positive (cathode). This assay is based on the fragmentation of DNA separated on an agarose gel (Figure 3.14). The visualization of DNA migration on the gel is facilitated by the use of intercalating dyes that bind and stain DNA. These dyes have been used to indicate DNA quantity, size and quality (Haines *et al.*, 2015).

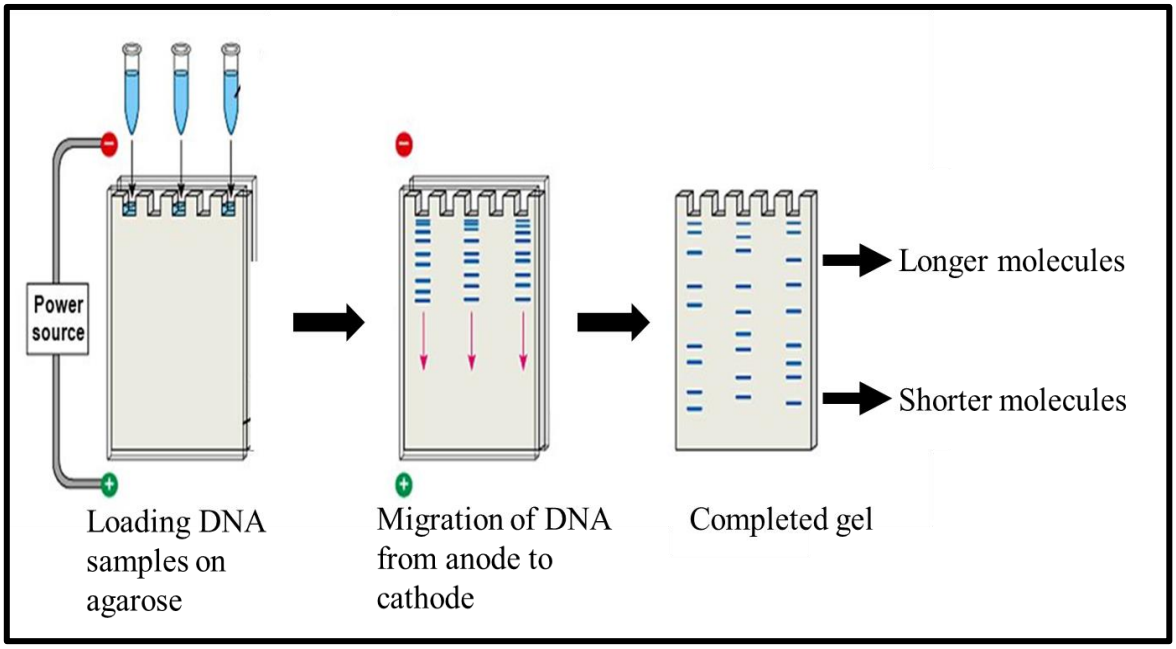

Figure 3.14 : The separation of DNA fragments bases on their size and charge on an agarose gel (Prepared by author).

3.15.2 Protocol

Hek293 cells were exposed to various AFB_1 concentrations for 24hrs, with untreated cells serving as the control. Following treatment, the supernatants were discarded, and cells were rinsed 1x with 5 ml 0.1 M PBS. Thereafter, 600 µl cell lysis solution (EDTA, Tris-Cl, 0.1% SDS) was added to the flasks of treated cells and left at room temperature (RT) for 5 minutes. The flasks were then scraped, and the constituents were transferred to 1.5 ml eppendorf tubes then stored at -80˚C overnight. To thawed samples, 600 µl potassium acetate was added and the samples were vortexed, then invert mixed for 8 minutes. The samples were vortexed once more and centrifuged (13000

rpm for 5 min) and the clear supernatant was decanted into eppendorf tubes. To the tubes with the supernatants, 600 µl of isopropanol was added and the tubes were invert mixed for 5 minutes then centrifuged (13000 rpm for 5 min). After centrifugation the supernatant was decanted to a new 1.5 ml eppendorf, leaving behind the pellet and isopropanol was added to the tubes (60 µl supernatant, 200 µl pellet) accordingly. The tubes were invert mixed for 5 minutes and centrifuged (13000 rpm for 5 min). The pellet was noted in each tube, pellets were combined for each treatment and 300 µl of ethanol was added to the final pellet then vigorously vortexed followed by centrifugation (13000 rpm for 5 minutes).The ethanol was removed carefully noting the clean white pellet and the tubes were dried on an absorbent towel for 1hr. Furthermore, 40 µl of DNA hydration solution (1x TE solution) was added to the pellet. Then the samples were vortexed and placed in a water bath (65˚C) for 15 minutes. The samples were allowed to cool for 15 minutes and stored at -80˚C. The concentration of DNA for each sample was measured using Nanodrop (Nanodrop 2000) and the obtained concentrations were standardized to the lowest concentration (100 ng/µl).

3.15.2.1 Agarose gel

A 2% agarose gel (2 g agarose powder in 100 ml 1x TBE buffer) was prepared. The standardized DNA samples were prepared with loading dye (10 µl : 10 µl) then loaded in to gels, a DNA ladder of 1kilo base pairs (kb) was used as a marker for the migration of DNA samples in the gel and the gels were electrophoresed (120 V) monitoring the migration of the samples. The gels were then viewed using Molecular Imager® Chemidoc™ XRS and Bio-Rad imaging system.

3.16 STATISTICAL ANALYSIS

GraphPad Prism V5 software was used for the analysis of results. Data was presented as mean ± standard deviation (SD). The significant differences among groups were determined using One-way analysis of variance (ANOVA) and Tukey's multiple comparisons post-test. The unpaired student *t*-tests with Welch's correction was also used to measure the significant difference between two sample means. A value of $p < 0.05$ was accepted as an indication of statistical significance. All the data represented was obtained from at least three replicates of each experiment, and experiments were repeated to confirm the results.

CHAPTER 4 : RESULTS

4.1 CELL VIABILITY

4.1.1 MTT assay

The toxicity of AFB_1 in Hek293 cells was assessed using the MTT assay. The results show that at lower AFB_1 concentrations (log 0.097 - 0.699) a slight increase in Hek293 cell viability was observed relative to the control (Figure 4.1). However, a dose dependent decrease was observed at higher AFB_1 concentrations (log 1.0 - 2.0). Analysis of the curve disclosed that 32.60 µM of AFB_1 inhibited cell proliferation by inducing 50% toxicity in Hek293 cells (IC_{50}).

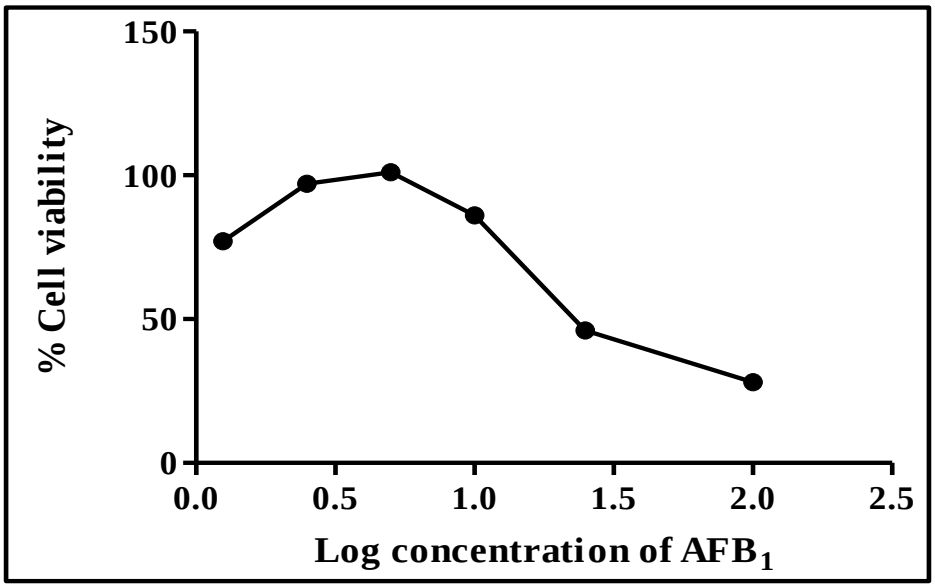

Figure 4.1 : Viability of Hek293 cells after 24 hr treatment with different AFB_1 concentrations. A dose dependent decline in cell viability was observed at high AFB_1 concentrations.

4.1.2 ATP assay

The intracellular levels of ATP were evaluated using the Cell Titre Glo ™ assay. AFB_1 induced a decrease in ATP levels in Hek293 cells in a dose dependent manner (Figure 4.2, $p < 0.0001$ using ANOVA, Tukey's post-test). Significant decreases in ATP concentration were noted at the IC_{50} ($p = 0.004$) and IC_{75} ($p = 0.0143$) relative to the control (Figure 4.2).

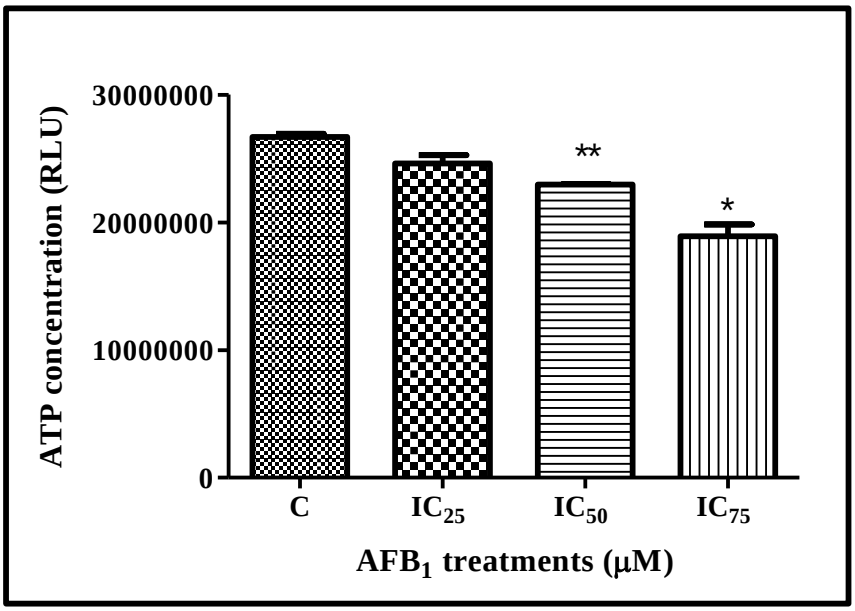

Figure 4.2 : The ATP concentration decreased in Hek293 cells after 24hr treatment with different concentrations of AFB_1 (**p = 0.0044 and *p = 0.0143, unpaired student t-test with Welch's correction).

4.2 OXIDATIVE STRESS

4.2.1 TBARS assay

The TBARS assay was used to quantify MDA levels, a marker of lipid peroxidation in Hek293 cells treated with different AFB_1 concentrations. The dose dependent decline in MDA levels was observed AFB_1 treated cells (Figure 4.3, $p < 0.0001$ using ANOVA, Tukey's post-test). The MDA levels dropped from 2.994±0.03402 µM in the control to 0.6432±0.006586 µM at the IC_{25} ($p < 0.0001$). In addition, the higher concentrations of AFB_1 induced a decrease from reported control MDA levels to 0.4829±0.006044 µM at IC_{50} ($p < 0.0001$), and 0.4509±0.007995 µM at IC_{75} ($p < 0.0001$) respectively (Figure 4.3).

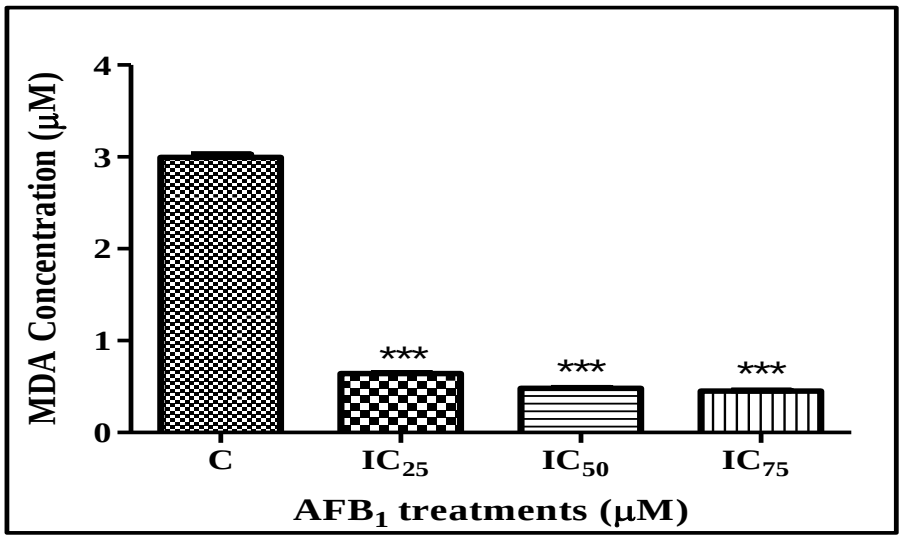

Figure 4.3 : 24hr treatment with AFB_1 induced in a dose dependent decrease in MDA concentration in Hek293 cells (*** $p < 0.0001$ for all treatments, unpaired student *t*-test with Welch's correction).

4.2.2 NOS assay

The concentration of RNS in AFB_1-treated Hek293 cells was evaluated using the nitrates assay. An increase in nitrates concentration was observed in the IC_{25} and IC_{50} treated cells; an increase was also observed at the IC_{75} relative to the control, but was lower than the IC_{50} (Figure 4.4, $p = 0.0046$ using ANOVA, Tukey's post-test). When compared to the control (2.000±0.3608 µM), a non-significant increase to 2.625 ±0.7217 µM and 3.563±0.5413 µM was observed at IC_{25} and IC_{75} respectively, while a significant increase to 6.688±0.9021 µM was observed at IC_{50} ($p = 0.0404$, Figure 4.4).

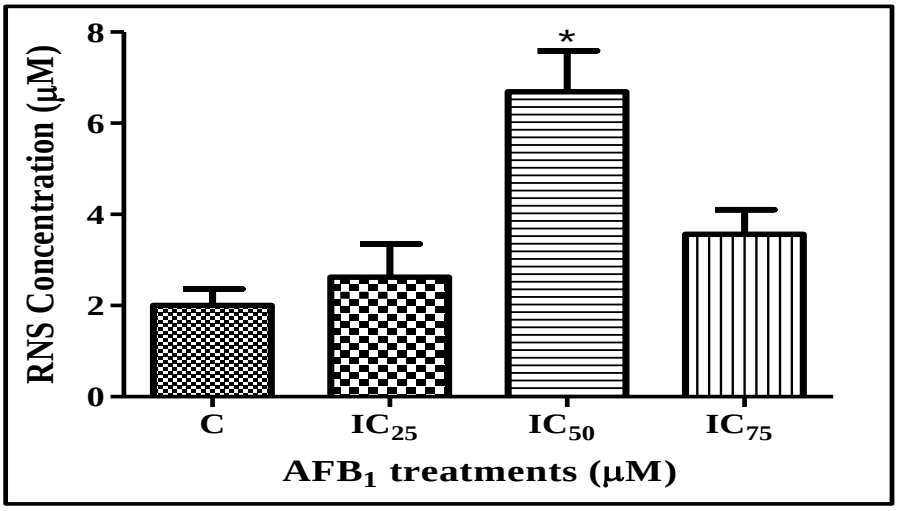

Figure 4.4 : Treatment with AFB_1 induced an increase in the production of reactive nitrogen species in Hek293 cells (*$p = 0.0444$, unpaired student *t*-test with Welch's correction).

4.2.3 GSH assay

The GSH assay was used for the quantification of GSH in treated Hek293 cells. The data revealed a concentration dependent increase in GSH levels at all AFB_1 concentrations (Figure 4.5, p = 0.0039 using ANOVA, Tukey's post-test). The GSH levels increased from 23200±486.6 RLU in the control to 68160±23650 RLU at IC_{25} (p = 0.1977), with significant increases to 102300±862.3 RLU at IC_{50} ($p < 0.0001$) and 105000 ±716.8 RLU at IC_{75} ($p < 0.0001$).

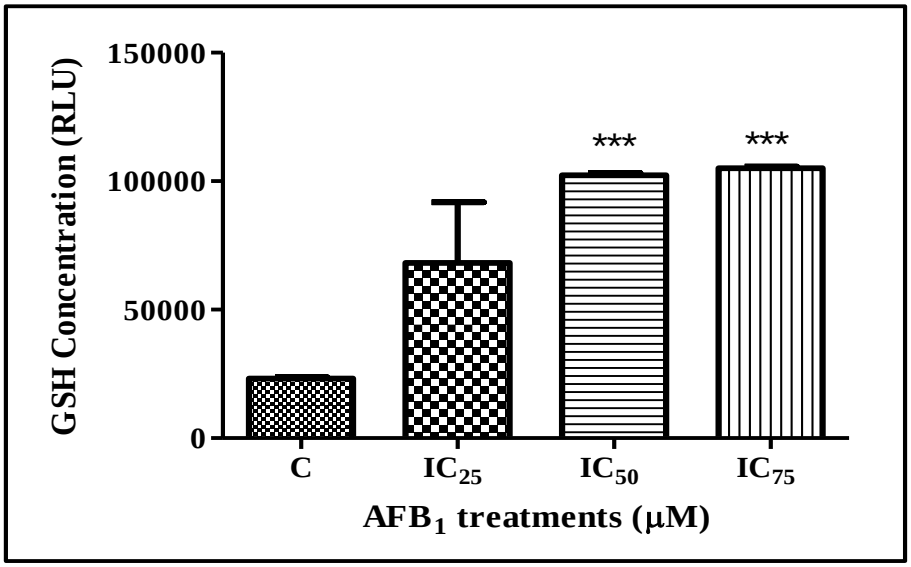

Figure 4.5 : Exposure to AFB_1 induced a dose dependent increase in GSH levels in Hek293 cells (***p < 0.0001, unpaired student t-test with Welch's correction).

4.2.4 Hsp70

The expression of proteins in AFB_1 treated Hek293 cells was determined using western blotting relative to the control. The expression of Hsp70 was upregulated in treated Hek293 cells compared to the control (Figure 4.6, $p < 0.0001$ using ANOVA, Tukey's post-test). The control expression was recorded as 0.8897±0.003612 RBI. An increase to 1.075±0.004250 RBI, 0.9927±0.002614 RBI, 0.9332±0.003711 RBI was observed at IC_{25} ($p < 0.0001$), IC_{50} ($p < 0.0001$) and at IC_{75} (p = 0.0005) concentrations respectively, relative to the control.

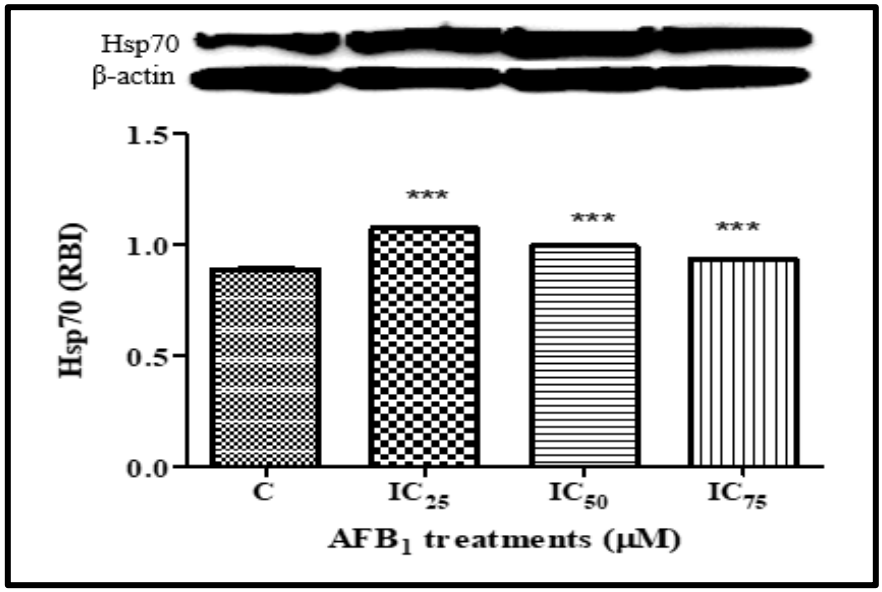

Figure 4.6 : Upregulated expression of stress protein Hsp70 after 24hr treatment with AFB_1 in Hek293 cells (***$p < 0.0001$, IC_{25} and IC_{50}; *** $p = 0.0005$, $IC_{75;}$ unpaired student *t*-test with Welch's correction).

4.2.5 Antioxidant response

The expression of proteins related to the antioxidant response in AFB_1 treated Hek293 cells was established using western blotting (Figure 4.7). Nrf-2 was significantly upregulated in AFB_1 treated Hek293 cells, an increase from the control expression of 0.09956±0.001364 RBI to 0.1740±0.003141 RBI was observed at the IC_{25} concentration ($p < 0.0001$). A further increase to 0.3511±0.003066 RBI was observed at IC_{50} concentration ($p < 0.0001$). In addition, an increase to 0.2060±0.001476 RBI at IC_{75} concentration was noted ($p < 0.0001$). SOD2 expression was increased from 1.069±0.008645 RBI in the control to 1.277±0.007789 RBI at the IC_{25} concentration of AFB_1 ($p < 0.0001$), a further increase to 1.195±0.003530 RBI and 1.486±0.007021 RBI for the IC_{50} ($p = 0.0009$) and IC_{75} ($p < 0.0001$) concentrations respectively. GPx was upregulated at the IC_{25} and IC_{50} concentration of AFB_1 to 1.070±0.02179 RBI ($p = 0.1459$) and 1.055±0.01705 RBI ($p = 0.1846$) respectively compared to the control expression of 1.024±0.008110 RBI; a significant increase to 1.143±0.006078 RBI relative to the control was noted at the IC_{75} ($p < 0.0001$). Catalase was significantly increased in AFB_1-treated Hek293 cells relative to the control. Upregulation from control expression (1.788±0.02214 RBI) to 2.501±0.01745 RBI at IC_{25} ($p < 0.0001$), 1.990±0.003122 RBI was at IC_{50} concentration ($p = 0.0029$) and 3.360±0.01842 RBI at the IC_{75} ($p < 0.0001$) AFB_1 concentration comparative to the control.

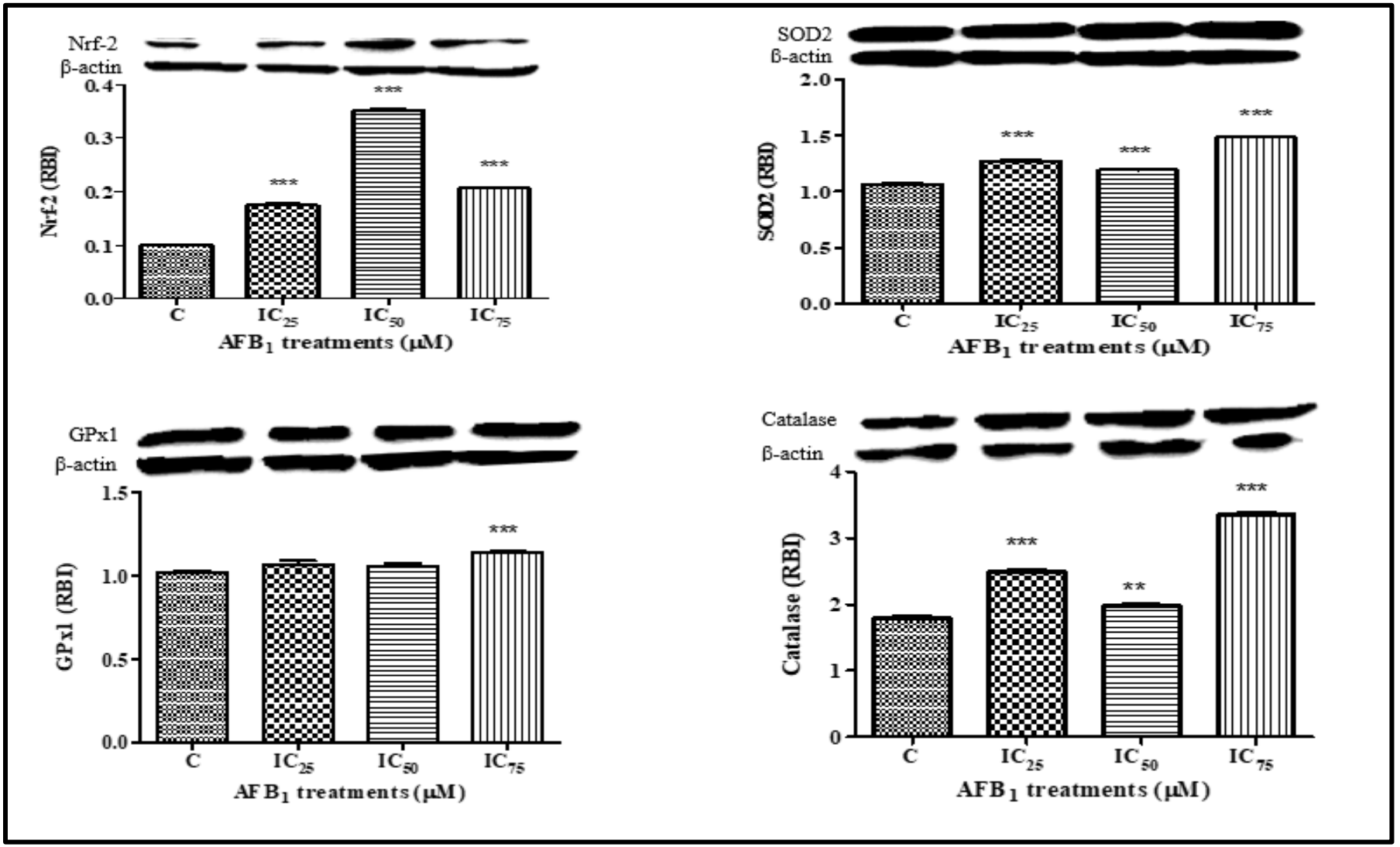

Figure 4.7 : The expression of antioxidant proteins Nrf-2 (***$p < 0.0001$), SOD2 (***$p < 0.0001$, IC_{25} and IC_{75}; ***$p = 0.0009$, IC_{50}), GPx (***$p < 0.0001$) and catalase (**$p < 0.0001$, IC_{25} and IC_{75}; ***$p = 0.0029$, IC_{50}) after 24hrs treatment with AFB_1 in Hek293 cells, unpaired student *t*-test with Welch's correction.

4.3 DNA DAMAGE

4.3.1 SCGE assay

The SCGE assay was performed to detect DNA fragmentation induced by DNA damage in treated Hek293 cells and the untreated cells served as the control. Large intact comet heads indicated no DNA fragmentation and the presence of comet tails lengths is an indication of DNA fragmentation. A significant dose-dependent increase in comet tail length was observed relative to the control (Figure 4.8, $p < 0.0001$ using ANOVA, Tukey's post-test). A significant increase from 6.244±0.1459 µm in the control to 7.046±0.1208 µm, 8.620±0.1370 µm, 9.109±0.1152 µm was observed for IC_{25} ($p < 0.0001$), IC_{50} ($p < 0.0001$) and IC_{75} ($p < 0.0001$) concentrations of AFB_1 respectively in treated Hek293 cells.

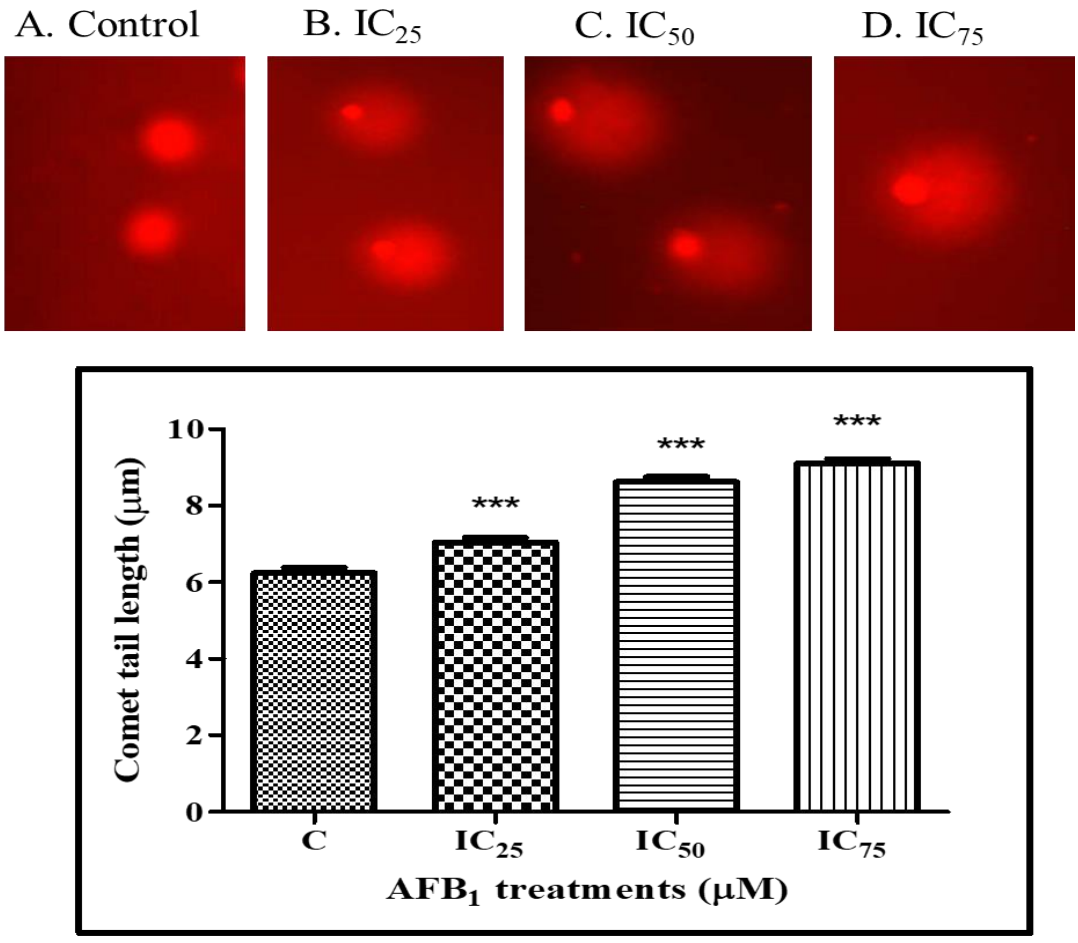

Figure 4.8 : Comet tails of Hek293 cells after 24hr treatment with AFB_1. A significant increase in comet tail length was observed in the treated cells relative to the control (***$p < 0.0001$, unpaired student *t*-test with Welch's correction).

4.3.2 DNA fragmentation

To further validate the damage to DNA in AFB_1 treated Hek293 cells, DNA fragmentation was assessed by running isolated DNA samples of the treated cells on an agarose gel; untreated cells served as the control. The genomic DNA of AFB_1 treated Hek293 cells showed fragmentation in treated cells except the control which indicated that AFB_1 exposure induced DNA double strand breaks in Hek293 cells.

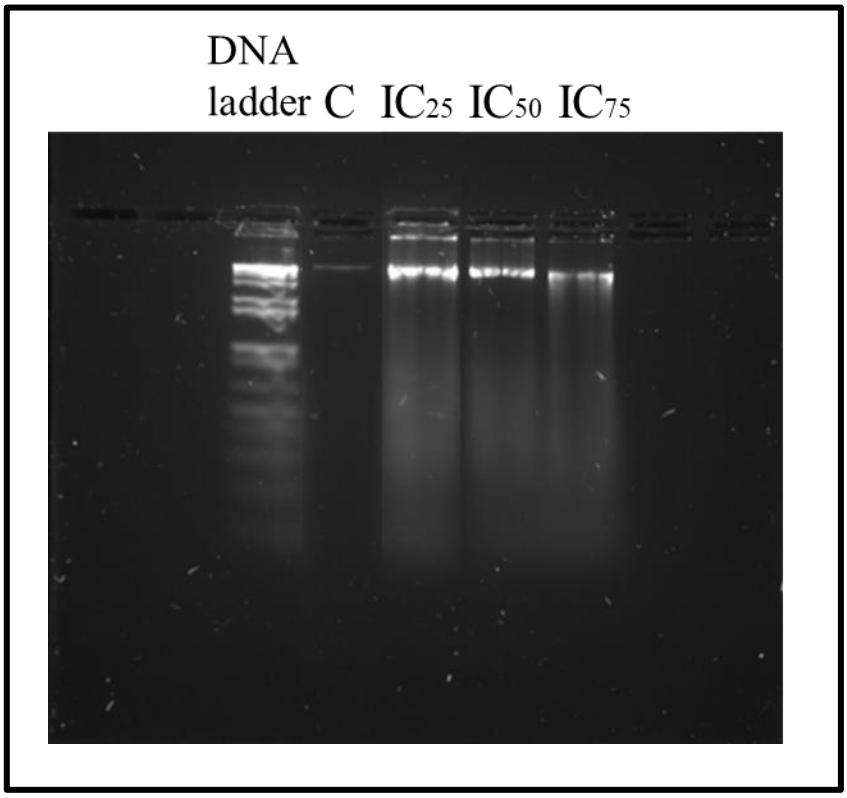

Figure 4.9 : Fragmentation of DNA induced by 24hr exposure to AFB_1 in Hek293 cells.

4.3.3 OGG1 expression

The expression of mRNA in Hek293 cells after 24hr exposure to AFB_1 was quantified using qPCR. A non-significant concentration dependent increase in OGG1 mRNA expression was observed at IC_{25} (p = 0.3837) and IC_{50} (p = 0.7867) concentrations in AFB_1 treated Hek293 cells, and an increase at IC_{75} (p = 0.2145) was observed compared to the control.

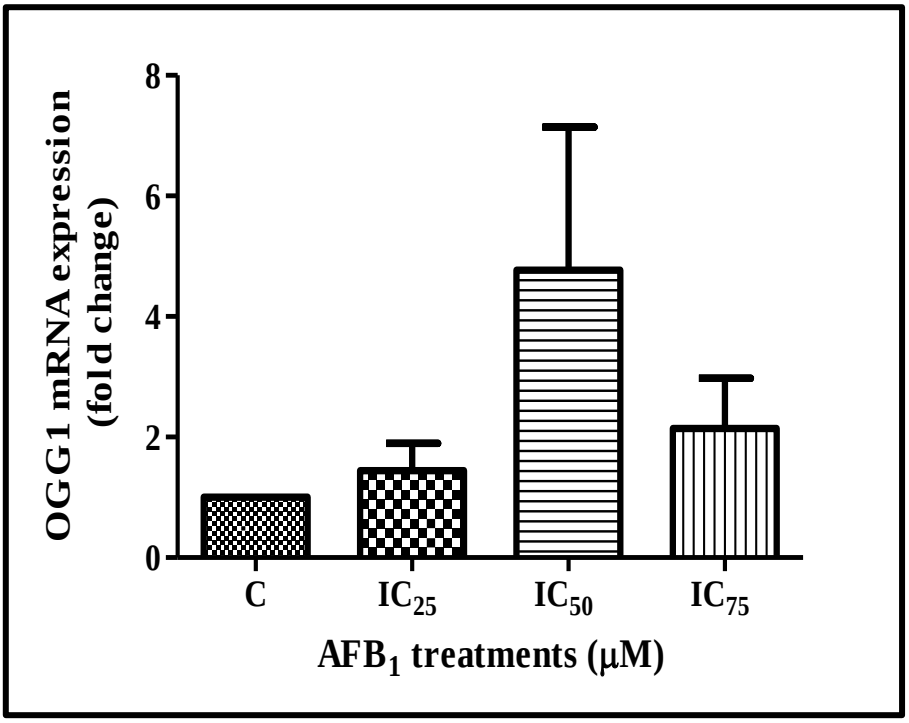

Figure 4.10 : Increased mRNA levels of OGG1 after 24 hr treatment with AFB_1 in Hek293 cells.

4.4 CELL DEATH

4.4.1 Caspase activity

Intracellular activities of caspases 8, 9 and 3/7 were measured using luminometry. Treatment of cells with AFB_1 decreased caspase 8 activity (Figure 4.11A) activity in Hek293 cells. There was a decrease to 4329000±724.6 RLU, 2025000±956800 RLU, 3289000±9904 RLU was noted at IC_{25} (p = 0.6847), IC_{50} (p = 0.1336) and IC_{75} (p = 0.0624) AFB_1 concentrations sequentially from control activity of 4421000±196700 RLU. Compared to the control (3216000±586800 RLU), only slight but non-significant increases in the activity of caspase 9 were observed (Figure 4.11B). Caspase 9 activity increased to 3337000±401700 RLU at IC_{25} (p = 0.8928), 3806000±49500 RLU at IC_{50} (p = 0.5082) and 3432000±90480 at IC_{75} (p = 0.7773). The increase in caspase 3 activity compared to the control (455900±13440 RLU) was not significant (Figure 4.11C). An increase at IC_{25} (p = 0.1252) to 617500± 61860 RLU and 541300±46180 RLU IC_{50} (p = 0.2177) were noted, while caspase 3 activity was similar to the control for the IC_{75} (p = 0.775) with 450700±9904 RLU in AFB_1 treated Hek293 cells.

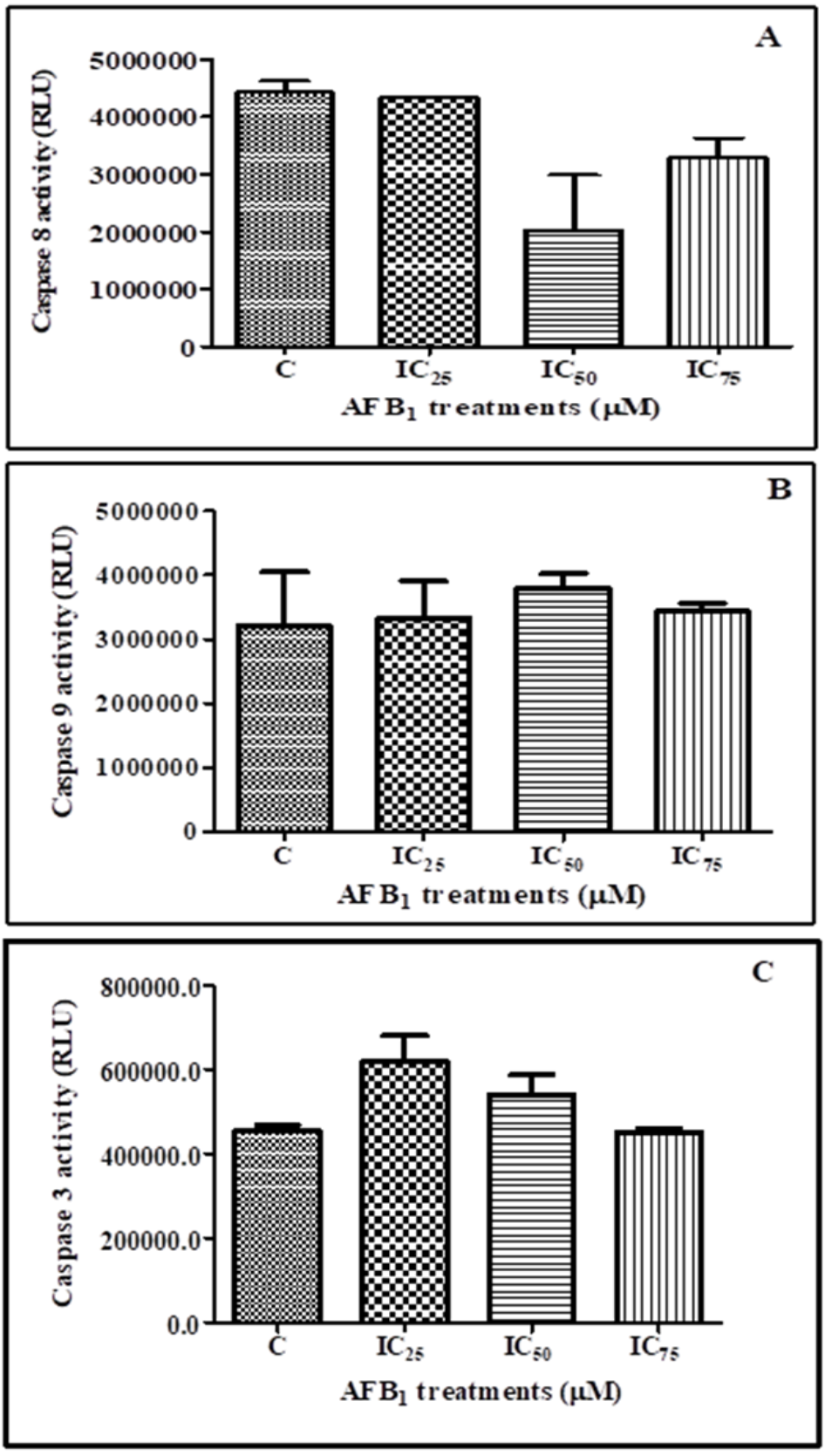

Figure 4.11 : The activity of initiator and executioner caspases in AFB_1 treated Hek293 cells, A) caspase 8, B) caspase 9 and C) caspase 3/7.

4.4.2 Apoptosis-related proteins

Evaluation of the expression apoptosis-related protein in AFB_1 treated Hek293 cells was ascertained using western blotting. Upregulation in the expressions of p53, Bax and c-Parp was observed in treated Hek293 cells comparative to the control (Figure 4.14). Control expression for p53 was recorded as 1.214±0.01316 RBI and were elevated to 2.046±0.02566 RBI at IC_{25} ($p < 0.0001$). In addition, an increase to 1.506±0.01500 RBI and 1.553±0.01318 RBI was observed at IC_{50} ($p < 0.0001$) and IC_{75} ($p < 0.0001$) concentrations respectively (Figure 4.12A). Regarding the expression of pro-apoptotic Bax protein, a significant concentration dependent increase was observed in AFB_1 treated Hek293 cells (Figure 4.12B). An increase from control expression of 0.5447±0.01588 RBI to 0.7113±0.01268 RBI was observed at IC_{25} ($p = 0.0004$) concentration with a noted significant increase to 0.8567±0.003298 RBI at IC_{50} ($p = 0.0010$) relative to the control, and an observed increase to 1.005±0.01354 RBI was noted at the IC_{75} ($p < 0.0001$) concentration. The expression of c-Parp (Figure 4.12C) showed an increase from 0.8430±0.003773 RBI in the control to 1.521±0.004865 RBI at IC_{25} ($p < 0.0001$), while an increase to 1.111±0.008022 RBI and 1.225±0.01154 RBI was noted at IC_{50} ($p < 0.0001$) and IC_{75} ($p < 0.0001$).

The expression of c-IAP was significantly increased in treated cells relative to the control (Figure 4.13A), an increase from 0.7220±0.005607 RBI in the control to 1.300±0.02637 RBI was noted at IC_{25} concentration ($p = 0.0002$). An increase from recorded control levels to 0.8199±0.01008 RBI and 0.9026± 0.1016 RBI was observed at the IC_{50} concentration ($p = 0.0011$) and IC_{75} concentration ($p < 0.0001$). A dose dependent increase in the expression of NF-κb (Figure 4.13B) was observed in AFB_1 treated Hek293 cells, the control expression of NF-κb was recorded as 1.272±0.009986 RBI, an increase from recorded control expression to 2.413±0.01762 RBI, 2.538±0.02202 RBI and 2.544±0.01727 RBI was noted at the IC_{25} concentration ($p < 0.0001$), IC_{50} concentration ($p < 0.0001$), and IC_{75} concentration ($p < 0.0001$) respectively.

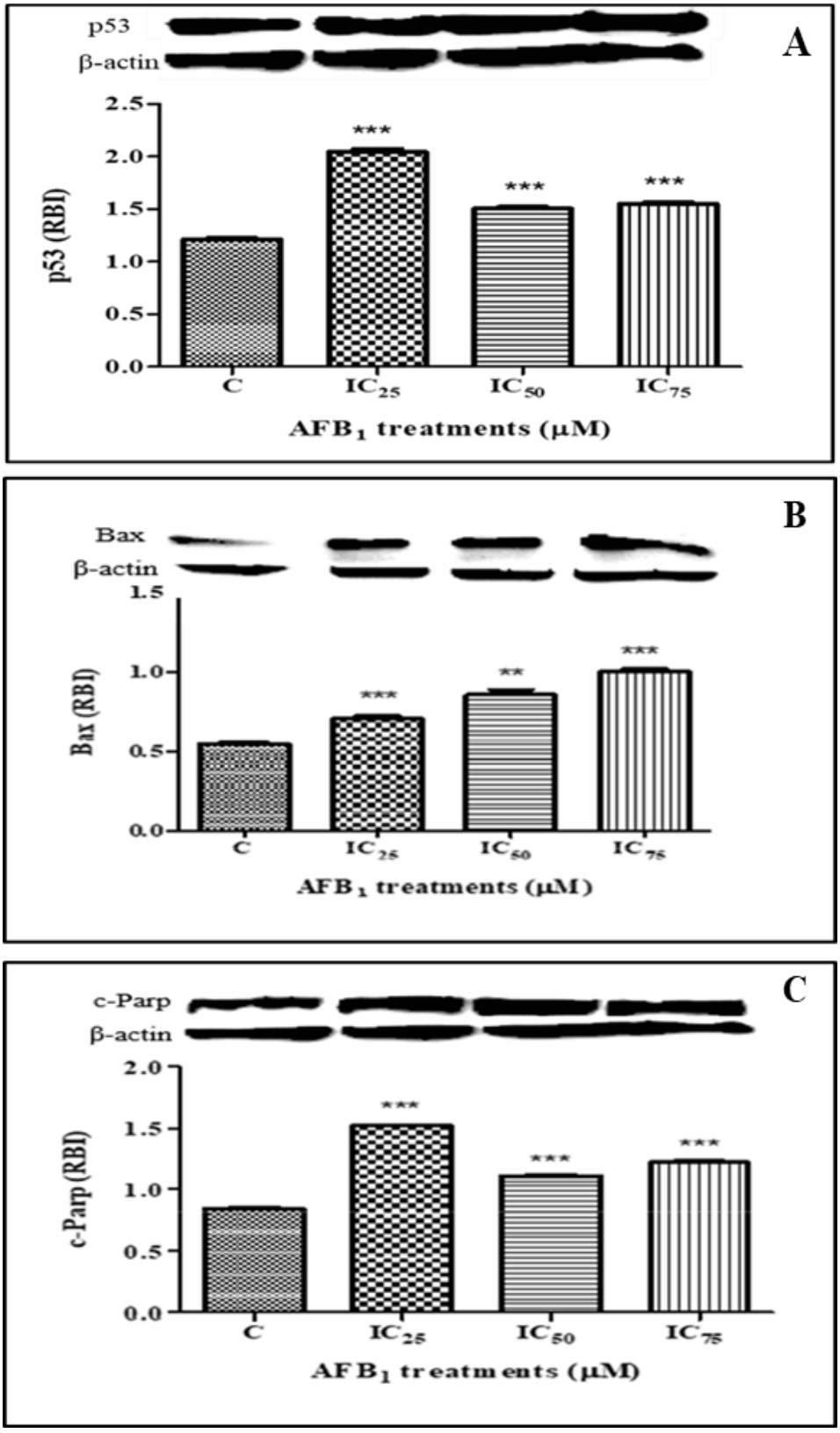

Figure 4.12 : The protein expression of p53 (***p < 0.0001), Bax (***p = 0.0004, IC_{25}; **p = 0.0010, IC_{50}; ***p < 0.0001, IC_{75}) and c-Parp IC_{25} (***p < 0.0001) were increased in AFB_1 treated Hek293 cells (unpaired student *t*-test with Welch's correction).

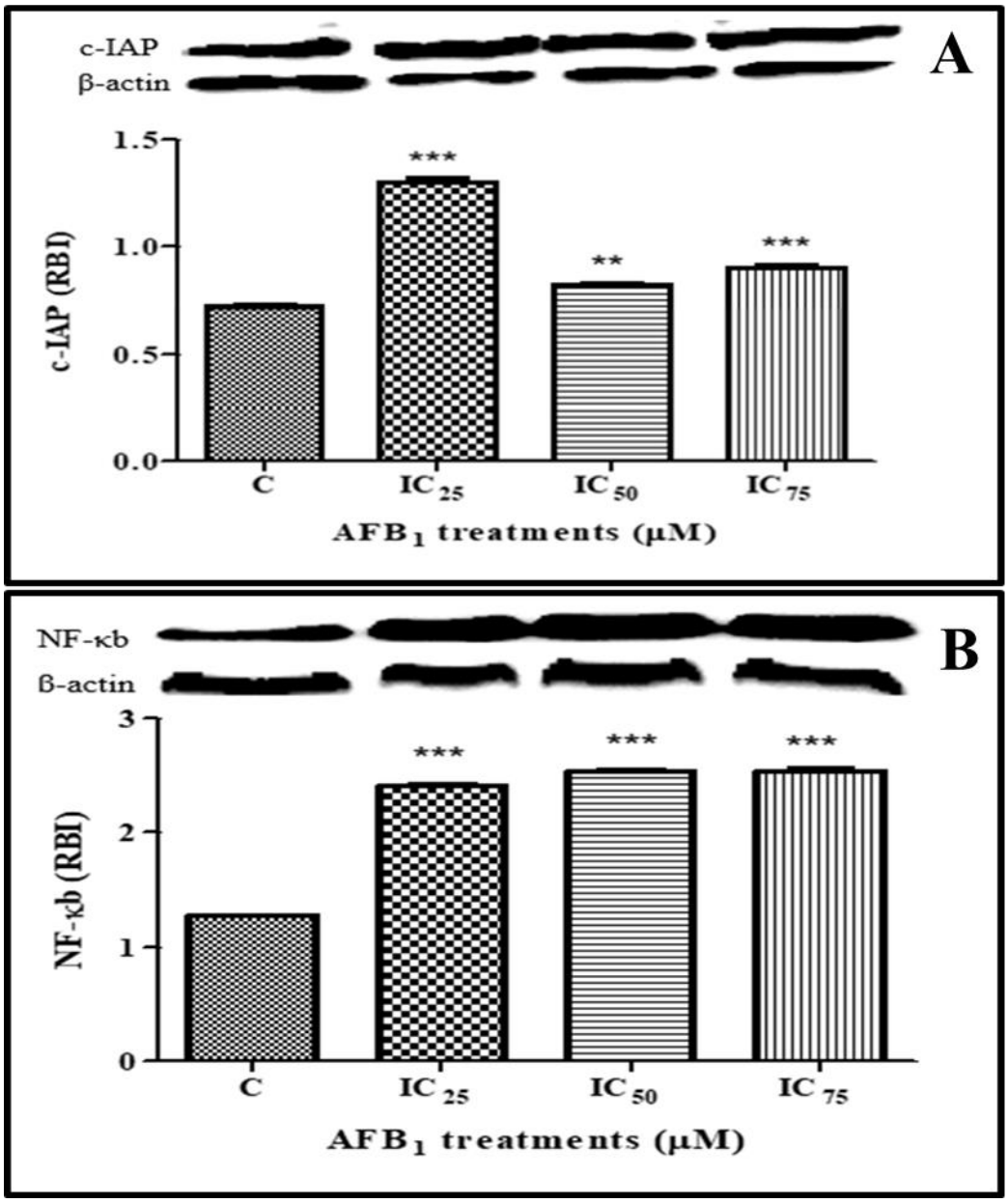

Figure 4.13 : Upregulated expression of c-IAP (***p = 0.0002, IC_{25}; **p = 0.0011, IC_{50}; ***p < 0.0001, IC_{75}) and NF-κb (***p < 0.0001) in AFB_1 treated Hek 293 cells (unpaired student t-test with Welch's correction).

4.4.3 Mode of cell death

The annexin V assay was used to detect apoptotic cells by measuring the exposure of phosphatidylserine (PS) on the outer leaflet of the cell membrane during apoptotic processes. Since annexin binds to PS, the findings indicate that AFB_1 decreased externalization of PS. Thus, annexin binding in treated cells was less compared to the control. Control apoptotic cells were recorded as

886100±21410 RLU (Figure 4.14). A decrease to 695300 ± 40650 RLU was observed at the IC_{25} (p = 0.0254) concentration and to 736800±39000 RLU at the IC_{50} (p = 0.0439) concentration relative to the control (Figure 4.14); phosphatidylserine externalisation at the IC_{75} was similar to the control (p = 0.9755).

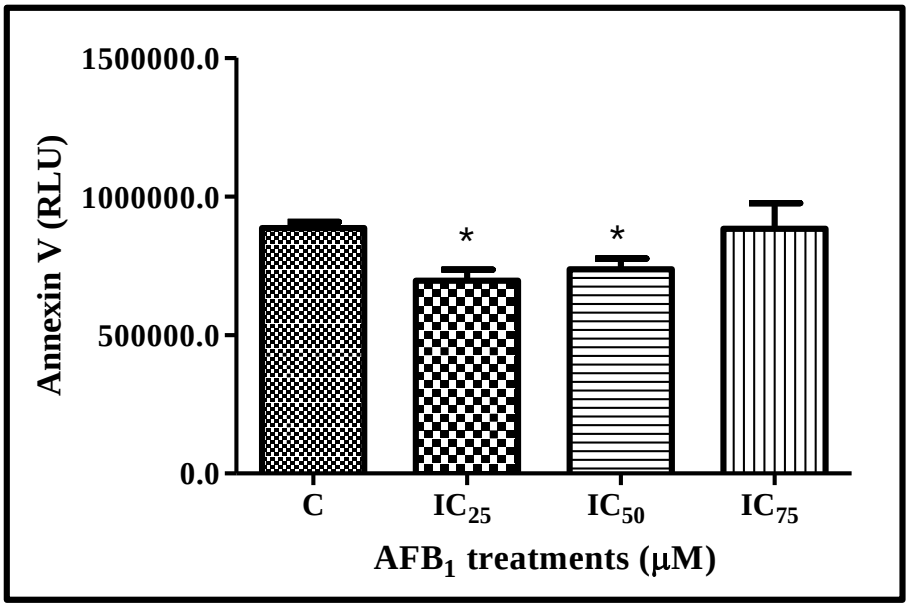

Figure 4.14 : AFB_1 induced a decrease in early apoptotic cells in treated Hek293 cells (*p = 0.0254, IC_{25}; *p = 0.0439, IC_{50}; unpaired student t-test with Welch's correction).

Necrotic cells were quantified to determine the mode of cell death induced by AFB_1 in treated Hek293 cells. The presence of necrotic cells was detected using the necrosis assay which measured the permeability of the plasma membrane to an impermeable fluorescent dye. Control necrotic cells were recorded as 886100±37080 RFU (Figure 4.15), a decrease to 695300±70410 RFU was observed at the IC_{25} (p = 0.2516) concentration. A further decrease relative to the control to 736800±67550 RFU and 882800±159700 RFU was noted at IC_{50} (p = 0.3033) and IC_{75} (p = 0.9873) concentrations respectively.

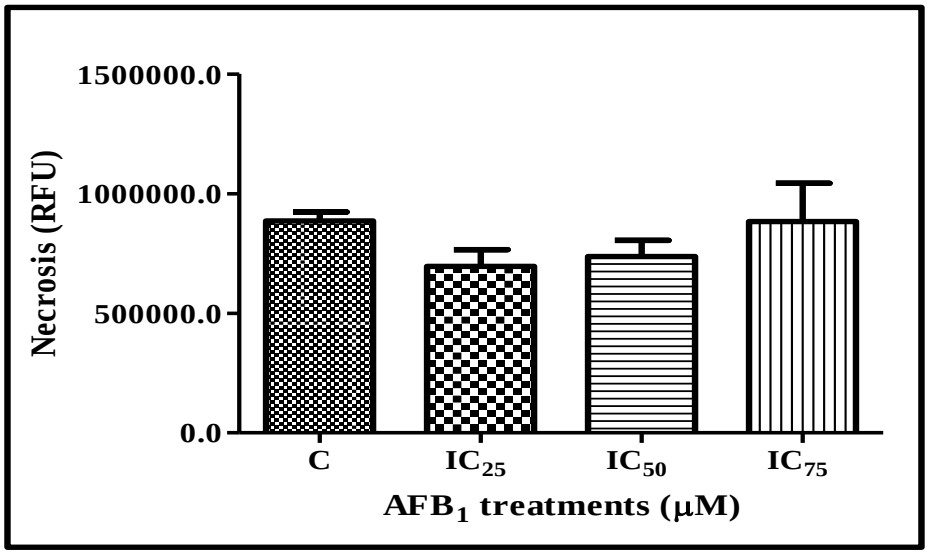

Figure 4.15 : 24hr treatment with AFB_1 decreased levels of necrotic cells in treated Hek293 cells.

Upon membrane damage cells release the enzyme lactate dehydrogenase (LDH) into the extracellular space and its release can indicate membrane damage (Kumar *et al.*, 2018). Extracellular LDH levels were quantified using the LDH assay. A non-significant decrease in LDH concentration occurred for all treatments (Figure 4.12). A decrease from 0.1657±0.02627 OD in the control to 0.1110±0.02078 OD, 0.1347±0.02050 OD, 0.1267±0.02858 OD was noted at the IC_{25} (p = 0.2012), IC_{50} (p = 0.4028) and IC_{75} (p = 0.3891) concentrations respectively (Figure 4.12).

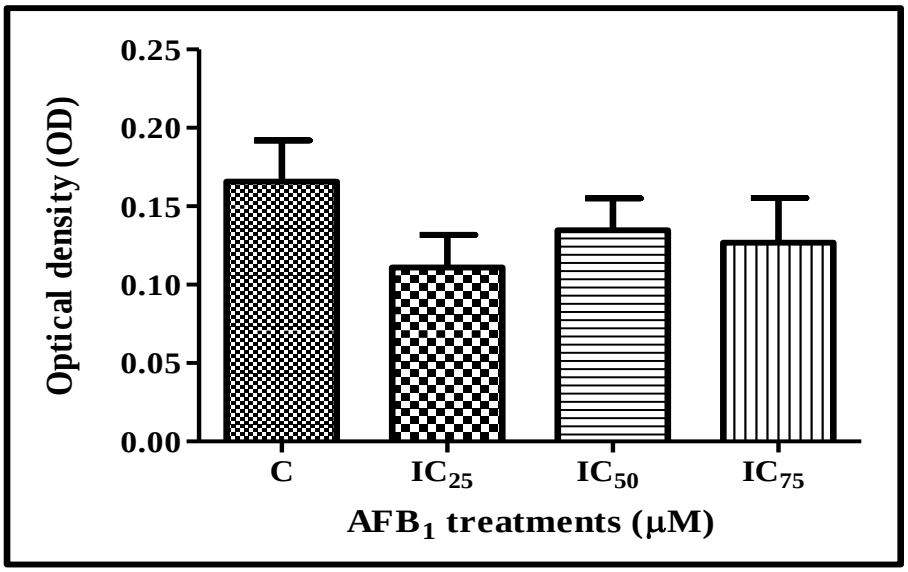

Figure 4.16 : Extracellular LDH levels decreased after 24hr treatment with AFB_1 in Hek293 cells.

CHAPTER 5 : DISCUSSION

This chapter describes in detail what the obtained results of this study indicate and further outlines the mechanism by which AFB_1 exerts its effects in Hek293 cells. Furthermore, the study limitations and recommendations are also included in this chapter.

Mycotoxins are a group of toxic secondary metabolites produced by fungi that colonise dietary staples. They present a growing health concern associated with mortality and morbidity in animals and humans. AFB_1 is of great concern worldwide because it is considered the most potent mycotoxin and is classified as a group 1 carcinogen (da Rocha *et al.*, 2014, Alshannaq and Yu, 2017, Zinedine and El Akhdari, 2019). Exposure to AFB_1 is mainly through the diet, as AFB_1 is frequently found as a contaminant in maize, peanuts and wheat which are major staple foods especially in South Africa (Alshannaq and Yu, 2017). Carcinogenic, immunotoxic, teratogenic and mutagenic effects have been reported in both humans and animals. Exposure is linked to several diseases including liver cancer in humans (Moosa, 2019) and nephrotoxicity in rats (Abdel-Hamid and Firgany, 2015, Asa *et al.*, 2018, Yilmaz *et al.*, 2018). However, AFB_1 effects on the human kidney have not been fully elucidated. This study therefore investigated the cytotoxic effects of AFB_1 exposure on Hek293 cells.

All living organisms require energy to survive; the energy is provided by the hydrolysis of ATP and is used for various cellular activities (Yong *et al.*, 2019). Mitochondria are the metabolic hub of cells that perform the essential function of oxidative phosphorylation, resulting in the production of ATP necessary for cell viability and survival (Yong *et al.*, 2019). The present study exposed Hek293 cells to different AFB_1 concentrations and cell viability was evaluated using the MTT assay. This study showed that viable Hek293 cells reduced the MTT salt to formazan and decreased cell viability (Figure 4.1). The result corroborates several studies that have demonstrated that AFB_1 decreases viability in human brain microvascular endothelial cells, hematopoietic stem cells, human brain macrovascular endothelial cells, human hepatocellular carcinoma cells and human epithelial colorectal adenocarcinoma cells (Qureshi *et al.*, 2015, Yip *et al.*, 2017, Al-Ouqaili, 2018, Huang *et al.*, 2018, Meneely *et al.*, 2018). The suggested decrease in mitochondrial succinate dehydrogenase activity or NADH (Stockert *et al.*, 2018), both essential components of the electron transfer, would negatively impact oxidative phosphorylation; ATP will be depleted and cell

viability is lost resulting in cell death (Yong *et al.*, 2019). The decrease in Hek293 cell viability corresponded with a dose-dependent decrease in ATP levels (Figure 4.2), and correlated with decreased ATP levels reported following AFB_1 administration to HepG2 cells (Liu *et al.*, 2014).

An attempt by the Hek293 cells to enhance the metabolic rate to replenish the depleted ATP could lead to oxidative stress, which is associated with an increased production of ROS (Forrester *et al.*, 2018). Several studies have demonstrated a role for AFB_1 in the onset of oxidative stress; AFB_1 forms ROS in rat liver, duck liver, mouse lung, chicken liver and the kidney of rats (Shen *et al.*, 1994, Shen *et al.*, 1996, El-Nekeety *et al.*, 2011, Abdel-Hamid and Firgany, 2015). Although mitochondria are a major source of ROS produced as by-products of cellular respiration in the ETC, they are also highly susceptible to ROS molecules and their harmful effects (Milkovic *et al.*, 2019). Specifically, mitochondria produce O_2^- from O_2 (Tong *et al.*, 2015, Di Meo *et al.*, 2016, Milkovic *et al.*, 2019). The O_2^- is converted to H_2O_2 in a dismutation reaction catalysed by SOD or it can react with NO to form peroxynitrite ($ONOO^-$) (Di Meo *et al.*, 2016). In this study, the increased SOD2 (Figure 4.7) and RNS (Figure 4.4) provide evidence of increased O_2^-. Furthermore, the noted increase in SOD2 expression at all AFB_1 exposures (Figure 4.7) can be attributed to the correspondingly increased expression of NF-κb (Figure 4.13A), as SOD2 is one of the antioxidant targets of NF-κb (Morgan and Liu, 2011).

H_2O_2 produced in the dismutation reaction has several fates. It may be converted to the potent OH^- using the Fenton reaction (Di Meo *et al.*, 2016). Both O_2^- and OH^- are able to oxidise cellular macromolecules including proteins and lipids (Di Meo *et al.*, 2016, Milkovic *et al.*, 2019). Decreased MDA levels at all doses of AFB_1 (Figure 4.3) is characteristic of decreased lipid peroxidation and implies that membranes were spared from the cytotoxic effects of free radicals (Figure 4.3); the decreased membrane damage is supported by decreased LDH release from all AFB_1-treated Hek293 cells (Figure 4.16). This protection could be conferred by the upregulation of another pathway for H_2O_2, where H_2O_2 is reduced to water using GSH (Tong *et al.*, 2015). Alternatively, catalase converts H_2O_2 to water and O_2 (Tong *et al.*, 2015, Di Meo *et al.*, 2016). These antioxidants protect cells from the deleterious effects of H_2O_2 (Dhawan, 2014). Protein expression of both GPx (Figure 4.7) and catalase (Figure 4.7) was increased for all AFB_1 treatments, but particularly for the IC_{75} AFB_1 treatment. The functioning of GPx is dependent on adequate reduced glutathione (GSH); increased GSH in all AFB_1-treated cells (Figure 4.5) was

employed in the reduction of lipid hydroperoxides and thus correlates with the observed decline in MDA levels at all doses of AFB_1 (Figure 4.3). Overall, decreased MDA (Figure 4.3) in this study suggests that the antioxidant response in human kidney cells sufficiently keeps ROS within levels suitable to maintain cellular homeostasis. Thus, the Hek293 cells are able to resist oxidative stress; this adaptive advantage is known to permit cancer cells to increase their metabolic rate, proliferate and to escape free radical damage (Sainz *et al.*, 2012) and may indicate a progression to cancer.

The antioxidant response is modulated by the upregulation of Nrf-2 (Figure 4.7) in all treated Hek293 cells. Nrf-2 is a transcription factor involved in the activation of antioxidants and cytoprotective enzymes that protect cells from excess oxidative stress by binding to antioxidant response elements (AREs) (Kavian *et al.*, 2018). Despite an overwhelming antioxidant response, the upregulated expression of the stress response protein, Hsp70 (Figure 4.6) at all AFB_1 doses demonstrates that AFB_1 induced oxidative stress in Hek293 cells. Several studies also show the involvement of AFB_1 in the induction of oxidative stress in rat kidney, splenic lymphocytes of broilers, and heart tissues of rats (Abdel-Hamid and Firgany, 2015, Chen *et al.*, 2016, Yilmaz *et al.*, 2018).

Oxidative damage to DNA is also possible during episodes of oxidative stress. It may manifest as lesions on DNA, breaks in DNA strands or faulty links and base gaps in sequences (Wang *et al.*, 2018). Cells respond to oxidative DNA damage using the base excision repair (BER) pathway that employs enzymes such as OGG1, a DNA glycosylase involved in BER (Wang *et al.*, 2018, Vlahopoulos *et al.*, 2019). OGG1 is a marker of oxidative DNA damage (Wang *et al.*, 2018). The increase in OGG1 (Figure 4.10) may reflect increased strand breaks in DNA that require repair. Strand breaks in this study are indicated by DNA laddering (Figure 4.7) and increased comet tail lengths (Figure 4.8) both of which indicate oxidative damage to DNA. Since OGG1 is transcriptionally regulated by p53, as well as the observed increase in DNA damage, the upregulation of p53 (Figure 4.12) was not surprising. Failure to repair DNA results in activation of the cell death program by p53.

Cell death is mediated by multiple pathways, including apoptosis and necrosis (Jog and Caricchio, 2014). Intact and ruptured plasma membranes are considered as hallmarks of apoptosis and necrotic cell death respectively (Zhang *et al.*, 2018). The results of this study revealed a decrease in necrosis

(Figure 4.15). Evidence for the decreased necrosis is provided by the corresponding decrease in LDH (Figure 4.16) released from treated Hek293 cells at all concentrations of AFB_1; this effect was not dependent on dose. It is further supported by decreased MDA levels and lipid peroxidation (Figure 4.3) indicating reduced membrane damage. Thus, homeostasis is maintained, the influx of water and extracellular ions leading to cell swelling and rupture is prevented, and necrotic cell death is avoided (Zhang *et al.*, 2018). This indicates that treatment of cells with AFB_1 induced a decrease in necrotic cell death at all AFB_1 concentrations relative to the normal untreated cells.

Essential for the occurrence of apoptosis is a group of cysteine proteases (caspases) which become activated in response to pro-apoptotic signals (McIlwain *et al.*, 2013). In the present study, AFB_1 exposure lead to a decrease in caspase 8 activity (Figure 4.11A) in Hek293 cells indicating that the extrinsic pathway of apoptosis was not activated. The intrinsic pathway of apoptosis is controlled by the Bcl-2 family. Bax is a pro-apoptotic member of the Bcl-2 family (Aubrey *et al.*, 2018). The increase in Bax (Figure 4.12B), may have been triggered by upregulation of p53 (Figure 4.12A). The tumour suppressor protein p53, aids in DNA repair and can also initiate cell death, DNA damage was increased as described earlier. p53 activation results in transcription of pro-apoptotic PUMA and NOXA that bind to anti-apoptotic Bcl-2, freeing Bax to dimerize into the mitochondrial membrane forming pores that increase permeabilization of the mitochondrial outer membrane (Peng *et al.*, 2016, Aubrey *et al.*, 2018). This facilitates the release of cytochrome c, apoptosis inducing factor (AIF), endonuclease G, and Smac/DIABLO from the mitochondria (Peng *et al.*, 2016). Subsequently, cytochrome c binds to Apaf-1 forming an apoptosome and facilitating the autocatalytic activation of procaspase 9. Activated caspase 9 (Figure 4.11B) cleaves and activates the executioner caspase 3 (Figure 4.11C) leading to the cleavage of Parp. The cleavage of Parp (Figure 4.12C) renders the enzyme inactive which further explains the observed DNA fragmentation (Figure 4.9) and the progression to apoptosis (Peng *et al.*, 2016). Thus, the mitochondrial pathway of apoptosis was triggered in Hek293 cells after exposure to AFB_1.

Despite the upregulation of p53 (Figure 4.12A) and activation of caspases via the intrinsic pathway (Figure 4.11B), PS was not externalised (Figure 4.14) at all concentrations of AFB_1. Thus, a key hallmark of apoptosis did not occur; this translates to decreased cell death and suggests that the inhibition of the intrinsic pathway apoptosis might be a mechanism by which AFB_1 could cause cancer in kidney cells. Indeed, inhibition of cell death is a hallmark of cancer (Aubrey *et al.*, 2018).

Progression of the intrinsic pathway of apoptosis may also have been hindered by the expression of c-IAP (Figure 4.13A) that was upregulated in this study. Inhibitors of apoptosis (IAPs) have been reported to regulate cell death through caspase inhibition; however, despite their ability to bind to caspases, recent work has reported that cellular IAPs (c-IAPs) do not possess the ability to inhibit caspase activation (Kocab and Duckett, 2016).

It has been demonstrated that AFB_1 induces apoptosis in splenic lymphocytes, cardiomyocytes of rats, human bronchial epithelial (B-2A13) cells and human hepatocytes (Liu *et al.*, 2014, Chen *et al.*, 2016, Ge *et al.*, 2017). The induction of apoptosis in broiler hepatocytes as reported by Liu and Wang (2016) revealed that increased caspase 9 and caspase 3 activities and increased Bax expression lead to the activation of the intrinsic apoptotic pathway (Liu and Wang, 2016). In addition, Yang (2012) demonstrated that AFB_1 increased the activity of caspase 3, increased the expression of apoptotic Bax and c-Parp in B-2A13 cells (Yang *et al.*, 2012). Moreover, Liu *et al.* (2014) also discovered that AFB_1 induced an increase in the expression of apoptotic proteins p53 and Bax hence activation of caspase 3 in human hepatocytes (Liu *et al.*, 2014). The results of this study correlated with the previous finding as the expression of p53 (Figure 4.12A), Bax (Figure 4.12 B), caspase 9 (Figure 4.11A) and caspase 3 activity (Figure 4.11C), and c-Parp expression was increased resulting in activating the intrinsic pathway of apoptosis.

Even though c-IAPs are poor inhibitors of caspase activity, they have been linked to the regulation of the NF-κb signalling pathway, which can contribute to determination of cell fate (Kocab and Duckett, 2016). The results of this study revealed that AFB_1 increased the expression of NF-κb (Figure 4.13B) in treated Hek293 cells; NF-κb is an apoptosis regulator that activates survival genes. This may predispose kidney cells to the potential cancer-causing effects of AFB_1. It has been previously reported that AFB_1 increases NF-κb protein expression in broiler chicks, which correlates with the observed increased expression in Hek293 cells (Rajput *et al.*, 2019).

The results of this study suggested that AFB_1 induced a decrease in cell viability through the induction of oxidative stress which lead to cell death through the activation of the intrinsic pathway of apoptosis. Furthermore, no relationship was established between dosage and AFB_1 cytotoxicity in Hek293 cells. However, future studies may use concentrations greater than 100 µM and also evaluate the effects of chronic AFB_1 exposure as individuals are exposed to AFB_1 on a day to day

basis. However, methods of eradicating or minimizing the toxic effects of AFB_1 are essential to maintain human health. The Hek293 cell line was an appropriate model to use for evaluating the effects of AFB_1 on kidney cells as its exhibits the expression of membrane proteins and optimal biological activity of target proteins.

CHAPTER 6 : CONCLUSION

The results of this study are summarised in Figure 6.1. The present study demonstrated that exposure to high AFB_1 concentrations inhibited Hek293 cell viability evidenced by the noted decrease in ATP concentrations in treated cells. An overwhelming antioxidant response was demonstrated in AFB_1-treated Hek293 cells by the upregulation of Nrf-2, SOD2, GPx, Catalase and increased GSH levels which correlated with decreased lipid peroxidation and membrane damage in treated cells. Despite the perceived overwhelming antioxidant response, RNS production increased in AFB_1-treated Hek293 cells, subjecting cells to high levels of free radicals and resulting in oxidative stress, which was confirmed by the increased expression of Hsp70. In response to free radical production oxidative DNA damage was noted in treated Hek293 cells by increased mRNA levels of OGG1, increased comet tail lengths and fragmented DNA. Furthermore, the observed upregulated p53 in response to DNA damage failed to initiate DNA repair mechanisms, therefore apoptotic cell death mechanisms were activated. The upregulated Bax lead to activation of caspase 9 and 3/7, and subsequent execution of the intrinsic pathway of apoptosis. However, the increase in c-IAP expression hindered the extrinsic pathway of apoptosis by inhibiting caspase 8 activation in treated cells. Confirmation that AFB_1 induced apoptotic cell death in Hek293 cells was noted as necrotic cells decreased in treated cells. Survival mechanisms of escaping cell death induced by AFB_1 were observed in treated cells as NF-κb was upregulated and a decrease in externalisation of PS which is considered as a hallmark of apoptosis was observed.

Further studies need to ascertain the effects chronic exposure to AFB_1 as this study only investigated the effects of acute exposure to AFB_1 in human cells. Considering that most of AFB_1 susceptible foods are a major part of the South African diet, future studies might investigate possibilities of ameliorating the toxic effects of AFB_1 in humans using drugs or medicinal plants. Lastly, this study showed the need for the application of safety measures for controlling AFB_1 concentration in commercially produced products.

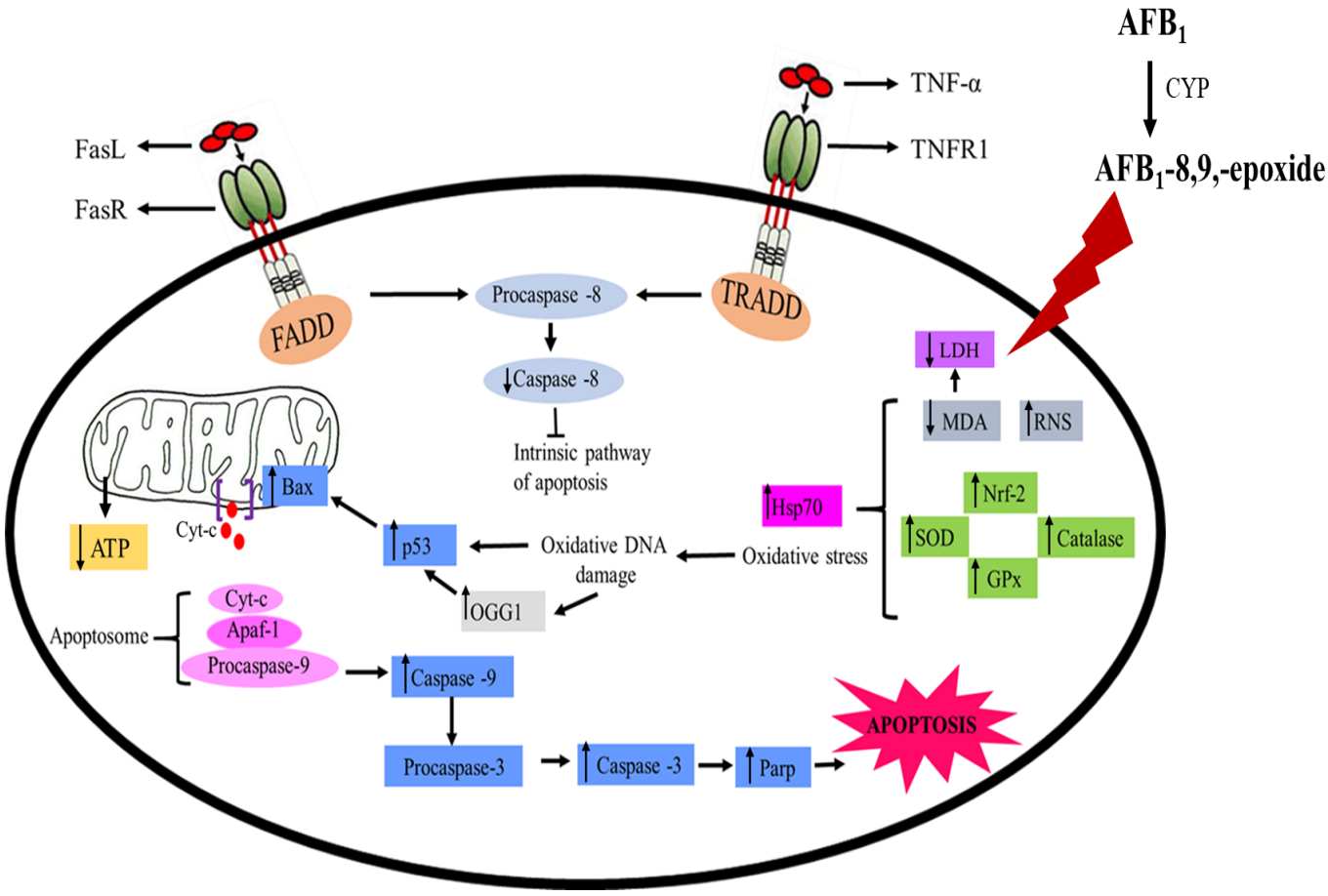

Figure 6.1 : Proposed mechanisms by which AFB_1exerts its toxic effects on Hek293 cells.

REFERENCES

ABDEL-HAMID, A. A. & FIRGANY, A. E.-D. L. 2015. Vitamin E supplementation ameliorates aflatoxin B1-induced nephrotoxicity in rats. *Acta histochemica,* 117**,** 767-779.

ADAN, A., KIRAZ, Y. & BARAN, Y. 2016. Cell proliferation and cytotoxicity assays. *Current pharmaceutical biotechnology,* 17**,** 1213-1221.

AL-HAMMADI, S., MARZOUQI, F., AL-MANSOURI, A., SHAHIN, A., AL-SHAMSI, M., MENSAH-BROWN, E. & SOUID, A.-K. 2014. The cytotoxicity of aflatoxin B1 in human lymphocytes. *Sultan Qaboos University Medical Journal,* 14**,** e65.

AL-OUQAILI, M. T. S. 2018. Depending on HPLC and PCR, detection of aflatoxin B1 extracted from Aspergillus flavus strains and it's cytotoxic effect on AFB treated-hematopoietic stem cells obtained from human umbilical cord. *Asian Journal of Pharmaceutics (AJP): Free full text articles from Asian J Pharm,* 12.

ALSHANNAQ, A. & YU, J.-H. 2017. Occurrence, toxicity, and analysis of major mycotoxins in food. *International journal of environmental research and public health,* 14**,** 632.

ASA, S. A., EL-SHAYMAA, E., MOSELHY, W. A., HASSAN, N. E.-H. Y. & HASSAN, A. A. 2018. Aflatoxin induced renal toxicity in Albino rats and the ameliorative effect of green tea aqueous extract: Histological, Morphometric and Immunohisto-chemical Study. *Journal of Experimental and Applied Animal Sciences,* 2**,** 273-285.

AUBREY, B. J., KELLY, G. L., JANIC, A., HEROLD, M. J. & STRASSER, A. 2018. How does p53 induce apoptosis and how does this relate to p53-mediated tumour suppression? *Cell death and differentiation,* 25**,** 104.

AYALA, A., MUÑOZ, M. F. & ARGÜELLES, S. 2014. Lipid peroxidation: production, metabolism, and signaling mechanisms of malondialdehyde and 4-hydroxy-2-nonenal. *Oxidative medicine and cellular longevity,* 2014.

BASU, S. 2007. The enigma of in vivo oxidative stress assessment: isoprostanes as an emerging target. *Scandinavian Journal of Food and Nutrition,* 51**,** 48-61.

BBOSA, G. S., KITYA, D., LUBEGA, A., OGWAL-OKENG, J., ANOKBONGGO, W. W. & KYEGOMBE, D. B. 2013a. Review of the biological and health effects of aflatoxins on body organs and body systems. *Aflatoxins-recent advances and future prospects,* 12**,** 239-265.

BBOSA, G. S., KITYA, D., ODDA, J. & OGWAL-OKENG, J. 2013b. Aflatoxins metabolism, effects on epigenetic mechanisms and their role in carcinogenesis. *Health,* 5**,** 720-726.

BBOSA, G. S., KITYA, D., ODDA, J. & OGWAL-OKENG, J. 2013c. Aflatoxins metabolism, effects on epigenetic mechanisms and their role in carcinogenesis. *Health,* 5**,** 14.

BERNABUCCI, U., COLAVECCHIA, L., DANIELI, P. P., BASIRICÒ, L., LACETERA, N., NARDONE, A. & RONCHI, B. 2011. Aflatoxin B1 and fumonisin B1 affect the oxidative status of bovine peripheral blood mononuclear cells. *Toxicology in vitro,* 25**,** 684-691.

CÂMARA, N. O. S., ISEKI, K., KRAMER, H., LIU, Z.-H. & SHARMA, K. 2017. Kidney disease and obesity: epidemiology, mechanisms and treatment. *Nature Reviews Nephrology,* 13**,** 181.

CARVAJAL-MORENO, M. 2015. Metabolic changes of aflatoxin B1 to become an active carcinogen and the control of this toxin. *Immunome Research,* 11**,** 1.

CHEN, J., CHEN, K., YUAN, S., PENG, X., FANG, J., WANG, F., CUI, H., CHEN, Z., YUAN, J. & GENG, Y. 2016. Effects of aflatoxin B1 on oxidative stress markers and apoptosis of spleens in broilers. *Toxicology and industrial health,* 32**,** 278-284.

COULOMBE JR, R. A. 1994. Nonhepatic disposition and effects of aflatoxin B1. *The Toxicology of Aflatoxins.* Elsevier.

CSONKA, C., PÁLI, T., BENCSIK, P., GÖRBE, A., FERDINANDY, P. & CSONT, T. 2015. Measurement of NO in biological samples. *British journal of pharmacology,* 172**,** 1620-1632.

DA ROCHA, M. E. B., FREIRE, F. D. C. O., MAIA, F. E. F., GUEDES, M. I. F. & RONDINA, D. 2014. Mycotoxins and their effects on human and animal health. *Food Control,* 36**,** 159-165.

DE OLIVEIRA, C. A. & CORASSIN, C. H. 2014. Aflatoxins. Future Medicine.

DENG, J., LING, Z., NI-YA, Z., KARROW, N. A., CHRISTOPHER, S. K., DE-SHENG, Q. & LV-HUI, S. 2018. Aflatoxin B1 metabolism: Regulation by phase I and II metabolizing enzymes and chemoprotective agents. *Mutation research/reviews in mutation research*.

DHAWAN, V. 2014. Reactive oxygen and nitrogen species: general considerations. *Studies on Respiratory Disorders.* Springer.

DI MEO, S., REED, T. T., VENDITTI, P. & VICTOR, V. M. 2016. Role of ROS and RNS sources in physiological and pathological conditions. *Oxidative Medicine and Cellular Longevity,* 2016.

EL-NEKEETY, A. A., MOHAMED, S. R., HATHOUT, A. S., HASSAN, N. S., ALY, S. E. & ABDEL-WAHHAB, M. A. 2011. Antioxidant properties of Thymus vulgaris oil against aflatoxin-induce oxidative stress in male rats. *Toxicon,* 57**,** 984-991.

ELWAHAB, H. A. 2017. The role of the glutathione system in regulating the levels of ROS neutralisation in the endothelial cells of the blood-brain barrier.

ESCOBAR, M. L., ECHEVERRÍA, O. M. & VÁZQUEZ-NIN, G. H. 2015. Necrosis as programmed cell death. *Intech Open Science***,** 419-34.

FERNANDES, T., FERRÃO, J. & BELL, V. 2017. Mycotoxins, food and health. *J. Nutr. Health Food Sci,* 5**,** 1-10.

FIUME, L., MANERBA, M., VETTRAINO, M. & DI STEFANO, G. 2014. Inhibition of lactate dehydrogenase activity as an approach to cancer therapy. *Future medicinal chemistry,* 6**,** 429-445.

FORRESTER, S. J., KIKUCHI, D. S., HERNANDES, M. S., XU, Q. & GRIENDLING, K. K. 2018. Reactive oxygen species in metabolic and inflammatory signaling. *Circulation research,* 122**,** 877-902.

GE, J., YU, H., LI, J., LIAN, Z., ZHANG, H., FANG, H. & QIAN, L. 2017. Assessment of aflatoxin B1 myocardial toxicity in rats: mitochondrial damage and cellular apoptosis in cardiomyocytes induced by aflatoxin B1. *Journal of International Medical Research,* 45**,** 1015-1023.

GLASSOCK, R. J. & RULE, A. D. 2016. Aging and the kidneys: anatomy, physiology and consequences for defining chronic kidney disease. *Nephron,* 134**,** 25-29.

GUENGERICH, F. P. 2015. Human cytochrome P450 enzymes. *Cytochrome P450.* Springer.

HAINES, A. M., TOBE, S. S., KOBUS, H. J. & LINACRE, A. 2015. Properties of nucleic acid staining dyes used in gel electrophoresis. *Electrophoresis,* 36**,** 941-944.

HEDSTRÖM, M. & MATTIASSON, B. 2015. Screening of self-assembled monolayer for aflatoxin B1 detection using immune-capacitive sensor. *Biotechnology Reports,* 8**,** 144-151.

HUANG, S., ZHENG, N., FAN, C., CHENG, M., WANG, S., JABAR, A., WANG, J. & CHENG, J. 2018. Effects of aflatoxin B1 combined with ochratoxin A and/or zearalenone on metabolism, immune function, and antioxidant status in lactating dairy goats. *Asian-Australasian journal of animal sciences,* 31**,** 505.

HUSSAIN, Z., KHAN, M. Z. & HASSAN, Z. 2008. Production of aflatoxins from Aspergillus flavus and acute aflatoxicosis in young broiler chicks. *Pak. J. Agri. Sci,* 45**,** 95-102.
JALALI, M., ZABOROWSKA, J. & JALALI, M. 2017. The Polymerase Chain Reaction: PCR, qPCR, and RT-PCR. *Basic Science Methods for Clinical Researchers.* Elsevier.
JEDRZEJCZAK-SILICKA, M. 2017. *History of cell culture,* InTech.
JOG, N. R. & CARICCHIO, R. 2014. The role of necrotic cell death in the pathogenesis of immune mediated nephropathies. *Clinical immunology,* 153**,** 243-253.
KAVIAN, N., MEHLAL, S., JELJELI, M., SAIDU, N. E. B., NICCO, C., CERLES, O., CHOUZENOUX, S., CAUVET, A., CAMUS, C. & AIT DJOUDI, M. 2018. The Nrf2-antioxidant response element signaling pathway controls fibrosis and autoimmunity in scleroderma. *Frontiers in immunology,* 9**,** 1896.
KIRK, G. D., LESI, O. A., MENDY, M., SZYMANSKA, K., WHITTLE, H., GOEDERT, J. J., HAINAUT, P. & MONTESANO, R. 2005. 249 ser TP53 mutation in plasma DNA, hepatitis B viral infection, and risk of hepatocellular carcinoma. *Oncogene,* 24**,** 5858.
KNIGHTS, K. M., ROWLAND, A. & MINERS, J. O. 2013. Renal drug metabolism in humans: the potential for drug–endobiotic interactions involving cytochrome P450 (CYP) and UDP-glucuronosyltransferase (UGT). *British journal of clinical pharmacology,* 76**,** 587-602.
KOCAB, A. J. & DUCKETT, C. S. 2016. Inhibitor of apoptosis proteins as intracellular signaling intermediates. *The FEBS journal,* 283**,** 221-231.
KRALIK, P. & RICCHI, M. 2017. A basic guide to real time PCR in microbial diagnostics: definitions, parameters, and everything. *Frontiers in microbiology,* 8**,** 108.
KUMAR, P., MAHATO, D. K., KAMLE, M., MOHANTA, T. K. & KANG, S. G. 2017. Aflatoxins: a global concern for food safety, human health and their management. *Frontiers in microbiology,* 7**,** 2170.
KUMAR, P., NAGARAJAN, A. & UCHIL, P. D. 2018. Analysis of cell viability by the lactate dehydrogenase assay. *Cold Spring Harbor Protocols,* 2018**,** pdb. prot095497.
KUMAR, V. V. 2018. Aflatoxins: Properties, toxicity and detoxification. *Nutrition and Food science International Journal,* 6**,** 555696.
KUTSCHERA, U. & NIKLAS, K. J. 2013. Metabolic scaling theory in plant biology and the three oxygen paradoxa of aerobic life. *Theory in Biosciences,* 132**,** 277-288.
LAKSHMANAN, I. & BATRA, S. K. 2013. Protocol for Apoptosis Assay by Flow Cytometry Using Annexin V Staining Method. *Bio-protocol,* 3.
LAWRENCE, E. A., DOHERTY, D. & DHANDA, R. 2018. Function of the nephron and the formation of urine. *Anaesthesia & Intensive Care Medicine,* 19**,** 249-253.
LI, H., XING, L., ZHANG, M., WANG, J. & ZHENG, N. 2018. The toxic effects of aflatoxin B1 and aflatoxin M1 on kidney through regulating L-proline and downstream apoptosis. *BioMed research international,* 2018.
LI, W., SANG, Y. & ZHANG, G. 2017. Combined cytotoxicity of aflatoxin B1 and deoxynivalenol to hepatoma HepG2/C3A cells. *World Mycotoxin Journal,* 10**,** 387-399.
LING, X. C. & KUO, K.-L. 2018. Oxidative stress in chronic kidney disease. *Renal Replacement Therapy,* 4**,** 53.
LIU, Y., DU, M. & ZHANG, G. 2014. Proapoptotic activity of aflatoxin B1 and sterigmatocystin in HepG2 cells. *Toxicology reports,* 1**,** 1076-1086.
LIU, Y. & WANG, W. 2016. Aflatoxin B1 impairs mitochondrial functions, activates ROS generation, induces apoptosis and involves Nrf2 signal pathway in primary broiler hepatocytes. *Animal Science Journal,* 87**,** 1490-1500.

LUI, C., CADY, N. C. & BATT, C. A. 2009. Nucleic acid-based detection of bacterial pathogens using integrated microfluidic platform systems. *Sensors,* 9**,** 3713-3744.
MARCHESE, S., POLO, A., ARIANO, A., VELOTTO, S., COSTANTINI, S. & SEVERINO, L. 2018. Aflatoxin B1 and M1: Biological properties and their involvement in cancer development. *Toxins,* 10**,** 214.
MCILWAIN, D. R., BERGER, T. & MAK, T. W. 2013. Caspase functions in cell death and disease. *Cold Spring Harbor perspectives in biology,* 5**,** a008656.
MENEELY, J. P., HAJŠLOVÁ, J., KRSKA, R. & ELLIOTT, C. T. 2018. Assessing the combined toxicity of the natural toxins, aflatoxin B1, fumonisin B1 and microcystin-LR by high content analysis. *Food and chemical toxicology,* 121**,** 527-540.
MILKOVIC, L., CIPAK GASPAROVIC, A., CINDRIC, M., MOUTHUY, P.-A. & ZARKOVIC, N. 2019. Short Overview of ROS as Cell Function Regulators and Their Implications in Therapy Concepts. *Cells,* 8**,** 793.
MISIHAIRABGWI, J., EZEKIEL, C., SULYOK, M., SHEPHARD, G. & KRSKA, R. 2019. Mycotoxin contamination of foods in Southern Africa: A 10-year review (2007–2016). *Critical reviews in food science and nutrition,* 59**,** 43-58.
MOOSA, M. 2019. The state of kidney transplantation in South Africa. *SAMJ: South African Medical Journal,* 109**,** 235-240.
MOOSA, M., VAN DER WALT, I., NAICKER, S. & MEYERS, A. 2015. Important causes of chronic kidney disease in South Africa. *South African Medical Journal,* 105**,** 320-327.
MORGAN, M. J. & LIU, Z.-G. 2011. Crosstalk of reactive oxygen species and NF-κB signaling. *Cell research,* 21**,** 103.
MUSLEH, M., AL-OUQAILI, M. & AL-KUBAISI, S. 2017. *A Molecular Study of Aflatoxin and its Toxic Effect on Hematopoietic Stem Cells.* M. Sc. Thesis, Department of Biology, College of Education for Pure Sciences ….
NANDHAKUMAR, S., PARASURAMAN, S., SHANMUGAM, M., RAO, K. R., CHAND, P. & BHAT, B. V. 2011. Evaluation of DNA damage using single-cell gel electrophoresis (Comet Assay). *Journal of pharmacology & pharmacotherapeutics,* 2**,** 107.
NAVARRO, E., SERRANO-HERAS, G., CASTAÑO, M. & SOLERA, J. 2015. Real-time PCR detection chemistry. *Clinica chimica acta,* 439**,** 231-250.
PENG, X., YU, Z., LIANG, N., CHI, X., LI, X., JIANG, M., FANG, J., CUI, H., LAI, W. & ZHOU, Y. 2016. The mitochondrial and death receptor pathways involved in the thymocytes apoptosis induced by aflatoxin B1. *Oncotarget,* 7**,** 12222.
PFEFFER, C. & SINGH, A. 2018. Apoptosis: a target for anticancer therapy. *International journal of molecular sciences,* 19**,** 448.
PIZZORNO, J. 2015. The Kidney Dysfunction Epidemic, Part 1: Causes. *Integrative Medicine: A Clinician's Journal,* 14**,** 8.
QURESHI, H., HAMID, S. S., ALI, S. S., ANWAR, J., SIDDIQUI, A. A. & KHAN, N. A. 2015. Cytotoxic effects of aflatoxin B1 on human brain microvascular endothelial cells of the blood-brain barrier. *Medical mycology,* 53**,** 409-416.
RAJPUT, S., SUN, L., ZHANG, N.-Y., KHALIL, M., LING, Z., CHONG, L., WANG, S., RAJPUT, I., BLOCH, D. & KHAN, F. 2019. Grape Seed Proanthocyanidin Extract Alleviates AflatoxinB1-Induced Immunotoxicity and Oxidative Stress via Modulation of NF-κB and Nrf2 Signaling Pathways in Broilers. *Toxins,* 11**,** 23.
RAMPAL, G., KHANNA, N., THIND, T. S., ARORA, S. & VIG, A. 2012. Role of isothiocyanates as anticancer agents and their contributing molecular and cellular mechanisms. *Med. Chem. Drug Discovery,* 3**,** 79-93.

RAUNIO, H., KUUSISTO, M., JUVONEN, R. O. & PENTIKÄINEN, O. T. 2015. Modeling of interactions between xenobiotics and cytochrome P450 (CYP) enzymes. *Frontiers in pharmacology,* 6**,** 123.

RISS, T. L., MORAVEC, R. A., NILES, A. L., DUELLMAN, S., BENINK, H. A., WORZELLA, T. J. & MINOR, L. 2016. Cell viability assays. *Assay Guidance Manual [Internet]*. Eli Lilly & Company and the National Center for Advancing Translational Sciences.

ROEBUCK, B. D., JOHNSON, D. N., SUTTER, C. H., EGNER, P. A., SCHOLL, P. F., FRIESEN, M. D., BAUMGARTNER, K. J., WARE, N. M., BODREDDIGARI, S. & GROOPMAN, J. D. 2009. Transgenic expression of aflatoxin aldehyde reductase (AKR7A1) modulates aflatoxin B1 metabolism but not hepatic carcinogenesis in the rat. *Toxicological sciences,* 109**,** 41-49.

RUSHING, B. R. & SELIM, M. I. 2018. Aflatoxin B1: A review on metabolism, toxicity, occurrence in food, occupational exposure, and detoxification methods. *Food and chemical toxicology*.

SAINZ, R. M., LOMBO, F. & MAYO, J. C. 2012. Radical decisions in cancer: redox control of cell growth and death. *Cancers,* 4**,** 442-474.

SALBITANI, G., BOTTONE, C. & CARFAGNA, S. 2017. Determination of reduced and total glutathione content in extremophilic microalga Galdieria phlegrea. *Bio Protoc.,* 7**,** e2372.

SHARMA, V., SHARMA, C., PALIWAL, R., PRACHETA, S. S. & SHARMA, S. 2011. Ameliorative effects of Curcuma longa and curcumin on aflatoxin B1 induced serological and biochemical changes in kidney of male mice. *Asian J Biochem Pharmaceut Res,* 2**,** 338-351.

SHEN, H.-M., SHI, C.-Y., LEE, H.-P. & ONG, C.-N. 1994. Aflatoxin B1-induced lipid peroxidation in rat liver. *Toxicology and applied pharmacology,* 127**,** 145-150.

SHEN, H.-M., SHI, C.-Y., SHEN, Y. & ONG, C.-N. 1996. Detection of elevated reactive oxygen species level in cultured rat hepatocytes treated with aflatoxin B1. *Free Radical Biology and Medicine,* 21**,** 139-146.

STEPANENKO, A. & DMITRENKO, V. 2015. HEK293 in cell biology and cancer research: phenotype, karyotype, tumorigenicity, and stress-induced genome-phenotype evolution. *Gene,* 569**,** 182-190.

STEWART, R. K., SMITH, G. B., DONNELLY, P. J., REID, K. R., PETSIKAS, D., CONLAN, A. A. & MASSEY, T. E. 1999. Glutathione S-transferase-catalyzed conjugation of bioactivated aflatoxin B1 in human lung: differential cellular distribution and lack of significance of the GSTM1 genetic polymorphism. *Carcinogenesis,* 20**,** 1971-1977.

STOCKERT, J. C., HOROBIN, R. W., COLOMBO, L. L. & BLAZQUEZ-CASTRO, A. 2018. Tetrazolium salts and formazan products in Cell Biology: Viability assessment, fluorescence imaging, and labeling perspectives. *Acta histochemica,* 120**,** 159-167.

SZNARKOWSKA, A., KOSTECKA, A., MELLER, K. & BIELAWSKI, K. P. 2017. Inhibition of cancer antioxidant defense by natural compounds. *Oncotarget,* 8**,** 15996.

SZYMAŃSKA, K., LESI, O. A., KIRK, G. D., SAM, O., TANIERE, P., SCOAZEC, J. Y., MENDY, M., FRIESEN, M. D., WHITTLE, H. & MONTESANO, R. 2004. Ser-249TP53 mutation in tumour and plasma DNA of hepatocellular carcinoma patients from a high incidence area in the Gambia, West Africa. *International journal of cancer,* 110**,** 374-379.

TAYLOR, S. C. & POSCH, A. 2014. The design of a quantitative western blot experiment. *BioMed research international,* 2014.

TONG, L., CHUANG, C.-C., WU, S. & ZUO, L. 2015. Reactive oxygen species in redox cancer therapy. *Cancer letters,* 367**,** 18-25.
VAN VLEET, T. R., MACÉ, K. & COULOMBE, R. A. 2002. Comparative aflatoxin B1 activation and cytotoxicity in human bronchial cells expressing cytochromes P450 1A2 and 3A4. *Cancer research,* 62**,** 105-112.
VLAHOPOULOS, S., ADAMAKI, M., KHOURY, N., ZOUMPOURLIS, V. & BOLDOGH, I. 2019. Roles of DNA repair enzyme OGG1 in innate immunity and its significance for lung cancer. *Pharmacology & therapeutics,* 194**,** 59-72.
WANG, R., LI, C., QIAO, P., XUE, Y., ZHENG, X., CHEN, H., ZENG, X., LIU, W., BOLDOGH, I. & BA, X. 2018. OGG1-initiated base excision repair exacerbates oxidative stress-induced parthanatos. *Cell death & disease,* 9**,** 628.
WANGIKAR, P., DWIVEDI, P., SINHA, N., SHARMA, A. & TELANG, A. 2005. Teratogenic effects in rabbits of simultaneous exposure to ochratoxin A and aflatoxin B1 with special reference to microscopic effects. *Toxicology,* 215**,** 37-47.
YANG, X.-J., LU, H.-Y., LI, Z.-Y., BIAN, Q., QIU, L.-L., LI, Z., LIU, Q., LI, J., WANG, X. & WANG, S.-L. 2012. Cytochrome P450 2A13 mediates aflatoxin B1-induced cytotoxicity and apoptosis in human bronchial epithelial cells. *Toxicology,* 300**,** 138-148.
YAO, H., HRUSKA, Z. & DI MAVUNGU, J. D. 2015. Developments in detection and determination of aflatoxins. *World Mycotoxin Journal,* 8**,** 181-191.
YILMAZ, S., KAYA, E., KARACA, A. & KARATAS, O. 2018. Aflatoxin B1 induced renal and cardiac damage in rats: Protective effect of lycopene. *Research in veterinary science,* 119**,** 268-275.
YIP, K. Y., WAN, M. L. Y., WONG, A. S. T., KORACH, K. S. & EL-NEZAMI, H. 2017. Combined low-dose zearalenone and aflatoxin B1 on cell growth and cell-cycle progression in breast cancer MCF-7 cells. *Toxicology letters,* 281**,** 139-151.
YONG, J., BISCHOF, H., BURGSTALLER, S., SIIRIN, M., MURPHY, A., MALLI, R. & KAUFMAN, R. J. 2019. Mitochondria supply ATP to the ER through a mechanism antagonized by cytosolic Ca2+. *eLife,* 8.
ZANGER, U. M. & SCHWAB, M. 2013. Cytochrome P450 enzymes in drug metabolism: regulation of gene expression, enzyme activities, and impact of genetic variation. *Pharmacology & therapeutics,* 138**,** 103-141.
ZEB, A. & ULLAH, F. 2016. A simple spectrophotometric method for the determination of thiobarbituric acid reactive substances in fried fast foods. *Journal of analytical methods in chemistry,* 2016.
ZHANG, Y., CHEN, X., GUEYDAN, C. & HAN, J. 2018. Plasma membrane changes during programmed cell deaths. *Cell research,* 28**,** 9.
ZHANG, Z., LU, H., HUAN, F., MEGHAN, C., YANG, X., WANG, Y., WANG, X., WANG, X. & WANG, S. L. 2014. Cytochrome P450 2A13 mediates the neoplastic transformation of human bronchial epithelial cells at a low concentration of aflatoxin B1. *International journal of cancer,* 134**,** 1539-1548.
ZINEDINE, A. & EL AKHDARI, S. 2019. Food Safety and Climate Change: Case of Mycotoxins. *Handbook of Research on Global Environmental Changes and Human Health.* IGI Global.

APPENDIX

Appendix A

Table A1: MTT assay raw data used to calculate AFB_1 IC_{50}

AFB_1 concentration (µM)	**Log concentration**	**OD1**	**OD2**	**OD3**	**OD4**	**Average**	**% cell viability**
0		0,23	0,219	0,245	0,265	0,2398	
1,25	0,097	0,177	0,152	0,185	0,226	0,1850	77
2,5	0,398	0,206	0,221	0,248	0,251	0,2315	97
5	0,699	0,206	0,261	0,209	0,288	0,2410	101
10	1,000	0,197	0,169	0,226	0,236	0,2070	86
25	1,398	0,108	0,107	0,133	0,097	0,1113	46
50	1,699	0,242	0,27	0,184	0,184	0,2200	92
75	1,875	0,247	0,162	0,13	0,12	0,1648	69
100	2,000	0,056	0,099	0,047	0,063	0,0663	28

Appendix B : Nitric oxide synthase (NOS)assay

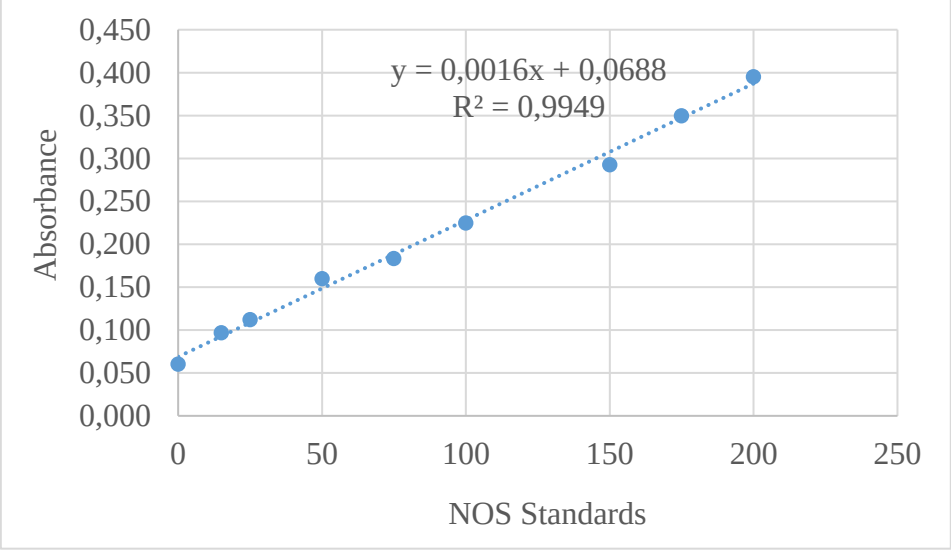

Figure B1 : Standard curve generated from NOS standards.

Appendix C : Protein standardisation

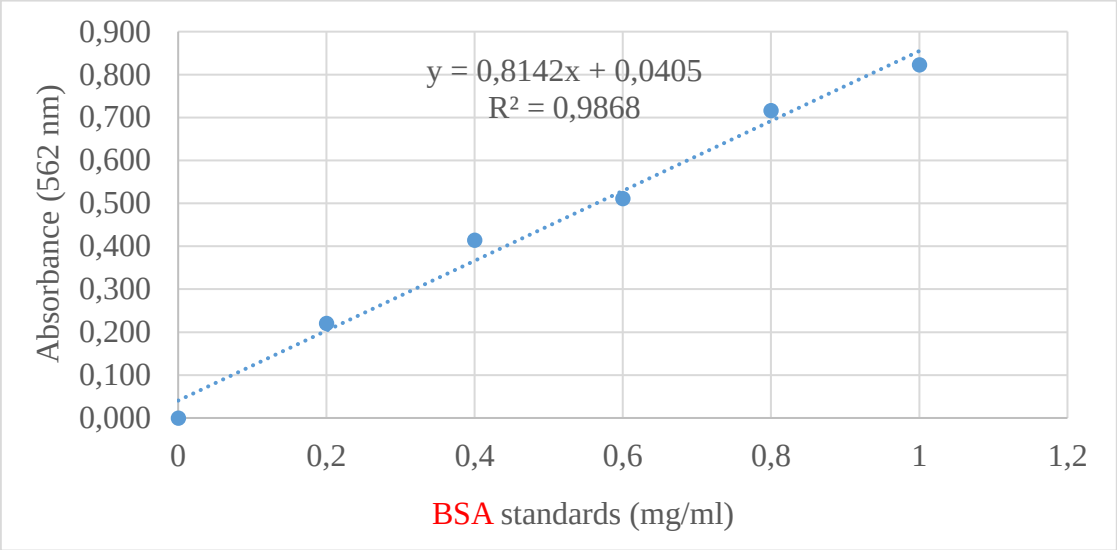

Figure C1 : Protein standardisation curve

Appendix D : Quantitative polymerase reaction (qPCR)

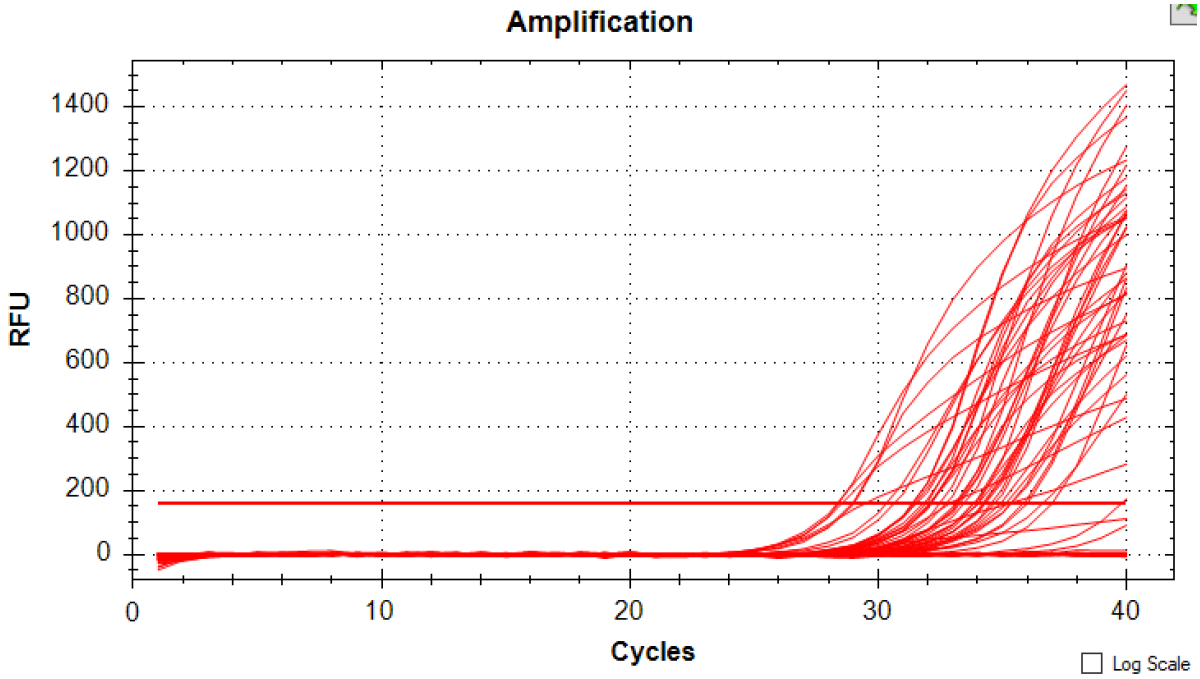

Figure D1 : The amplification of OGG1 gene.

Appendix E : Plagiarism report

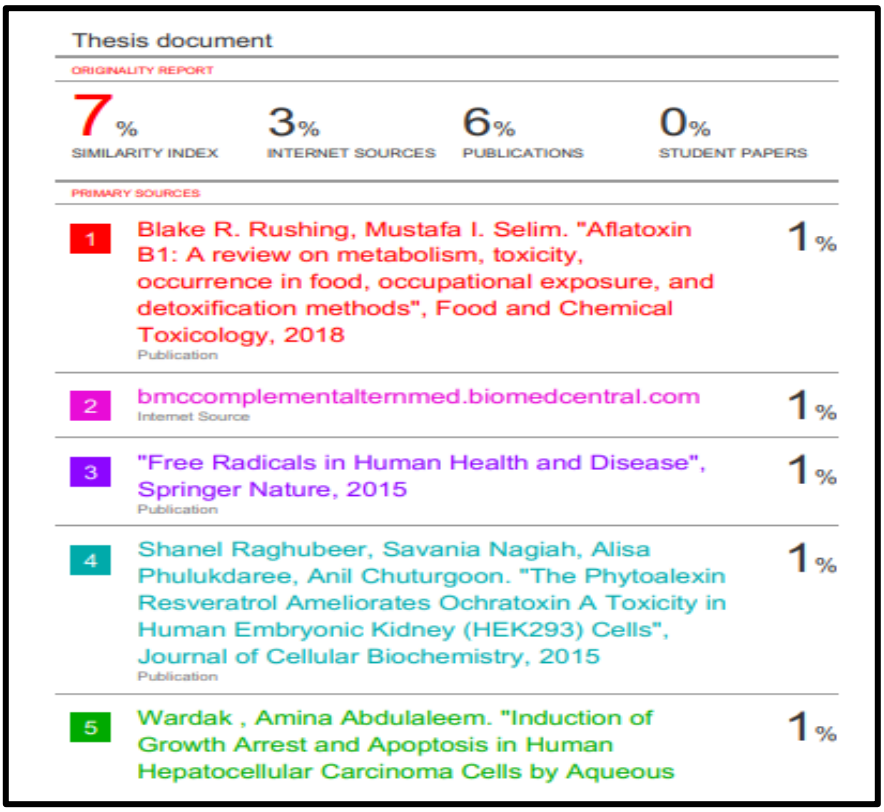

Thesis document

ORIGINALITY REPORT

7%	3%	6%	0%
SIMILARITY INDEX	INTERNET SOURCES	PUBLICATIONS	STUDENT PAPERS

PRIMARY SOURCES

1	Blake R. Rushing, Mustafa I. Selim. "Aflatoxin B1: A review on metabolism, toxicity, occurrence in food, occupational exposure, and detoxification methods", Food and Chemical Toxicology, 2018 Publication	1%
2	bmccomplementalternmed.biomedcentral.com Internet Source	1%
3	"Free Radicals in Human Health and Disease", Springer Nature, 2015 Publication	1%
4	Shanel Raghubeer, Savania Nagiah, Alisa Phulukdaree, Anil Chuturgoon. "The Phytoalexin Resveratrol Ameliorates Ochratoxin A Toxicity in Human Embryonic Kidney (HEK293) Cells", Journal of Cellular Biochemistry, 2015 Publication	1%
5	Wardak , Amina Abdulaleem. "Induction of Growth Arrest and Apoptosis in Human Hepatocellular Carcinoma Cells by Aqueous	1%

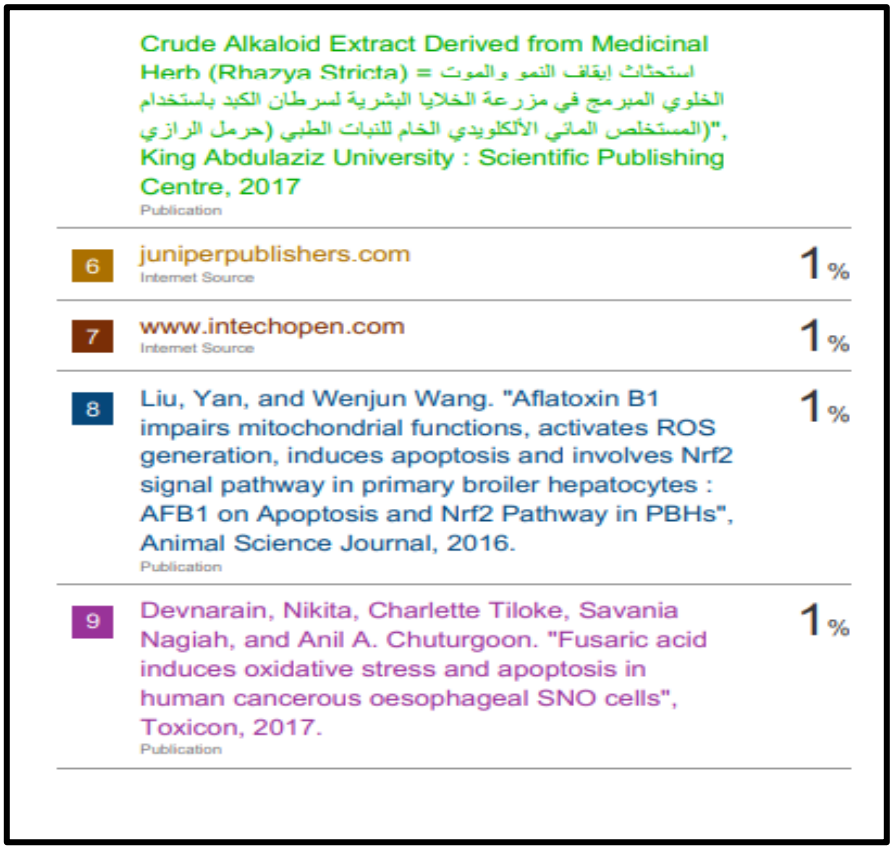

Crude Alkaloid Extract Derived from Medicinal Herb (Rhazya Stricta) = استحثاث إيقاف النمو والموت الخلوي المبرمج في مزرعة الخلايا البشرية لسرطان الكبد باستخدام المستخلص المائي الألكلويدي الخام للنبات الطبي (حرمل الرازي)", King Abdulaziz University : Scientific Publishing Centre, 2017
Publication

6	juniperpublishers.com Internet Source	1%
7	www.intechopen.com Internet Source	1%
8	Liu, Yan, and Wenjun Wang. "Aflatoxin B1 impairs mitochondrial functions, activates ROS generation, induces apoptosis and involves Nrf2 signal pathway in primary broiler hepatocytes : AFB1 on Apoptosis and Nrf2 Pathway in PBHs", Animal Science Journal, 2016. Publication	1%
9	Devnarain, Nikita, Charlette Tiloke, Savania Nagiah, and Anil A. Chuturgoon. "Fusaric acid induces oxidative stress and apoptosis in human cancerous oesophageal SNO cells", Toxicon, 2017. Publication	1%